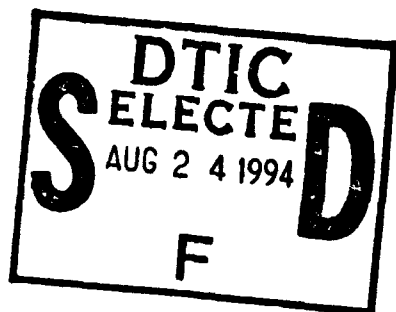
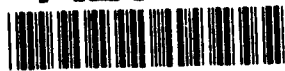


NAVAL POSTGRADUATE SCHOOL
Monterey, California

①

AD-A283 618



THESIS

94-26835



Course Module for AA2021: Wing Structural Design Project

By

Stephen A. Burris, P.E.

March 1994

Thesis Advisor:

Gerald H. Lindsey, Ph.D.

Approved for public release: distribution is unlimited

DTIC QUALITY INSPECTED 1

94 8 23 02 5

Unclassified

SECURITY CLASSIFICATION OF THIS PAGE

Form Approved
OMB No. 0704-0188

REPORT DOCUMENTATION PAGE

1a. REPORT SECURITY CLASSIFICATION Unclassified		1b. RESTRICTIVE MARKINGS	
2a. SECURITY CLASSIFICATION AUTHORITY		3. DISTRIBUTION/AVAILABILITY OF REPORT Approved for public release: distribution is unlimited	
2b. DECLASSIFICATION/DOWNGRADING SCHEDULE		4. PERFORMING ORGANIZATION REPORT NUMBER(S)	
5. MONITORING ORGANIZATION REPORT NUMBER(S)		6a. NAME OF PERFORMING ORGANIZATION Naval Postgraduate School	
6b. OFFICE SYMBOL (If applicable)		7a. NAME OF MONITORING ORGANIZATION Naval Postgraduate School	
6c. ADDRESS (City, State, and ZIP Code) Monterey, CA 93943-5000		7b. ADDRESS (City, State, and ZIP Code) Monterey, CA 93943-5000	
8a. NAME OF FUNDING/SPONSORING ORGANIZATION		8b. OFFICE SYMBOL (If applicable)	
8c. ADDRESS (City, State, and ZIP Code)		9. PROCUREMENT INSTRUMENT IDENTIFICATION NUMBER	
10. SOURCE OF FUNDING NUMBERS		PROGRAM ELEMENT NO.	
PROJECT NO.		TASK NO.	
WORK UNIT ACCESSION NO.		11. TITLE (Include Security Classification) Course Module for AA2021: Wing Structural Design Project	
12. PERSONAL AUTHOR(S) Stephen Allen Burris, P.E.			
13a. TYPE OF REPORT Master's Thesis		13b. TIME COVERED FROM _____ TO _____	
14. DATE OF REPORT (Year, Month, Day) March 1994		15. PAGE COUNT 132	
16. SUPPLEMENTARY NOTATION The views expressed in this thesis are those of the author and do not reflect the official policy or position of the Department of Defense or the U.S. Government.			
17. COSATI CODES		18. SUBJECT TERMS (Continue on reverse if necessary and identify by block number)	
FIELD	GROUP	SUB-GROUP	
19. ABSTRACT (Continue on reverse if necessary and identify by block number) <p>This thesis defined a fundamental approach for aircraft wingbox design appropriate for an introductory course in aircraft structures based upon material strength and stiffness requirements. The process developed sought to encompass major conceptual engineering design considerations that ranged from load estimation at various points in the subsonic flight envelope, to initial structural sizing and layout. The goal was to present a process that could be readily conducted via hand calculations and applied by any student entering basic aircraft structures design.</p> <p>The sequence of analysis began with application of a comprehensive panel code method developed by NASA Ames Research Center known as PMARC. Loads obtained from the code were then used to formulate a strength of materials study of the structure subjected to combined bending, shear and torsion. The static load approach allowed initial estimation of component sizing based upon material or buckling allowable stress selection. Finally, the study demonstrated a strength to weight ratio comparison.</p> <p>Several calculation examples and computer-based spreadsheets were prepared for rapid analysis of multiple option design scenarios. Since the study employed analysis methods that could be performed without the aid of a finite element routine or extensive computer programming knowledge, it serves as a good introduction for the entry and intermediate level structural engineer.</p>			
20. DISTRIBUTION/AVAILABILITY OF ABSTRACT <input checked="" type="checkbox"/> UNCLASSIFIED/UNLIMITED <input type="checkbox"/> SAME AS RPT. <input type="checkbox"/> DTIC USERS		21. ABSTRACT SECURITY CLASSIFICATION Unclassified	
22a. NAME OF RESPONSIBLE INDIVIDUAL Prof. Gerald H. Lindsey, Ph.D.		22b. TELEPHONE (Include Area Code) (408) 656-2311	
		22c. OFFICE SYMBOL AA/Li	

DD Form 1473, JUN 86

Previous editions are obsolete.

SECURITY CLASSIFICATION OF THIS PAGE

S/N 0102-LF-014-6603

Unclassified

Approved for public release: distribution is unlimited

Course Module for AA2021:
Wing Structural Design Project

by Stephen A. Burris, P.E.
Lieutenant Commander, United States Navy
B.S., United States Naval Academy, 1982

Submitted in partial fulfillment
of the requirements for the degree of


MASTER OF SCIENCE IN AERONAUTICAL ENGINEERING

from the

NAVAL POSTGRADUATE SCHOOL


March 1994

Author:


Stephen A. Burris

Approved by:


Gerald H. Lindsey, Thesis Advisor


Edward M. Wu, Second Reader


Daniel J. Collins, Chairman
Department of Aeronautics and Astronautics

Accession For	
NTIS CRA&I	<input checked="checked" type="checkbox"/>
DTIC TAB	<input type="checkbox"/>
Unannounced	<input type="checkbox"/>
Justification	
By	
Distribution /	
Availability Codes	
Dist	Avail and/or Special
A-1	

ABSTRACT

This thesis defined a fundamental approach for aircraft wingbox design appropriate for an introductory course in aircraft structures based upon material strength and stiffness requirements. The process developed sought to encompass major conceptual engineering design considerations that ranged from load estimation at various points in the subsonic flight envelope to initial structural sizing and layout. The goal was to present a process that could be readily conducted via hand calculations and applied by any student entering basic aircraft structures design.

The sequence of analysis began with application of a comprehensive panel code method developed by NASA Ames Research Center known as PMARC. Loads obtained from the code were then used to formulate a strength of materials study of the structure subjected to combined bending, shear and torsion. The static load approach allowed initial estimation of component sizing based upon material or buckling allowable stress selection. Finally, the study demonstrated a strength to weight ratio comparison.

Several calculation examples and computer-based spreadsheets were prepared for rapid analysis of multiple option design scenarios. Since the study employed analysis methods that could be performed without the aid of a finite element routine or extensive computer programming knowledge, it serves as a good introduction for the entry and intermediate level structural engineer.

TABLE OF CONTENTS

I. INTRODUCTION	1
II. LOAD ANALYSIS	3
A. REQUIREMENTS	3
B. REVIEW OF AVAILABLE METHODS	4
C. PMARC	5
1. Validation Study Summary	6
2. User Interface Issues	7
D. SAMPLE PROBLEM RESULTS	10
III. STRENGTH ANALYSIS	15
A. BOUNDARY CONDITION DEFINITION	15
1. Shear Diagram Construction	18
2. Bending Moment Diagram	19
3. Torsional Moment	23
B. BENDING STRESS ANALYSIS	27
1. Area Determination	28
2. Determination of Allowable Stress	30
3. Spar Placement Considerations	31
4. Straight Wing Approach	33
5. Swept Wing Considerations	34
C. SHEAR STRESS ANALYSIS	37
1. Shear Flow due to Torsion	37
2. Shear Flow due to Applied Loads	38
D. VARIATION IN OPERATIONAL CONDITIONS	41
E. SKIN SIZING	42

IV. BUCKLING CONSIDERATIONS	46
A. STIFFENER SPACING	46
B. STIFFENER SIZING	49
1. Initial Size Estimate	50
2. Uniform Thickness Approach	54
3. Stringer Cross-Section Stability	55
V. STRENGTH TO WEIGHT	58
A. BENDING STRENGTH TRADE STUDY	58
1. Material Selection	58
2. Forward Spar Location	60
B. INSTABILITY IMPLICATIONS	60
C. ADVANCED MATERIAL CONSIDERATIONS	61
VI. SUMMARY	63
A. FUTURE AREAS OF STUDY	63
1. Aerodynamic Investigations	63
2. Advanced Structural Analysis	64
B. CONCLUSION	66
APPENDIX A	68
A. WAKE INITIALIZATION	68
B. ANALYTICAL VALIDATION	71
C. COMPUTER-BASED VERIFICATION	76
D. EXPERIMENTAL DATA COMPARISON	77
APPENDIX B	79
APPENDIX C	114
A. LOCATING THE FORWARD SPAR	114
B. RIB SPACING CONSIDERATIONS	116
APPENDIX D	121
LIST OF REFERENCES	122

INITIAL DISTRIBUTION LIST	124
---------------------------------	-----

I. INTRODUCTION

This thesis provides a systematic approach to the preliminary design of an aircraft wingbox structure that employs a two spar support base. The method chosen was based upon an applied elasticity approach as described by Allen and Haisler [Ref. 1:pp. 145-233] using strength and stiffness specifications as the design target. The intent of this effort was to provide insight into the flow of engineering design decisions that begin in load determination and end with preliminary structural layout. As a result of this work, several study sections were developed for incorporation into the current aeronautical engineering curriculum at the Naval Postgraduate School (NPS) to be presented in the undergraduate and graduate core structural engineering courses.

The organization of this thesis begins with determination of the static load boundary condition applied to an airfoil of arbitrary geometry. To solve the low speed problem for designs encountering flight speeds up to and including Mach number 0.6, a potential flow panel code method was chosen that allowed user definition of wing geometry, and total aircraft, if desired. The code was used in this research to calculate spanwise force and moment information; however, it is also capable of providing pressure distribution information along the surface of the structure as well.

Once the loads were obtained along the span from the code, they were used as a series of discrete point loads. From this information traditional bending and shear diagrams were constructed for use in the strength analysis. As part of the instructional

module for the Introductory Aircraft Structures, AA 2021, a teaching guide and automated spreadsheet routine were developed to aid in presenting this material in a four hour lecture series.

The thesis continues with a review of the buckling stability of a wing cover subjected to the stresses projected from a shear flow solution. Using the methods described in Sechler and Dunn, an analysis of a stiffened wing section was conducted to determine potential stringer size, geometry and total number required to support the structure at a given cross-section [Ref. 2:pp. 154-258]. As these chapters are presented, several design questions arise from the structural engineer's perspective that are presented and answered.

At the conclusion of the research, several follow-on topics were presented for future thesis work by students at NPS. Since this work does support an ongoing design effort that is a fundamental segment of the curriculum for all students within the department, this work can serve as a valuable reference for use in future aircraft design reviews and competitions.

II. LOAD ANALYSIS

A. REQUIREMENTS

The very nature of design requires tools that support creative and interactive development of aircraft structures. Interactive flexibility demands that the designer must be able to quickly analyze several options feeding back to arrive at a configuration that best suits the requirements at hand. The boundary condition imposed upon an aircraft structure is the result of an external pressure distribution, internal structural weight and internal pressure distribution associated with a given flight envelope. These components of the overall boundary condition can then be idealized in a number of ways. Any method chosen to idealize the boundary condition to allow solution of its impact on the strength of a structure, necessitates the capability to adapt to arbitrary geometries and provide meaningful, accurate data in a reasonable amount of time.

Several Computational Fluid Dynamics (CFD) methods exist today that provide very reliable data for nearly all aspects of the flight envelope. Unfortunately these methods also require extensive training and experience in grid generation, input data preparation, interpretation of results, etc.; in addition to tremendous computer processing time. Another drawback to CFD is the time associated with development of an individually tailored analysis grid which can require several weeks of effort.

Earlier estimation methods employing conversion of 2-d airfoil data into 3-d wing results, as described by Nicholai [Ref. 3:pp. 2-1:2-9] and Raymer [Ref. 4:pp. 342-344]

tend to leave many students searching for specific solutions to problems that are not covered by generic tables or charts.

B. REVIEW OF AVAILABLE METHODS

For the reasons listed above, the CFD approach was rejected for use in an introductory to intermediate level approach to load determination. Since most tactical naval aircraft operate in both the supersonic and subsonic flight regimes, methods of load approximation are required in both arenas. The problem of estimating supersonic loads was believed to be reasonably approximated by the application of 2-d gas dynamics to obtain the external resultant pressure. Since all supersonic aircraft also operate in the subsonic regime, the load calculation method chosen for this work was for those loads associated with flight operations in the 0.0-0.6 Mach number regime. One area this thesis did not address concerns the load approximation for flight in the transonic regime. For first order approximations at those speeds, the reader is encouraged to review the methods depicted in Raymer [Ref. 4:pp 293-297].

Several analytical and empirical approximations in the subsonic range have been developed throughout the years to aid the designer in a quick approximation of the loads experienced along the span of a wing. Two of the more recognized approaches include DATCOM and Schrenk's approximation. Unfortunately during previous work, several students found these methods lacking in sufficient detail when confronted with changing geometries, (consider the case of high-lift devices), or actual changes in airfoil cross-section, (i.e., wash-out). However these methods did prove to be useful in

validating computer solution methods. *A key design lesson learned in the application of any computer solution is a thorough validation of expected results from a second approach at one or more known benchmarks.*

Students are exposed to potential flow theory early in the aeronautical engineering curriculum at NPS and generally understand the underlying principles of most panel code solution methods. Prior to replacement of the department's VAX computer network system, a panel code produced by NASA Langley known as SUB had been used extensively as a design tool by many students. During the interim between the loss of the VAX and complete system integration of a UNIX based Silicon Graphics_{TM} workstation network, the department sought to incorporate a new panel code routine for use by the aerospace engineering student body.

C. PMARC

During 1993 LCDR Dave Porter, USN, obtained a panel code method from NASA Ames known as Panel Method Ames Research Center (PMARC), for use in his thesis research. The software was accompanied by an additional routine, also developed by NASA Ames, known as General Visualization System (GVS). This second routine allows a 3-d graphical interpretation of the output from PMARC, which includes color display of pressure distribution, streamline generation, wireframe modeling and solid surface rendering.

PMARC enabled the designer to rapidly construct a complex geometry and analyze flows around that geometry in the subsonic regime. Since the code allowed for assembly

of several component geometries, it allowed for load analysis of difficult layouts that were previously considered unworkable by most students in the preliminary design phase (a large fowler flap assembly is one example).

Installation of this code for use by the entire department did not occur without some additional effort beyond simple file transfer to the system file server. The first obstacle encountered with PMARC was a lack of adequate information for the first time user regarding the generation of input and interpretation of output. To reduce the learning requirements placed upon the user, an installation and introductory instruction manual [Ref. 5] was developed for use by all department members as a part of this thesis work. The second hurdle to overcome was development of a means to benchmark the performance of the code.

1. Validation Study Summary

This section highlights a few of the tests that were conducted to validate the output generated by PMARC. Although one set of validation results was provided by NASA Ames with the original documentation, they involve a rather complex wing-body combination that is not well-suited for generation and duplication by the average student user. One example of PMARC's capability to produce an acceptable 3-d lift curve slope using a NACA 4 Digit airfoil cross-section is presented in Figure 1.

The comparison depicted is made from a 2-d transformation method described by Nicholai [Ref. 3:p. 23] that uses the airfoil lift curve slope adjusted for overall geometry. Another comparison performed to verify the results was on a wing based using a

NACA 6 Digit airfoil. The comparison was made against wind tunnel data presented by Bertin and Smith using an unswept trapezoidal wing at low mach number [Ref. 6:pp. 253-257]. Those results are summarized in Figure 2.

Several validation studies were performed to check the accuracy of output, in addition to learning the correct data input procedures. These studies demonstrate a

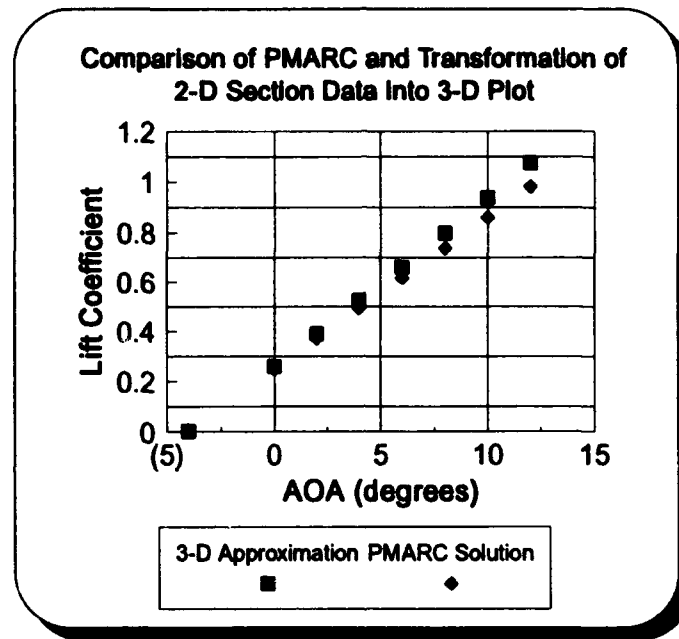


Figure 1

method for constructing wing shapes of various cross-sections using standard airfoil shapes, in addition to modeling individually tailored designs. A complete summary of these validation studies can be found in Appendix A.

2. User Interface Issues

Since PMARC allows for a wide range of analysis including boundary layer investigation, ground effect corrections, multiple geometries and oscillatory analysis, it

requires a sizable portion of input data in a FORTRAN format. The code does allow for quick generation of any wing shape that employs a NACA 4 Digit airfoil by employing an automatic panel generating scheme. However all other cross-sections require a specification of the geometry in 3-d space for all dividing sections; i.e., the root and tip cross-section. To provide easier body generation, the code allows several different axis orientation systems to build component geometries. During the development of a user's guide, the benefit of templates proved invaluable in reducing data input file construction time and minimization of data entry errors. A model template directory was constructed on the IRIS_{TM} computer system that was accessible to all users. This directory contained

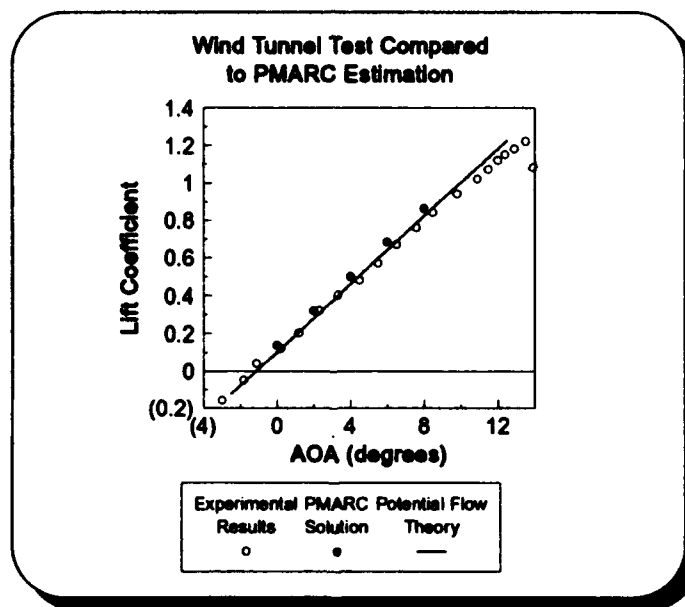


Figure 2

examples of the construction of several NACA 4 Digit airfoil sections and one NACA 6 Digit custom cross-section design. With less than a few hours of instruction and practice, the average user can construct a NACA 4 Digit wing in approximately 10 minutes. Given

the coordinates of a custom cross-section, most users can construct an input file using one of the templates in approximately 20 minutes. This short construction time proves to be very useful in a time-constrained design syllabus.

For introductory design work, the force and moment coefficient output of PMARC was determined to be easiest to use for most students investigating strength requirements of a given design proposal. However, the availability of pressure data offers some interesting possibilities for advanced study that will be addressed later in this report. The lift and drag coefficient data provides information for each individual panel, a summary of all columns of panels along the span, component summary (the right wing for example) and complete assembly summary in the case of an entire aircraft. For this project the column summaries were used to develop an approximate discrete load acting at the centroid of each column section. The column in this output is based upon the resultant force and moment that is obtained by grouping all of the panels around a section of the airfoil between two neighboring spanwise station locations. For instance, if the wing panels divided the wing into ten equally spaced segments starting from centerline, the first column corresponds to the first segment, and all panels acting on the upper and lower surface of that segment. In this analysis, the resultant loads due to lift and drag for the column have been assigned to discrete locations within each column, i.e., the center of the column in the spanwise direction and the center of pressure in the chordwise direction.

D. SAMPLE PROBLEM RESULTS

The geometry chosen for analysis is depicted in Figure 3, including operating condition data. To demonstrate the procedure used in developing the instructional modules, one aircraft configuration was chosen to be used as a repetitive example for the design sections of coursework encountered throughout the structures discipline at NPS. This allowed students to compare results using different methods of analysis as their skill level and exposure to advanced methods increased.

This wing was chosen to support an aircraft operating at a gross weight of 150,000 lbs subjected to a maximum allowable load factor of 3.5 g's. To demonstrate the methodology involved, one flight operating condition was used for analysis and sizing throughout this paper, with a discussion to follow on how to apply these techniques to multiple flight operating conditions.

Given the allowable load factor, the condition chosen for analysis was slightly above the corner velocity. The wing was assumed capable of delivering a maximum lift coefficient of 1.35 at 572 ft/sec. Since the panel code is based upon potential flow, the analysis point was moved out away from $c_{L_{max}}$ in an effort to avoid substantial bias due to a lack of non-linear lift analysis capability in the routine. Using sea-level conditions of 0.53 mach and standard day density, the required c_L was determined via equation (1).

$$c_L = \frac{2nW}{\rho V^2 A_{ref}} \quad (1)$$

The result was a minimum c_L of 1.269 with the corresponding AOA to be determined from the 3-d lift curve versus Angle of Attack (AOA) diagram. To obtain a lift curve

Planform 1



$$c_r = 15ft$$

$$c_t = 5ft$$

$$\bar{c} = 10.83ft$$

$$\lambda = 0.33$$

$$A_{ref} = 1000ft^2$$

$$b = 100ft$$

Airfoil : NACA 4418

$$AR = 10.0$$

$$Re = 38,378,000$$

$$IMN = 0.5$$

$$Temp = 60^\circ F$$

Altitude = Sea Level

$$AOA = 2^\circ$$

Figure 3

diagram, a PMARC input file for this wing was created and evaluated at several different angles of attack. Table 1 is a summary of those results over various alphas. Using the data of

Table 1 and simple linear regression analysis, the corresponding AOA was found to be 9.025 degrees at the desired operating condition.

TABLE 1

Column	C_L
-2.0000	0.2022
0.0000	0.3972
2.0000	0.5905
4.0000	0.7841
6.0000	0.9755

This angle of attack was then used as the input for PMARC to obtain the spanwise load. The code's panel generation routine was employed for model construction. The routine provided a spacing technique that increased panel density near the leading edge, trailing edge and wingtips for improved solution fidelity. Figure 4 depicts the resultant column lift coefficient distribution along the semi-span of the right wing. In addition to the lift coefficient output, PMARC also provided extensive coefficient information in both the wind axis and body axis system. From a structural standpoint, the load analysis was based upon the normal and axial forces. Since these forces were computed to act through the center of pressure on the aircraft's chord line, some modification of the results was

required to determine structural boundary conditions acting at the structure's centroid.

Table 2 is a summary of the coefficients that were required along the span.

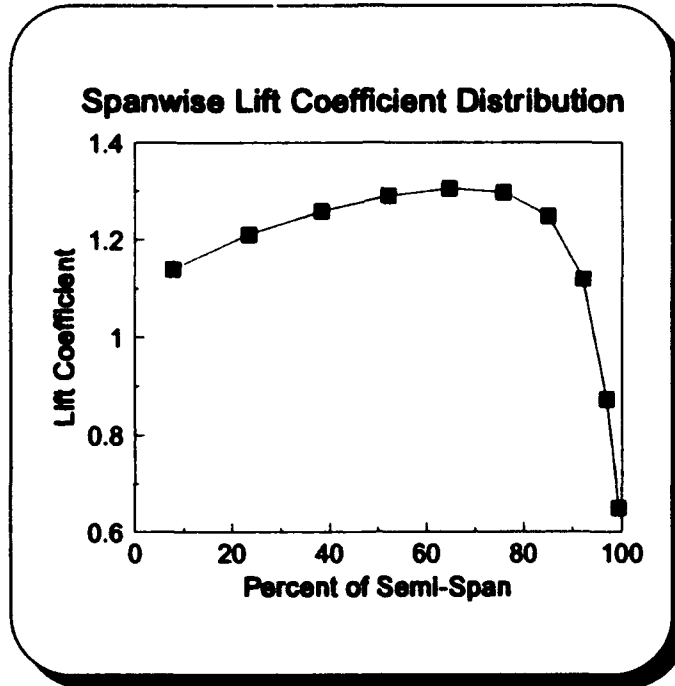


Figure 4

To simplify the following load analysis, the load was assumed to be a discrete load acting at the center of each column. To obtain the actual load, the force coefficients were multiplied by the planform area of each column and the freestream dynamic pressure. The moment acting at each column was obtained by multiplying the coefficient by planform area, dynamic pressure and the wing Mean Aerodynamic Chord (MAC, also referred to as \bar{c}). The moment is the resultant torque due to the normal force applied at the column center of pressure. The location of moment computation was based upon a user defined reference line specified within the input data file.

TABLE 2

Column	Fraction of Semi-Span	C_L	C_N	C_A	C_M
1.0000	0.0780	1.2723	1.2621	-0.1723	0.1256
2.0000	0.2330	1.3515	1.3398	-0.1877	0.1934
3.0000	0.3820	1.4066	1.3932	-0.2017	0.2641
4.0000	0.5210	1.4430	1.4283	-0.2121	0.3315
5.0000	0.6470	1.4604	1.4451	-0.2171	0.3903
6.0000	0.7580	1.4492	1.4343	-0.2137	0.4344
7.0000	0.8500	1.3906	1.3779	-0.1970	0.4537
8.0000	0.9210	1.2482	1.2396	-0.1619	0.4330
9.0000	0.9690	0.9951	0.9933	-0.1020	0.3569
10.0000	0.9940	0.7335	0.7597	0.0722	0.2451

III. STRENGTH ANALYSIS

A. BOUNDARY CONDITION DEFINITION

From the discussion in Chapter II of the panel code outputs along the semi-span of the wing, it is possible to obtain a reasonable approximation of the load pattern. This discussion will treat the wing as a composite of four bar elements as depicted in Figure 5. Note that these elements are not constrained to be symmetrical about the X or Z axis.

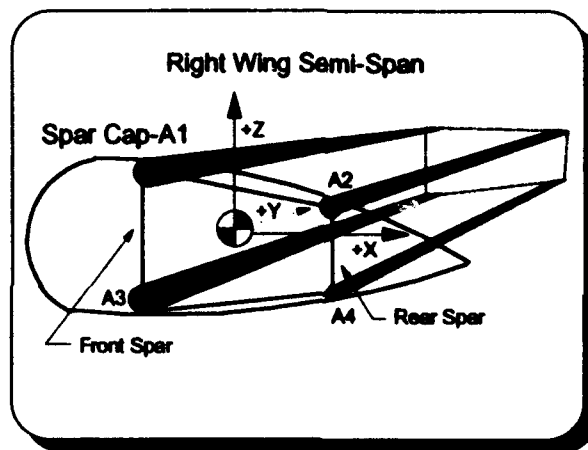


Figure 5

Figure 5 also depicts the orientation of the axis system that was used throughout most of the analysis. This sense of direction is consistent with the output from the panel code where coefficient data was obtained.

Since force and moment computation requires knowledge of the reference area, the planform area for each spanwise column must be determined. The panel code does provide the location in x,y,z coordinates for the corner points of each panel if instructed to do so within the input file. From these locations and simple trigonometric relationships,

the planform area of each column can be determined for use in the calculation of applied forces and moments. Figure 6 serves to describe the orientation of a positive load condition. Since this project was directed towards preliminary, vice detail engineering

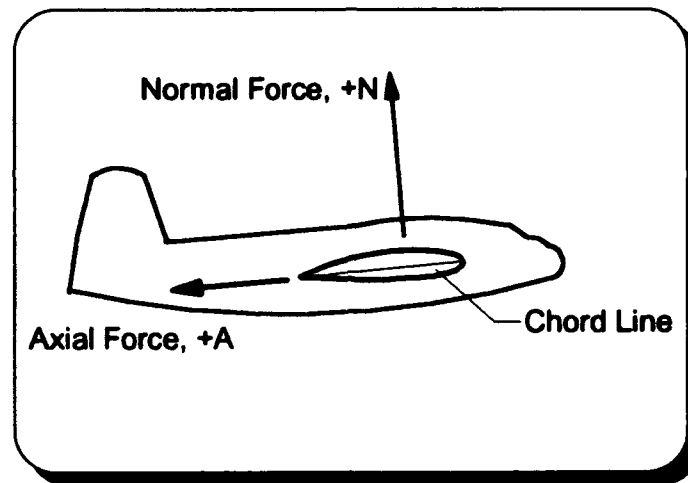


Figure 6

design, the problem was analyzed at the expected maximum load points near the wing root. However, this method can be applied throughout the semi-span to determine initial minimum sizing to meet strength requirements.

At this point in the design, a common question among new design students pertains to the choice of a two spar system. Since this four element structure is being initially designed to carry the bulk of normal stress due to bending, it follows that a two spar wingbox employing stiffened wing skins will generally provide a low cost, easily manufactured, lightweight structure. Another advantage as pointed out by Niu, [Ref. 7:pp. 247-263] was large interior volume for increased fuel capacity. These benefits seem well suited for large commercial and military carriers.

This project began by assuming the simplest possible configuration based upon a two spar arrangement. As loads increase and size constraints decrease in a design project, the feasibility of the two spar structure begins to diminish. The designer needs to look at his results during analysis and determine if they appear reasonable. For example, if the load factor requirement is increased, the spar cap cross-section will also increase. Additionally, the wall thickness of the front and rear spar webs must also be rising to meet the increased shear requirements. As these components grow in size, the designer needs to consider the effect of adding one or more additional spars to begin reducing the structure's internal cross-section dimensions (and ideally total wing weight).

Operating requirements may steer the designer in other directions, as evidenced in current tactical military aircraft structural design. Generally these aircraft demand high strength, while also minimizing vertical wing depth to allow for high speed operation. Most tactical aircraft also require multiple load paths for enhanced survivability if subjected to hostile fire. Consider the ramifications of a fore and aft spar structure that has been severed at the leading face of the wingbox (forward spar) under a maximum loading condition. The unexpected load path may prove too weak to carry the new load distribution, resulting in catastrophic failure. Such a design problem may seem overwhelming at this point to the beginning structural engineer. Hence, this project has been constrained to a problem that readily allows solution via hand calculations within the classroom without reliance on finite element or energy methods.

1. Shear Diagram Construction

Returning to the normal and axial force coefficients, the resultant loads acting at each spanwise station of the wing are depicted in Figure 7. These loads provided the basis for calculation of the shear in the z and x direction across the face of each section. Due to the assumption that the load acted at discrete points, the shear was assumed constant across each column element. The means of estimating shear along the semi-span was to start at the wing tip with zero shear and sum the loads moving inboard to the aircraft centerline. Figure 8 represents the shear loads for the two axes along the semi-span of the wing. For modeling considerations, the wing was assumed to be a continuous structure

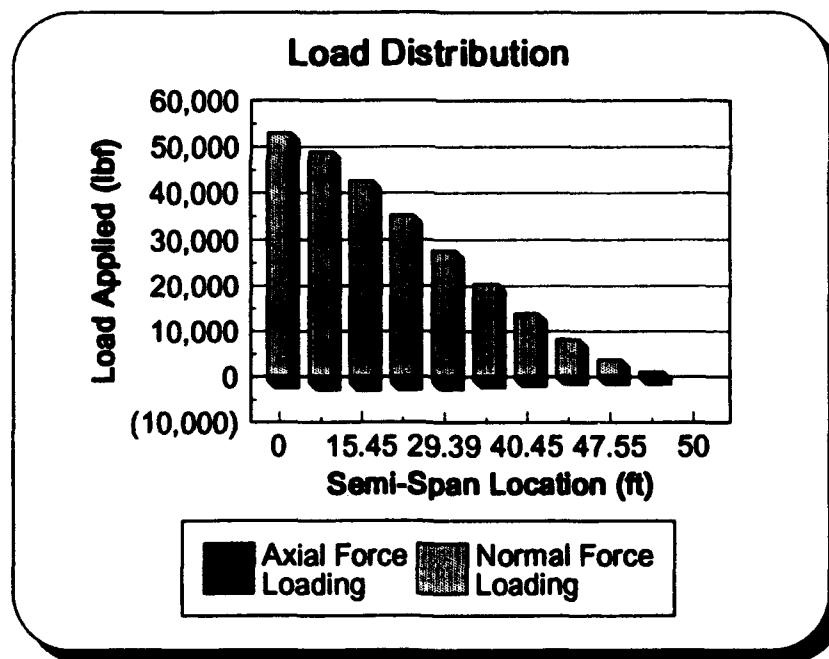


Figure 7

extending through the aircraft centerline; however, strength analysis modeling was based upon a cantilever beam fixed at the aircraft centerline and extending out the right wing.

All shear values were assumed to change at the left face of each column section moving along the y axis.

2. Bending Moment Diagram

The bending moment diagrams for the load condition previously selected are presented in Figure 9. These diagrams prove a bit more challenging to construct due to the number of repetitive calculations involved. Since the design engineer is likely to consider hundreds, or even thousands of load and geometry combinations during the design sequence, construction of these diagrams is a prime candidate for automated calculation.

These diagrams proved quicker to build with the aid of a spreadsheet by starting at the fixed end of the wing, on centerline. Figure 10 serves as an example of the calculations for the moment on the left face of column 8 near the right wingtip. The resultant moment for each face was calculated by summing up the product of all forces to the right of a cut section and their respective distances to the cut. These sums provided the data for the approximate moment at the left face of each column section.

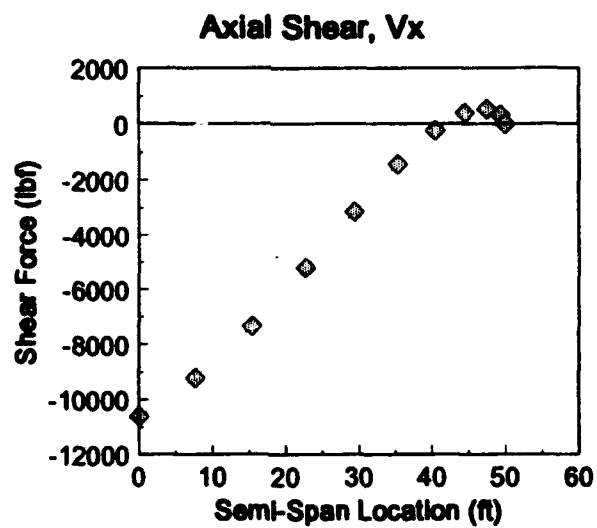
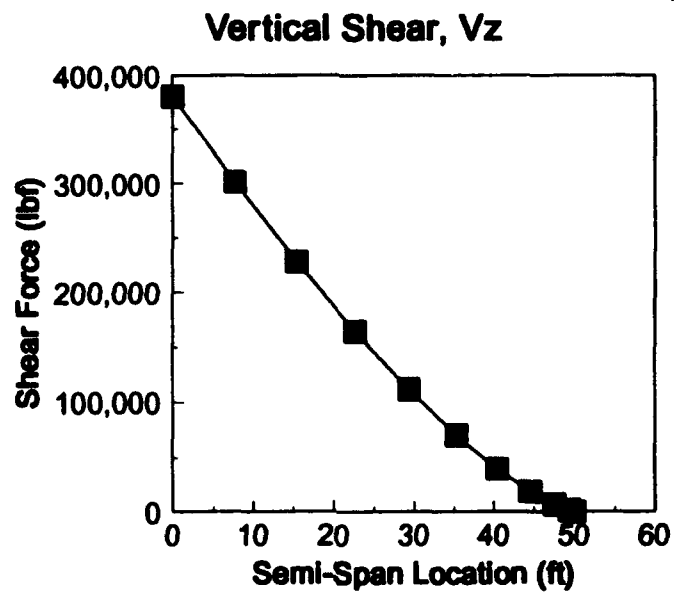


Figure 8

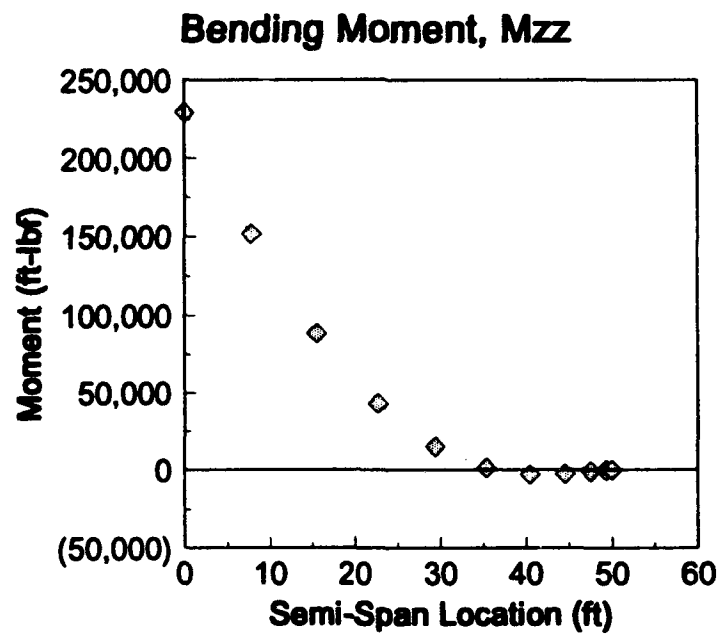
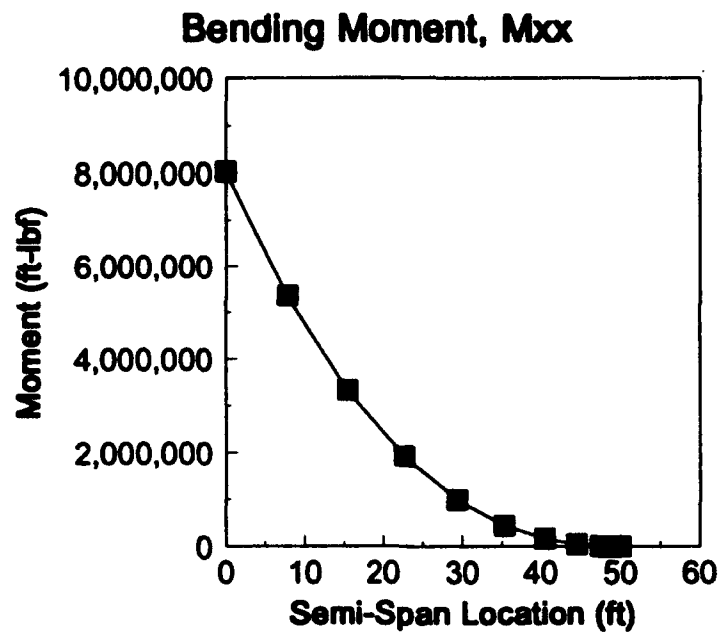


Figure 9

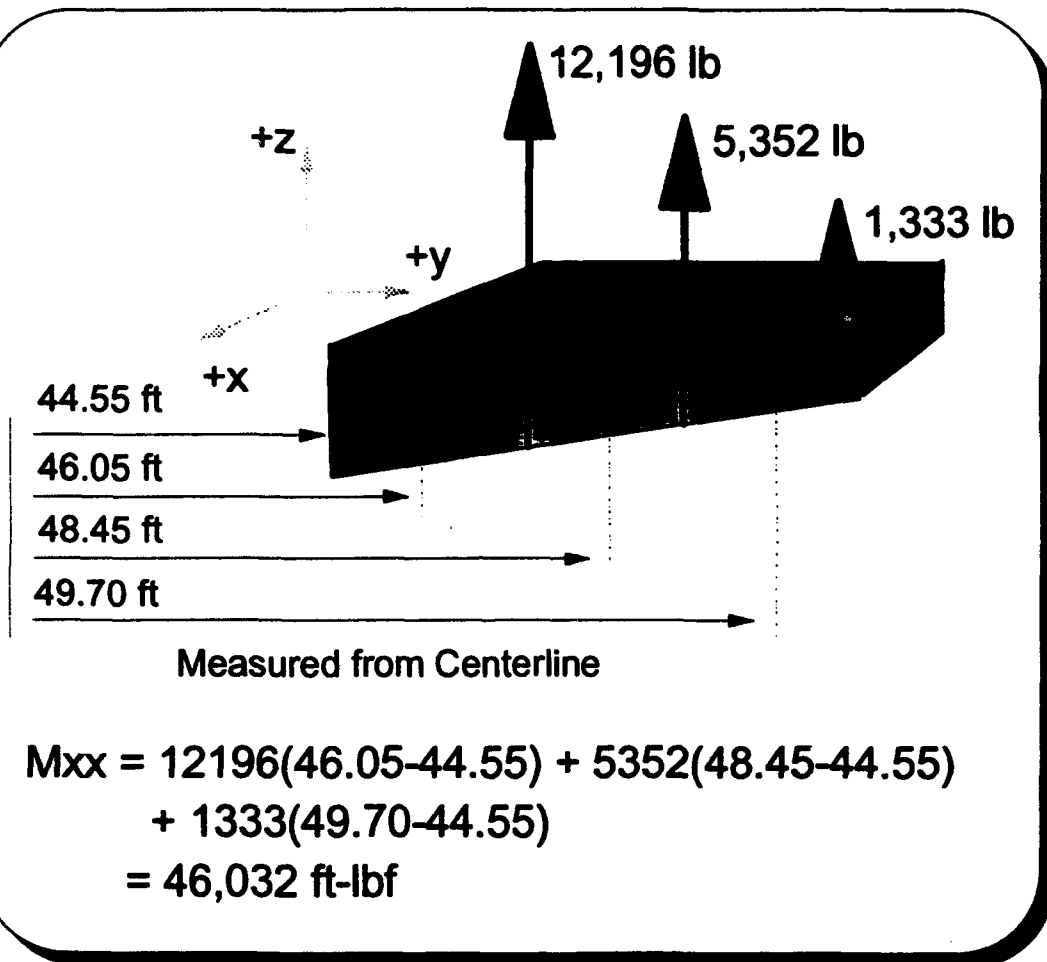


Figure 10

3. Torsional Moment

Production of the torsional moment diagram depicting M_{yy} along the semi-span requires the transfer of several couples prior to the final diagram construction. PMARC provides a value for the pitching moment coefficient for each column of panels based upon the planform area of each column and referenced to the Mean Aerodynamic Chord (MAC) of the overall wing structure. Equation (2) serves to illustrate the relation between c_M , and the actual moment produced, M .

$$M = \frac{1}{2} \rho V^2 A_{ref} \bar{c} c_M \quad (2)$$

It is important to understand that c_M and M can be used to specify moments anywhere on the wing cross-section. However the structural engineer is generally interested in the resultant moments found at the centroid of the cross-section under investigation. Anderson [Ref. 7:pp. 15-30] provides an extensive discussion of the integral approach to resolving the pressure force acting on the surface of the wing into normal and axial components. These forces can then be resolved into a single pair of forces acting at the center of pressure on the structure. If these forces, N and A are applied at the center of pressure (x_{cp}), there is no induced pitching moment along the chord line. Figure 11 depicts the order of transformation required to obtain a usable relationship.

Since the center of pressure is unlikely to be located at the cross-section's centroid, a relationship must be determined that can relate the moment arm distance obtained between x_{cp} and the selected reference. Returning to Anderson's [Ref. 7:p. 30]

discussion of normal forces and resultant moments, the center of pressure is defined via equation (3).

$$x_{CP} = \frac{M_{LE}}{N} \quad (3)$$

Note that this relationship only applies at the Leading Edge (LE), which is the basis for the transformation depicted in Figure 11. Another important aspect to equation (3) is the definition of positive orientation for the moment produced. Conventional aerodynamic notation directs that any force acting on the wing cross-section which causes a nose-up

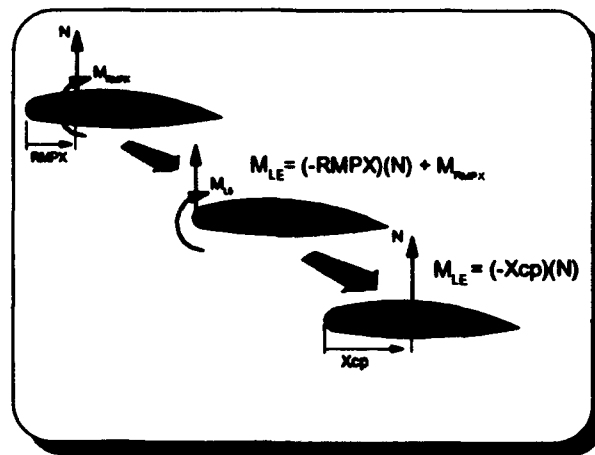


Figure 11

rotation of the wing leading edge is deemed positive, (note that positive lift results in a negative M_{LE}). It is also important to realize that aerodynamic sign convention for moments and forces may not coincide with the convention required of structural analysis. It is the design engineer's responsibility to properly translate the appropriate sign when moving among the two disciplines.

Since any moment can be expressed as the sum of two or more vector components (the components being moments themselves), any moment obtained along the

chord, where its location and corresponding normal force is known, can be used to obtain the center of pressure. Since PMARC allows specification of the line about which it calculates c_M (specified as RMPX), and provides c_N as an output, it is possible to locate the center of pressure. Figure 12 highlights the relationship graphically among all relevant measurements for a swept wing (referenced to the $X=0.0$ datum line). Equation (4) is used to solve for the location of XCP when provided with the necessary input and output data from PMARC.

$$XCP = RMPX - \frac{M_{RMPX}}{N} \quad (4)$$

In equation (4), N is the normal force obtained from the normal force coefficient c_N , (note that the output format of the code labels c_N under the format of c_L in the body axis system

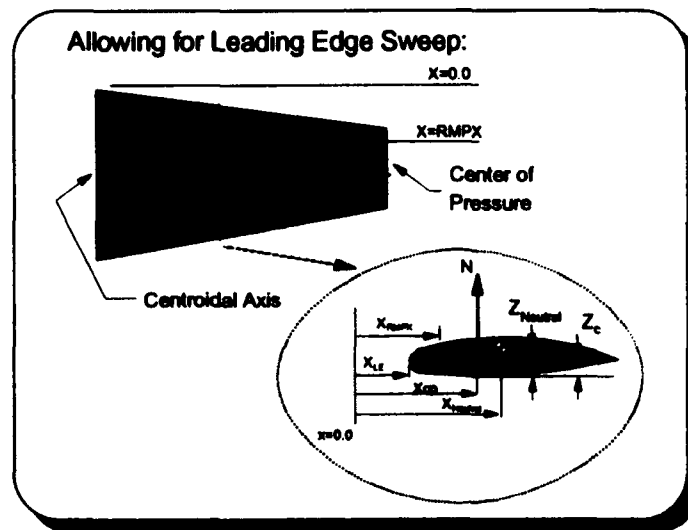


Figure 12

and reserves c_L as an output of the wind axis system). Likewise, M_{RMPX} is the moment obtained from equation (2) using the output of the code labeled c_M (for the pitching

moment output in the code there is no difference between c_m in the wind axis and the body axis system).

The remaining translation required involves the effect of the normal force acting at the center of pressure in relation to the centroid of the cross-section. The resultant moment on the centroid is readily determined as listed in equation (5).

$$m_{YN} = N(X_{neutral} - X_{CP}) \quad (5)$$

Where $X_{neutral}$ is based upon the location of the centroid, also referred to as \bar{x} in later sections. Note that equation (5) specifies m_{YN} vice M_{YY} , this is due to the fact that the chord line in many airfoils does not pass through the centroid. To account for this line of action, equation (6) solves for m_{YA} , which can then be summed with m_{YN} , to yield the desired resultant torque for an individual column cross-section, m_{YY} . Once the resultant moment, m_{YY} , has been obtained at each discrete column section, the resultant torsion experienced at a cross-section can be determined. As previously depicted in the bending moment discussion, beginning at the right wingtip and summing the column torsion values yields the resultant torsion, M_{YY} , experienced along the span.

$$m_{YA} = (Z_{neutral} - Z_C)A \quad (6)$$

Due to the format of the output of PMARC, the torsion solution is obtained for each column center, vice the left face; recall that shear analysis was performed at each column's inboard face. Figure 13 is the final result for total torsion applied to the center of each column along the right semi-span of the wing. Since Figure 13 was derived from a solution of equations (5) and (6), an interesting dilemma arises for the designer. Each of

these equations assumes that the centroid is already known. Therefore, Figure 13 cannot actually be developed prior to completion of the next section involving solution of the

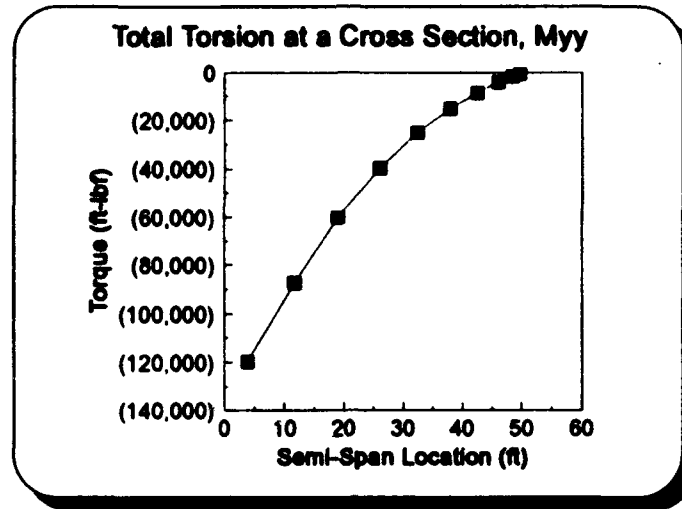


Figure 13

bending stresses due to N and A. However, it is presented at this time to provide the reader with a sense of relative magnitude in relation to the shear and bending diagrams previously developed.

B. BENDING STRESS ANALYSIS

The four spar caps represented by the four areas in Figure 5 will be assumed to initially carry the primary bending loads that give rise to M_{xx} and M_{zz} . Since bending occurs in both directions, and none of the areas were assumed to be symmetrical, the bending stress can be found from Allen and Haisler [Ref. 1:pp. 166-170]. Assuming the centroid is known and the size of each area is known, equation (7) serves to calculate the normal stress, σ_{yy} , carried at each spar cap.

Application of equation (7), in conjunction with an allowable working stress can be used to determine the location of the centroid and size of the four spar caps.

$$\sigma_{yy} = \left[\frac{M_{xx}I_{xx} + M_{yy}I_{yy}}{I_{xx}I_{yy} - (I_{xy})^2} \right] x - \left[\frac{M_{xx}I_{xy} + M_{yy}I_{yy}}{I_{xx}I_{yy} - (I_{xy})^2} \right] z \quad (7)$$

Although optimization routines do exist in industry today that can quickly identify the preferred location and distribution of the four areas [Ref. 8], observing the interaction of the four areas in relation to an allowable stress constraint proves very beneficial in the learning environment.

The operational envelope requirements set for this exercise included a +3.5 to -1.0 g load factor boundary. Analysis of the upper surface of the wing reveals that at the maximum load factor of +3.5 g's, the structure will experience a significant compressive load. Based upon information that will be presented in the buckling analysis section, the maximum allowable stress level for the upper surface is the material yield stress limit, which represents the maximum buckling stress for the stringers. However the lower spar cap allowable stress level for the material chosen was set at the ultimate tensile stress. Buckling instability of the lower surface did not present the same challenge as the upper surface because of the differences in design load requirements.

1. Area Determination

As mentioned above, an iterative solution performed by the student in design proved very rewarding in understanding the demands placed upon various points within the cross-section. Accomplishment of this task was performed with the aid of a spreadsheet. By initializing all four areas to some arbitrary amount, and then beginning a

sequence of variations, the average student could arrive at an acceptable solution within approximately ten minutes for a given flight condition. Appendix B provides a sample of the spreadsheet used in this manner. Figure 14 is a review of key dimensions employed by the spar cap area calculation spreadsheet.

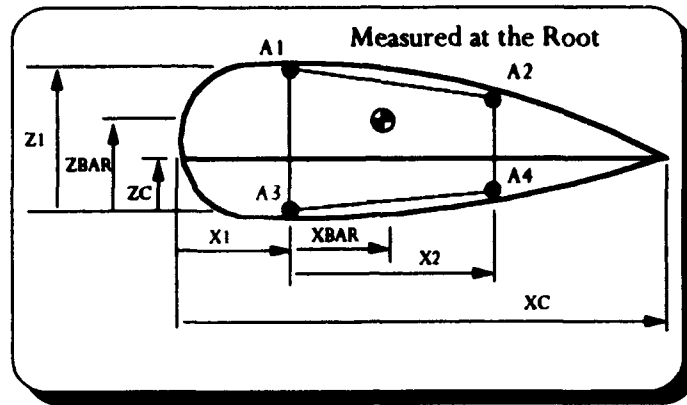


Figure 14

The spreadsheet requires the input of A1 through A4, the values of M_{xx} and M_{zz} , and the geometry constraints of the wing cross-section at the spanwise location under investigation. As the areas are input, \bar{x} , \bar{z} , I_{xx} , I_{zz} and I_{zx} are calculated. Having obtained these values, the routine goes on to evaluate the stress at points 1 through 4, using equation (7). While observing the total area and the stress levels for the four points, the designer brings points 1 and 3 to their respective allowable stress levels, and minimizes the total area by varying areas at points 1 through 4. The most productive method discovered for minimizing the time involved, employed a rapid change of areas in sections 1 and 3 until these sections are close to meeting the appropriate allowable stress levels. At that point the rear sections are varied until their change begins to significantly alter the stress carried in each respective forward member. At this point it becomes important to

start monitoring the total area to determine which changes in individual section areas leads to a reduction in total area. The process is terminated when the solution with the smallest total area is found.

This problem was worked on the basis of a prior material selection and the assumption that construction of stiffeners, skin and spar caps would be done with the same material. The method will also work for different material build-ups as long as a modulus weighted moment of inertia approach is applied. The problem can also be worked from the position of picking an allowable stress first and then determining what materials can sustain the expected stress levels.

2. Determination of Allowable Stress

For those regions of the structure that are subjected to maximum loads that are tensile in nature, it is of prime importance to ascertain what load condition and stress level should be chosen to achieve the desired factor of safety. The following discussion was applied to this project in determining the allowable stress level for maximum tensile loads for any material where yield and ultimate strength test data were available.

Begin with a comparison of two-thirds of the ultimate tensile stress to the yield stress value. The smaller of these two values will determine the eventual allowable stress and limit load analysis conditions, assuming a factor of safety of 1.5. When two-thirds of the ultimate stress is the lower value, analyze all loading problems at the ultimate load ($1.5 \times \text{Limit Load}$). For this case set $\sigma_{\text{allowable}} = \sigma_{\text{ultimate}}$. However, if initially the yield stress value proved to be the smaller value, the problem should still be analyzed at the ultimate

load. Although, in this situation the allowable stress level is reduced such that $\sigma_{allowable} = \frac{3}{2}\sigma_{yield}$. Recall that the limit load is the maximum load used for design purposes that the structure is expected to encounter in its normal operational routine. The ultimate load is derived simply from the concept of ensuring the existence of a margin of safety in design calculations.

Since the upper surface of the wing was subjected to large compression loads and stringer buckling was the design constraint, the material yield stress was chosen as the allowable stress. If, after a buckling analysis was performed, the column length between ribs was determined to be unacceptable (resultant weight increase), one option would be to incrementally reduce the allowable stress below the yield value. This reduction in stress carried will tend to increase the weight of the spar caps, forcing a strength to weight trade study to compare spar cap increase in weight, to weight reduction due to increased rib spacing (which results in fewer ribs).

3. Spar Placement Considerations

During the calculation of the stress levels at each corner point in the cross-section of the root chord wingbox, the location of the front and rear spars was assumed to be known. These parameters are not fixed at the outset of the design process, but rather represent one additional consideration and potential optimization that will require the designer's attention. Reviewing Figure 15 can provide a little insight on the considerations at hand.

Figure 15 depicts the location used for the analysis in this design. However, it is important to understand the range of flexibility involved, and associated implications. In his presentation on layout techniques, Niu [Ref. 9:p. 254] presents his range of forward spar location to be 12-17% of the chord. He also suggests the rear spar requires positioning at 55-60% chord to accommodate installation of a 30% aileron and flap section.

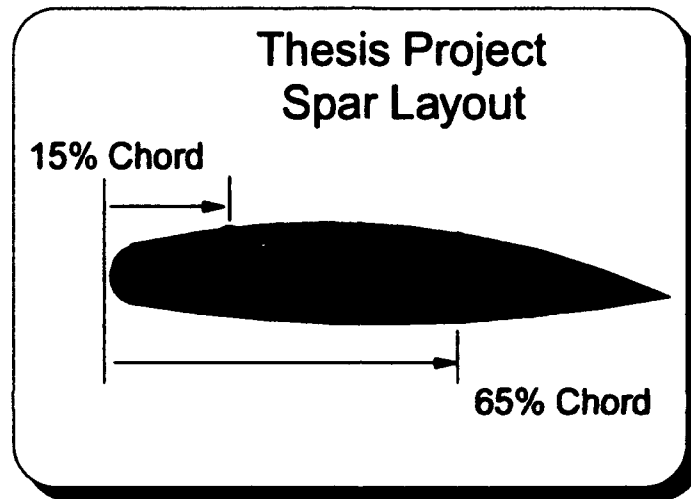


Figure 15

Given this range of values, where does the designer place the spar locations? Often the aft spar is positioned based upon aerodynamic considerations like attachment requirements to accommodate a flap or aileron system that is necessary for control of the vehicle. For this project the rear wall of the wingbox was fixed at 65% chord. Again reviewing Figure 15, as the forward spar moves aft, the overall height of the wingbox is increased while the distance between spars is reduced. Locating the front spar then becomes more of a structural optimization problem that strives to maximize I_{xx} , I_{zz} and I_{xz} .

to give minimum total spar cap area. Also, moving the forward spar aft, generally tends to reduce overall wingbox cross-sectional area. This serves to increase the shear flow around the surface for a given torsional loading. For the beginning designer, the recommendation is to make an initial comparison at the potential fore and aft locations of each spar to evaluate the magnitude of the differences found. For a swept wing design, torsion may prove to be the design driver as one proceeds out the semi-span. Appendix C offers further insight into the options available in a study on various locations for both the front and rear spar.

4. Straight Wing Approach

Once the initial effective area has been determined, allowing computation of the three moments of inertia, it is possible to enter all required elements into equation (7) for determination of the effective stress at a particular location. The only caution offered in the use of equation (7) involves maintaining a consistent use of orientation. For analysis of the wing root, the evaluation method chosen in this attempt involved determination of all forces and moments applied to a positive face at the desired analysis location.

Figure 16 serves to illustrate the orientation chosen. The cut depicted is intended to occur at an infinitesimal distance from the centerline of the wing.

Since all axes pass through the centroid for this portion of the analysis, it is important to monitor the sign convention for both the distance measured from the neutral axis and the allowable stress levels used during area determination. The sign orientation for positive x and z was based upon Figure 16. The sign convention employed for the

allowable stress assumed all compressive stresses to be negative and tensile stresses as positive. Appendix B also lists the results of the effective stress determination for several operating conditions.

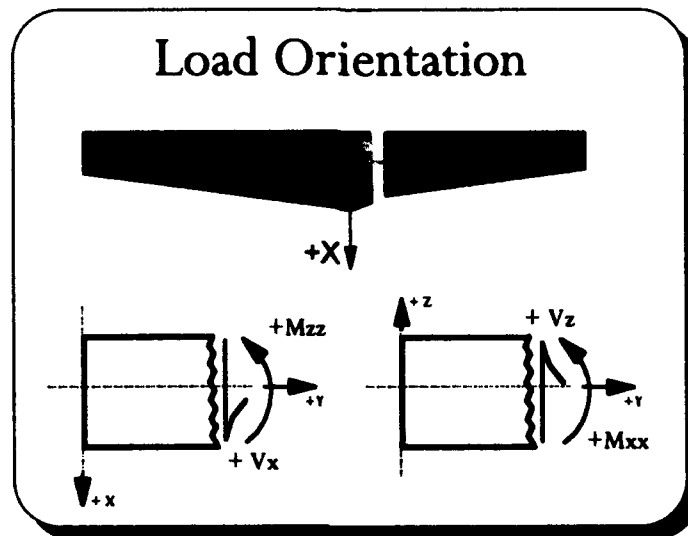


Figure 16

5. Swept Wing Considerations

One of the key advantages in using PMARC for initial load determination was that it allowed analysis of virtually any geometry in wing design. So the initial procedures for obtaining the loads applied to the exterior of any structure operating subsonically, will always remain the same. However, as Figure 17 illustrates, application of those loads will dramatically depend upon wing geometry chosen. In fact, it is a function of both external geometry (wingsweep and dihedral) as well as internal geometry (rib and spar orientation).

Figure 17 is taken from a broader discussion presented by Niu, where he depicts the internal structural layout of a wide range of current commercial transport aircraft that

incorporate swept wing designs [Ref. 9:pp. 278-281]. Since the panel code output is consistent with alignment shown in Figure 17-(a), one might think that particular layout would prove quicker to analyze. However, structural analysis involves working with an axis of bending and cross-sections perpendicular to it. The axis of bending will coincide with the line of centroids along the span, which can be taken as a first approximation as

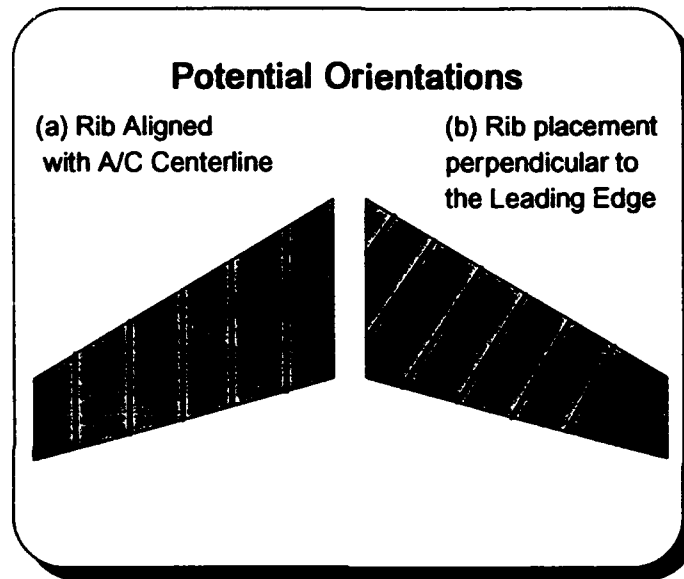


Figure 17

40% of the distance between spars. The axial forces from PMARC must be resolved into a component transverse to the bending axis and along it as shown in Figure 18. The transverse direction will be along the rib, and the spanwise component will be along the stringer. The latter will add a tensile component to the bending stresses.

To accomplish this task the following methodology is proposed:

- Resolve the loads obtained from PMARC into normal and axial components oriented with the rib direction.
- Modify equation (7) to account for the axial load component.
- Update the spanwise position of areas one through four in stress calculations.

Figure 18 hopefully serves to illustrate transforming the applied load into meaningful component requirements. This information provides the basis for modification of the analysis routines presented in Appendix B. At this level of complexity in the analysis, the amount of effort and time consumed rapidly begins to multiply. This should provide the

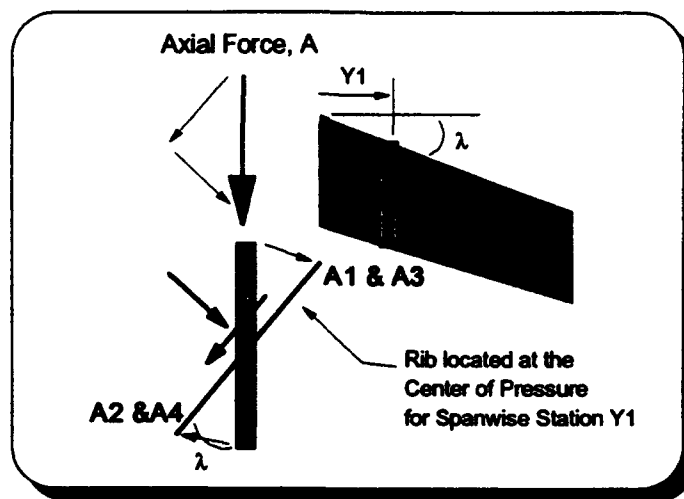


Figure 18

reader with an understanding of the requirement for more sophisticated techniques for analysis as the structure begins to depart from conventional beam appearance.

C. SHEAR STRESS ANALYSIS

To allow for quick computation of the expected shear on the spar webs and wing covers, a lumped mass approach, assuming constant shear flow between centers, was employed. Figure 19 illustrates the combination of shear flow due to torsion, and shear flow resulting from transverse loadings.

1. Shear Flow due to Torsion

Since the torque across the cross-section was solved in an earlier section as the resultant moment M_{yy} , the remaining solution requires minimal effort. Equation (8) forms

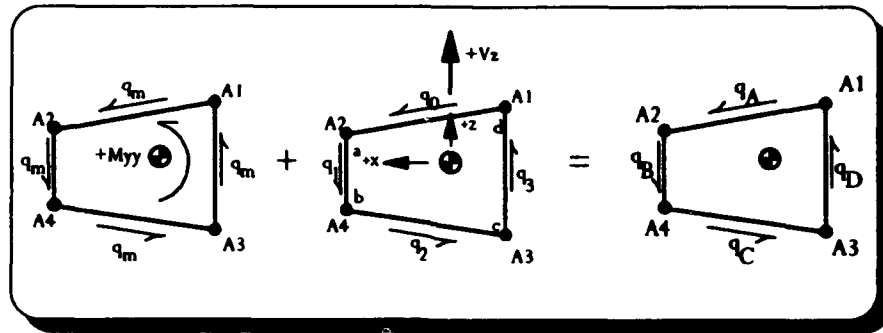


Figure 19

the basis of a constant value of shear flow that is imposed on all faces between the lumped mass centers. Note that equation (8) requires A to be the cross-section area located within the region bordered by centers A1 through A4.

$$q_m = \frac{M_{yy}}{2A} \quad (8)$$

Again, consistent sign convention is essential to a correct solution. Unlike bending, multiple sign errors throughout this analysis can result in potentially unrecognizable final solution errors, that in turn can generate a structurally deficient design. The next chapter

will reveal the importance of accurate shear flow estimation, since q_A serves as the basis for the buckling analysis.

2. Shear Flow due to Applied Loads

The middle segment of Figure 19 also has a straight forward, although longer method of solution. For both single-cell, as the current illustration depicts, and multicell analysis, a set of linear simultaneous equations must be solved. To obtain the appropriate number of equations in a multicell problem, the additional constraint of all cells adhering to the same angular rotation or deformation must also be applied. The starting point in determining q_0 is the relation between q_i and q_{i+1} as defined in equation (9).

$$q_{i+1} = q_i + \left[\frac{-V_z I_{zz} + V_x I_{zx}}{I_z I_{xx} - (I_{zx})^2} \right] Q_x - \left[\frac{V_x I_{xx} - V_z I_{zx}}{I_z I_{xx} - (I_{zx})^2} \right] Q_z \quad (9)$$

Allen and Haisler provide a discussion on the derivation of equation (9) and related multicell problems [Ref. 1:pp. 205-228]. Applying equation (9) to the middle drawing in Figure 19, q_1 , q_2 and q_3 can be related to the shear flow q_0 . All that remains for the single-cell problem is the formulation of one last equation allowing solution of q_0 . At this point one has the option of analyzing a single face at a given cross-section, or a differential element containing a combination of opposing faces. Figure 20 has been provided as a simplified schematic of the options available. The solution involves either equating the moments produced by the shear flows in the webs and skins to the equivalent moments produced by the resultant shear forces at that cross-section; or summing the moments to zero for equilibrium of the shear flows and shear forces acting on the differential element. The results presented in Appendix B are based upon analyzing the

shear flow due to concentrated shear forces on the same (positive) face. In this situation the moments are required to be equal.

The moments were considered about A3 since it provides no torque effect from shear flows q_2 and q_3 . Having solved for q_0 , equation (9) can again be applied, solving in sequence shear flows q_1 through q_3 . These results are algebraically summed to obtain the final shear flow in each spar web and wing cover (again, note the importance of consistent

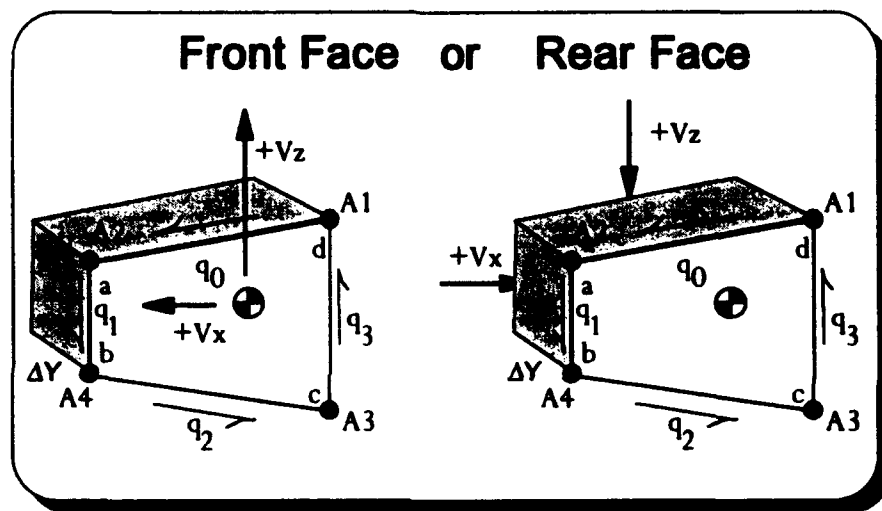


Figure 20

orientation). Figure 21 is the final solution with proper orientation for the operating condition picked thus far.

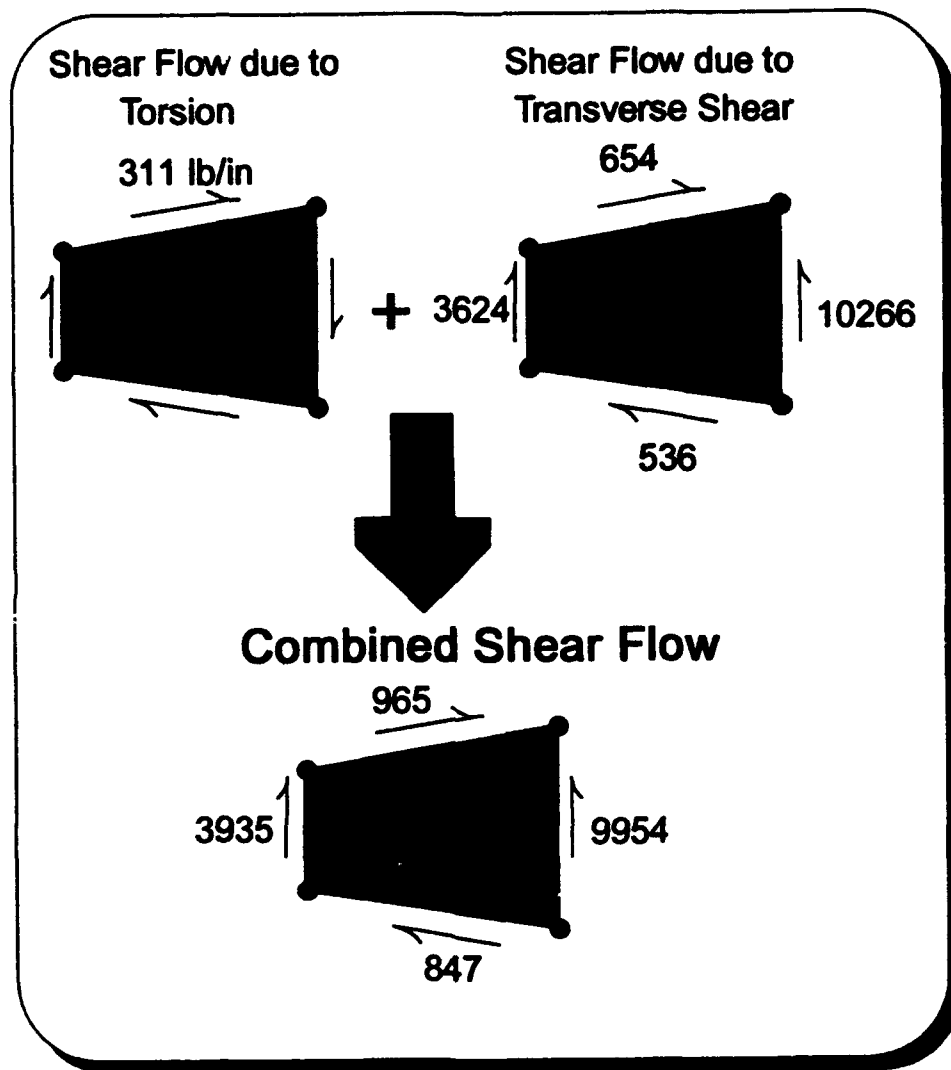


Figure 21

D. VARIATION IN OPERATIONAL CONDITIONS

The previous figures illustrated the shear flow developed due to the operating conditions that exist at point I in Figure 22. Before attempting to size the skin thickness, several other operating conditions warrant investigation to determine which condition develops the largest shear flow within the entire flight envelope. The four points illustrated in Figure 22 encompass flight at high and low angles of attack, in addition to maximum positive and negative load factors. In developing the curves associated with the maximum lift, a simple rule of thumb was employed to relate $c_{l_{max}}$ of the 2-d airfoil section, to $c_{l_{max}}$ of the 3-d wing structure. Obtaining both the positive and negative values of $c_{l_{max}}$

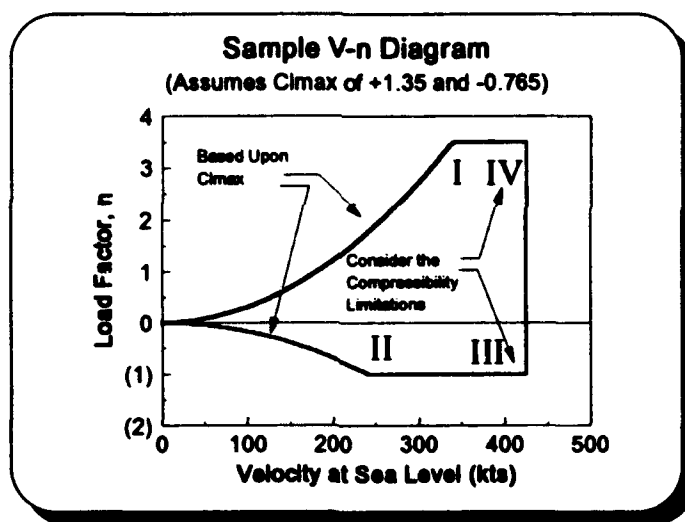


Figure 22

for a NACA 4418 airfoil from Abbot and Doenhoff [Ref. 10:p. 492], 90% of those values were then substituted as $c_{l_{max}}$ into equation (1) to determine the corresponding load factors. The data compendium (DATCOM) offers more extensive methods for estimating

the maximum lift of a wing operating in the subsonic through hypersonic flight regimes [Ref. 11: Sect 4.1.3.4].

Appendix B provides all stress levels and shear flows for conditions I through IV. For this particular design problem, condition I was the primary design constraint since all other operating points at sea level conditions developed stress levels below those of condition I. If, in a different design problem, one or more flight conditions develop stress levels that exceed the allowable limits after having sized the spar caps for a given condition, a logical sizing sequence must be employed to ensure the structure is properly sized to support flight at all locations. The following analysis routine is provided to aid in that form of design problem:

- Begin at condition I, note that if PMARC is used condition I is offset a small amount from the maximum lift line to avoid estimation errors in the nonlinear regime of the lift versus alpha curve.
- Having sized the structure, move to condition II. Maintain all spar cap sizes from condition I as the minimum values for condition II. If the allowable stress is exceeded at any point in condition II, increase spar cap areas as required. Set these new areas as the minimum spar cap sizes.
- Move to condition III; use the same procedure as that at condition II. Establish the new minimum areas and move to condition IV. Having completed condition IV, the structure is now assured to carry the applied loads throughout the expected flight envelope.

E. SKIN SIZING

Based upon a review of conditions I through IV, condition IV was found to develop the largest shear flow in the upper skin, where q_A was 1238 lb/in between spar caps. This value of shear flow was used to determine the minimum skin thickness required to carry

the applied load along the upper wing skin. If this value is substituted into equation (10) and $\tau_{allowable}$ is known, it is possible to solve for the minimum required skin thickness on the basis of strength alone.

$$\tau_{allowable} = \frac{q}{t} \quad (10)$$

Determining the value of $\tau_{allowable}$ is accomplished in the same manner as that employed to obtain the allowable normal stress which was calculated earlier. To review this method, first consider the values of τ_{yield} and $\frac{2}{3}\tau_{ultimate}$. If the $\frac{2}{3}\tau_{ultimate}$ proves to be the lower value, then set the allowable stress to the ultimate shear stress of the material. However, if the yield shear stress proved to be the lower number, then the allowable stress should be set to $\frac{3}{2}\tau_{yield}$. In both of these cases, the load used for analysis should always be the ultimate load using this criteria. For the calculations presented in Appendix B, material properties for 2024-T4 extruded aluminum were taken from Popov [Ref. 12:p. 554], however, a better approach is to develop specific material properties from the MILHANDBOOK-5F series. Using the information within Popov, the allowable shear stress was taken to be 32,000 psi, which requires a minimum skin thickness of 0.0387 in.

Having solved for the skin thickness t , it is also a responsibility of the designer to investigate any other constraints placed upon the vehicle by outside agencies or the final customer. Consider some of the following requirements as set forth by the Navy. Table 3 lists the minimum skin thickness requirements for a variety of materials that may be considered during the design process [Ref. 13:p. 17]. From Table 3, the minimum gauge requirement for aluminum construction is 0.026 in, since this is less than that required due

to the loads carried, the minimum thickness remains at 0.0387 in. Had the material considered been high strength, the minimum thickness may have been required to increase to comply with minimum gauge requirements, this can prove to be a major factor in considering a strength to weight study.

TABLE 3

Material	Minimum Gauge (in)
Corrosion-resistant Steel	0.008
Aluminum Alloys (Exterior)	0.026
Titanium Alloys	0.016
Superalloys	0.015
Graphite / Epoxy Skins	0.020
Boron / Epoxy Skins	0.020

One last consideration in the manufacturing effort concerns the availability of commercial stock material. For instance, if a roll of aluminum sheet is manufactured in a standard gauge thickness of 0.028 inches, yet the minimum thickness required calls for only 0.026 inches, what is required of the designer? To answer that question the design team would probably meet with the material supplier to determine the cost effectiveness of initiating a special production run, to provide a limited amount of material in the lighter gauge. The alternative to a special production run is acceptance of the associated excess material (and weight) to achieve a lower manufacturing cost. Table 4 is an excerpt from Appendix D which lists some of the dimensions used in production of commercial stock.

Note that several standards of measurement still exist today, and different manufacturers adopt one or more of these standards for use in their production runs.

In the analysis performed as part of this thesis, it was assumed to be cheaper to acquire commercially available aluminum sheet. After a review of the load requirements and the Navy's minimum thickness requirements for aluminum sheet, a minimum thickness of 0.0387 in is used to enter Table 4. With the information available, it appears that the smallest available gauge for use in the upper wing skin is on the order of 0.040 in, which corresponds to a number 18 gauge sheet in the American Standard. Using this value as the skin thickness t , and inserting it into equation (10) with the original shear flow, reveals an effective working shear stress of 30,948 psi in the upper wing cover.

TABLE 4

Gauge No.	American Std	Washburn Std	Birmingham Std	U.S. Standard
18	0.040	0.047	0.049	0.050
19	0.035	0.041	0.042	0.043
20	0.032	0.034	0.035	0.037
21	0.028	0.031	0.032	0.034

IV. BUCKLING CONSIDERATIONS

Having developed the initial estimate for spar cap sizes and approximated overall shear flow in the upper wing cover, it is now possible to begin to estimate the stability requirements of the upper surface. This process takes on two distinct aspects. The first phase involves determining the number and spacing of stiffeners to be employed. Once that has been accomplished, the designer must then choose the shape and size of the individual stringer elements. It is in this portion of the design that many interactions occur during calculations that open the door to a wide range of trade-offs that the designer must review. This diversity of possibilities in the design is perhaps one of the most challenging, yet rewarding aspects of the process for the apprentice designer.

A. STIFFENER SPACING

Recall that during the bending analysis, the allowable normal stress level for the upper surface was set at the material yield stress. One should also observe that the upper cover deals with two distinct forms of primary buckling analysis, column buckling of the stiffener and plate buckling for the skin itself. The plate buckling problem becomes the starting point, where the operating stress in the skin is kept below the buckling stress of the skin when treated as a flat plate. The methodology presented here is based upon an attempt to

preclude buckling throughout the wing structure in all flight conditions operated at or below ultimate load conditions.

The working shear stress now becomes the defining buckling shear stress for the wing skin. The dimensions of the plate shown in Figure 23 will be selected to prevent shear buckling. The equation for shear buckling of flat plates is given in equation (11) [Ref. 2:p. 172]. The desired output of equation (11) is the ratio of plate thickness to width.

$$\tau_{cr} = K_s \left[\frac{\pi^2 E}{12(1 - \nu^2)} \right] \left(\frac{t}{b} \right)^2 \quad (11)$$

Since the critical buckling stress is known, plus the skin thickness, t , it is possible to solve for plate width, b . The plate width is the distance between stringer attachment lines.

Referring to Figure 23, if the stringers are attached with a single row of closely spaced rivets, then b would represent the distance between these rivet lines, which are depicted by dashed lines along the span.

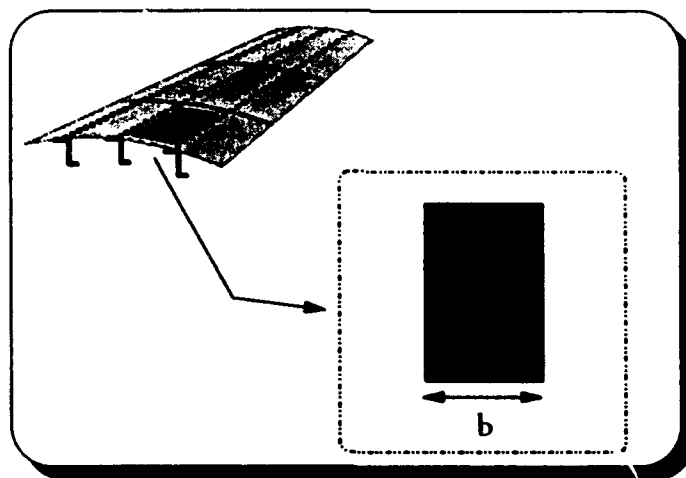


Figure 23

Before one solves for b explicitly in equation (11), several key constants have to be obtained. The first is the modulus of Elasticity, E . The results presented in Appendices B and C were based upon 2024 aluminum possessing a uniform modulus of elasticity of 10.6×10^6 lb/sq-in for aluminum plate. The constant ν is Poisson's ratio, and was taken to be 0.33. The final constant, K_s , is known as the shear buckling constant for use with the Euler buckling equation. The value of K_s reflects the type of support the plate has at its boundaries. It ranges from 5.35 for simply supported edges to 8.98 for four rigidly held edges in plates that are rectangular in shape [Ref. 2:p. 172]. Since ideal boundary conditions are seldom the rule in actual structures, review of several design handbooks can provide a range of values obtained from experience to use for K_s . Niu provides several illustrations of design charts for K_s that depend upon how each side of the plate is supported, the ratio of the plate length to width and the curvature of the surface of the plate [Ref. 9:pp. 138-140].

For simplicity of calculations, the value chosen in this analysis was based upon the discussion of Sechler and Dunn in their development of shear buckling for a flat plate. They provide a figure that theoretically estimates this constant for two different end supports. One curve is based upon simply supported sides, while the second employs clamped edge support. Since the actual aircraft skin panel support structure falls somewhere between these two locations, an average was taken for K_s , assuming the length of the plate (which will eventually determine the rib spacing) would be at least 5 times longer than the width of the plate. For these parameters the value of K_s was found to be 7.17. [Ref. 2:pp. 164-173]

Determination of the total number of stringers required along the upper cover necessitates the knowledge of the plate width between stringer attachment lines. Since the locations of the leading edge spar and trailing edge spar have already been fixed, the distance between them is also known. If the stringers are placed at equal distances between these two spars, equation (12) can be used to solve for total number of required stringers for the upper wing cover between the two spars. Note that the number of

$$n = \frac{\text{Total Width}}{b} - 1 \quad (12)$$

individual plate elements exceeds the number of stiffeners by one if the fore and aft edges are assumed to be bounded by the spar caps themselves. Solving for flight condition IV, $b=1.42$ in and $n=62$ total stringers at the wing root.

B. STIFFENER SIZING

This portion of the buckling analysis offers many possible variations to arrive at an acceptable solution. Rather than provide the student with an optimal solution, it was again determined to be more beneficial for the student to explore the effects of variations in a wide range of parameters. The first obvious question to arise in sizing of a stiffener stems from the geometry of the stringer itself. Niu is quick to point out the importance of the design engineer understanding more than optimum strength or minimum strength. In his description of the Y stringer, he indicates that it is a very strong support that can be easily attached during manufacture. However this same device is expensive and provides an inaccessible region on the inside skin surface that may become susceptible to corrosion

damage during the life of the aircraft. This region also precludes a visual inspection without complete removal of the stringer. Another concern of the designer is the interface of manufacturing processes involved in physically attaching a stringer. Questions to be asked include, "Does this design hinder the shop's ability to rivet or attach jig and alignment hardware?" Awareness of these factors at the earliest point in the process can produce enormous savings over the life of a program. [Ref. 9:pp. 141-142]

Keeping these ideas in mind, the Z section was chosen to demonstrate one method of stringer sizing. The Z geometry does not place enormous computational requirements on the designer, is readily attached and allows for visual inspection.

1. Initial Size Estimate

In an attempt to incorporate previous design experience and reduce the time for solution, two important ratios were taken from Niu as minimum weight *rules of thumb* and applied to the stringer cross-section build-up. The first, listed in equation (13), ratios the total cross-sectional area of the stringer to the cross-section of the plate located between two stringers.

$$A_s = 1.5(bt) \quad (13)$$

The second relation in equation (14) is taken specifically for use with the Z cross-section geometry and relates the skin thickness, t , to the thickness of the vertical web of the stringer, t_s .

$$t_s = 1.05 t \quad (14)$$

Returning to one last manufacturing consideration, actual construction of the stringer. One more cost study that may prove beneficial early in the process, is the choice

of stringer build-up. Possible options include commercial stock, limited production extrusions or bending operations to produce the desired section. If it is determined to be cost effective to bend a flat sheet into the appropriate Z section, one should observe that the value taken for t , now becomes constant for all three segments of the Z. Turning to Figure 24, it depicts one possible labeling of the required dimensions used in this analysis to arrive at the final geometry.

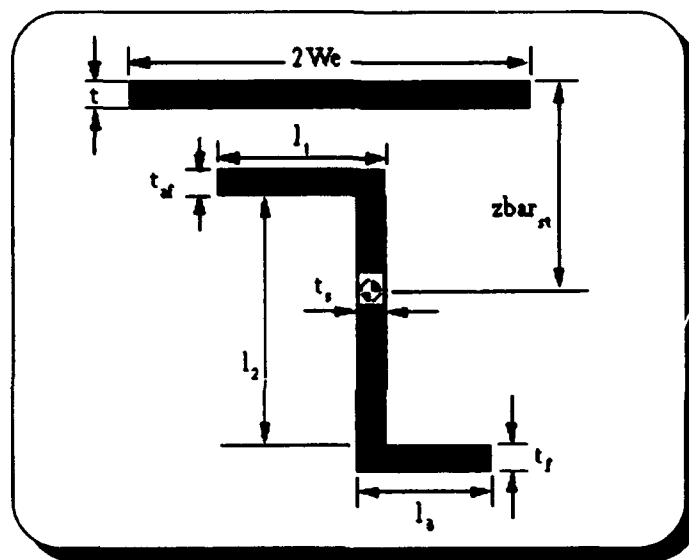


Figure 24

Also observe the segment defined by $2We$ in Figure 24. The value of $2We$ is taken from the concept of an effective width of skin acting in support of the attached stringer to prevent its compression buckling. It should not be confused with the width of the plate between stringers, which is greater than the effective width. In Figure 25, the general pattern of stress variation can be seen as one moves in a chordwise manner along the wing cover. As expected, the stress level rises in the vicinity of the stringers, which

must resist compression buckling. The stress carried then falls off to its low point midway between stringers where only the skin acts to carry the resultant load.

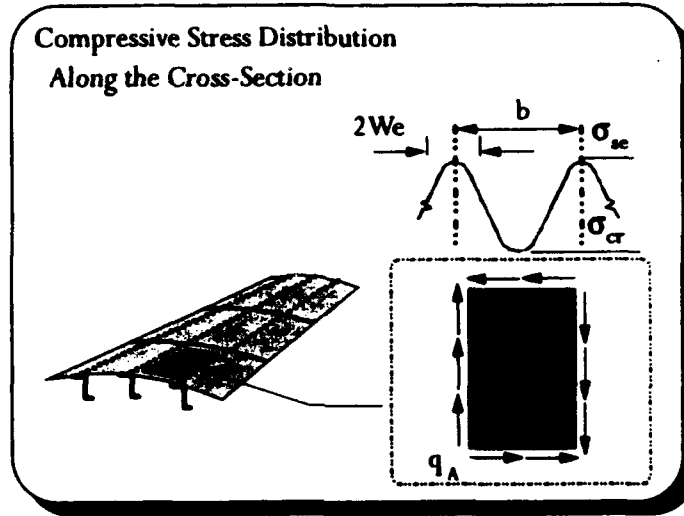


Figure 25

The effective width relates the stress carried at the supported edge, labeled σ_{se} , to the normal buckling stress of the plate section, referred to as the critical stress, σ_{cr} . Since the upper wing cover structure was initially sized to ensure the maximum normal stress level remained below the material yield stress, the value of σ_{se} is taken to be σ_{yield} . In the case of 2024 aluminum, the yield stress was assumed to be 44,000 psi. Using another form of the Euler buckling equation, the critical buckling stress for a flat plate can be used to determine σ_{cr} , as described in equation (15). Again, the values of K_c

$$\sigma_{cr} = K_c \frac{\pi^2 E}{12(1 - \nu^2)} \left(\frac{t}{b} \right)^2 \quad (15)$$

will vary depending upon the type of edge supports the flat plate encounters. The values of K_c range from 4.0 for the simply supported case, to 7.5 for all sides rigidly clamped. Again, taking an average of these values, $K_c=5.75$ was used for the solution of equation (15) in determining the critical stress of the plate sections between stringer attachments.

Substituting this value into equation (15) results in a buckling stress of 24,181 psi for flight condition IV in the upper skin plates along the wing root. It should be noted that the largest value the critical stress can become is the material's normal yield stress.

[Ref. 2:pp. 164-169]

Returning to the relation of the critical stress of a plate section and the stress carried at its edge supports, equation (16) defines this relationship in terms of the effective width of the skin attached to one stringer. Sechler and Dunn provide an extensive discussion on the development of equation (16) and determination of the period of oscillation associated with the loading pattern depicted in Figure 25 [Ref. 2:pp. 203-234].

$$We = \frac{b}{4} \left(1 + \frac{\sigma_{cr}}{\sigma_{se}} \right) \quad (16)$$

Using these inputs, the effective width is readily obtained as 0.74 in or 1.48 in for 2We as depicted in Figure 24. This information is now used in another Euler buckling problem that can determine the ratio of column required length to radius of gyration for the section shown.

2. Uniform Thickness Approach

If the stringer thickness is assumed to be uniform throughout (as in the case of a section produced by bending up a flat sheet), a starting point in estimating the required size is quickly obtained. Since the overall area of the stringer was determined via equation (13) and the thickness in equation (14), it becomes possible to relate the total length of the Z stringer sub-sections in the form of equation (17).

$$A_s = (l_1 + l_2 + l_3) t_s \quad (17)$$

Turning to prior design experience, the relative dimensions of the legs that produce a structure for optimum strength are specified in equations (18) and (19).

$$l_3 = 0.3 (l_2) \quad (18)$$

$$l_3 = 0.7 (l_1) \quad (19)$$

Once the length of each segment is known, it becomes possible to locate the center of gravity for the entire stringer cross-section that is depicted in Figure 26. This

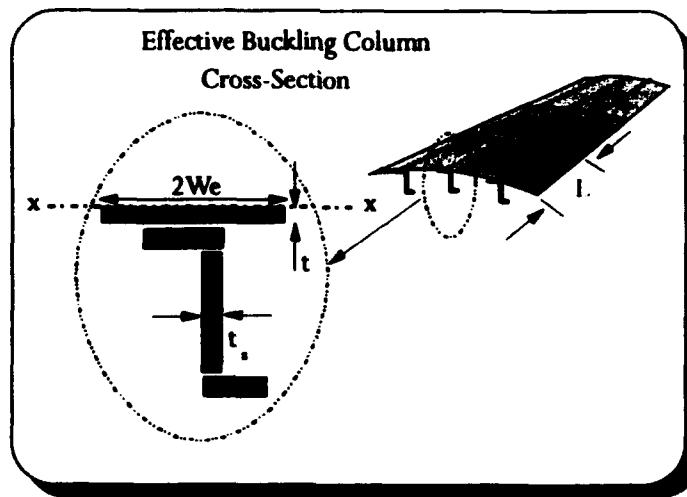


Figure 26

composite stringer includes the skin section of $2We$ and all three stringer segments.

Following determination of the centroid, the next requirement is to calculate the moment

of inertia, I_{xx} for the composite cross-section. It is the combination of effective skin width and the attached stringer that will act in unison as an individual column subjected to compressive buckling along the span (between the wing ribs). Recalling that the moment of inertia is related to the area of the cross-section, as illustrated in equation (20), it becomes possible to solve for the radius of gyration, r .

$$r^2 = \frac{I_{xx}}{A_{total}} \quad (20)$$

All that remains for this first approximation is determination of the required column length or rib spacing. For buckling beyond the proportional limit, The tangent modulus is inserted into the Euler column curve, and it is possible to develop equation (21), which can be used to solve for the column length, L .

$$\frac{\sigma_{cr}}{E} + m \left(\frac{\sigma_{cr}}{K} \right)^m = \frac{\pi^2}{\left(\frac{L}{\sqrt{C} r} \right)^2} \quad (21)$$

The constant m in equation (21) represents the inverse of the strain hardening exponent for the given material. In this analysis of 2024-T4 aluminum, m was 5. Similarly, K also represents a material property, it is known as the strength coefficient. It should be noted that K is generally provided in units of ksi; this requires consistent matching of units among the values substituted into equation (21). Throughout this analysis a value of $K=117$ ksi was used.

3. Stringer Cross-Section Stability

Although the results obtained above were based upon approximate size relationships obtained from previous design experience, it is still important to verify the

integrity of the stringer itself subjected to ultimate loading. The easiest means of analysis is accomplished by treating each individual segment of the Z stringer as a plate element subjected to compressive loading. Again returning to the Euler buckling relation, this time in the form of compressive plate loading, results in equation (22).

$$\sigma_{cr_i} = \frac{K_{c_i} \pi^2 E}{12(1 - \nu^2)} \left(\frac{t_i}{b_i} \right)^2 \quad (22)$$

The value of K_{c_i} varies depending upon the location of the individual stringer element.

Referring to Figure 24, note that the upper flange and lower flange pieces (described as parts 1 and 3), are assumed to act as a simply supported plate on three sides, with the fourth side free. Using the plate normal stress buckling results provided by Sechler and Dunn [Ref. 2:p. 168], reveals $K_1=K_3=0.50$. Similarly, the web section (part 2), is considered to be a simply supported on all four sides; thus $K_2=4.00$.

Now substituting these values into equation (22) allows calculation of the expected buckling stress for each individual plate element composing the stringer. For each element, the result is then compared to the yield stress. The lower of σ_{yield} and σ_{cr} is then referred to as $\sigma_{allowable}$, which is used to find the crushing stress, σ_{cc} , for the entire stringer. To determine this crushing strength begin by finding the allowable effective load in each element given by equation (23).

$$P_{i_{allowable}} = \sigma_{i_{allowable}} A_i \quad (23)$$

Once the allowable load in each element is determined, the crushing stress is determined via equation (24).

$$\sigma_{cc} = \frac{(P_1 + P_2 + P_3)}{(A_1 + A_2 + A_3)} \quad (24)$$

The importance of this check is to ensure that the crushing strength of the stringer is in

fact greater than the material yield stress. If the value comes up short, then the designer is forced to change the values of A_1 through A_3 until that goal is met. Recall that if the manufacturing intent is to construct the stringer from bending a single sheet of material, this places a restriction on area changes due to length changes only. However, if custom extrusions are being considered, then both length and thickness of the individual components are available for customizing to meet design strength requirements. Considering just these few variables that are open to design selection at only one operating condition, begins to portray the expansive nature of optimization involved with an aircraft's structural design life as thousands of variables surface for use in trade studies.

V. STRENGTH TO WEIGHT

This chapter offers the beginning designer some ideas and options of trade studies that can be used to optimize the previous design. These ideas are but a few of the many available. The distinction between this academic project, and actual manufacture of an aircraft, arises from the need to develop and understand principles on a small scale prior to their application in the field. The topics will be presented in the order of bending stress considerations, followed by instability constraints. However, the order of these studies also occur in a chronological sequence that supports the current sequence of teaching within the department.

A. BENDING STRENGTH TRADE STUDY

1. Material Selection

Since each material has a unique set of ultimate and tensile load properties, the value of $\sigma_{allowable}$ varies by a large amount over different types of conventional metals. Referring to equation (7) and inserting different values for the allowable stress will generate significant variations in the resultant areas that exist in the four spar caps. For each case considered, every material has a unique density associated with that material. For ease of comparison, consider a wing section at any given location along the span and assume it to be of unit length in the y direction. For instance, in this problem consider a chordwise segment that includes the wing from $y=0.00$ out to $y=1.00$.

Next assume the cross-section areas of the four spar caps, ($A_1 - A_4$), remain uniform throughout the entire section ($y=0.00 : y=1.00$). Consider the case of 2024 aluminum alloy, assumed to weigh 0.100 lb / cu-in. For the problem solved in Chapter III, the total weight of the spar caps for a unit depth at the wing root is indicated by equation (25).

$$W_{caps} = (A_1 + A_2 + A_3 + A_4)\rho \cdot a_{gravity} \quad (25)$$

Note that in equation (25), the density is assumed to be in units of mass / cu-ft. When the density is specified in that fashion, an adjustment for dimensions must be included to arrive at the correct units for total weight per unit span. For the density value listed above, the acceleration due to gravity has already been included. Table 5 is a quick summary of representative values for a few common engineering materials.

TABLE 5

Material	Weight / Volume (lb/in ³)	Ultimate Tensile Strength (ksi)	Yield Strength (ksi)
2024-T4 Aluminum	0.100	60	44
6061-T6 Aluminum	0.098	42	36
5Cr-Mo-V Steel	0.281	240	200
17-7PH Stainless	0.276	170	140
Titanium	0.162	115	110
Inconel 718	0.297	180	150

One should also notice the lack of two additional columns in Table 5, these include the cost per pound to acquire the material and a similar reference of cost per finished foot. Consider the case of titanium, for certain applications, the tooling required to shape a particular component may prove unacceptable in the overall cost constraint of

the project for a limited production run. The average student is unlikely to possess such detailed cost data, but should understand its impact when progressing to an industrial design team or contract review team.

2. Forward Spar Location

Earlier in chapter III, it was pointed out that the front spar location would generally occur between 12 - 17% of the chord. Since there is an available range to anchor the forward spar, this offers another opportunity to evaluate the effect of changing the spar's location. A series of spar locations might be investigated for a given operating condition, aircraft configuration and material selection to determine the optimum location of the forward spar. Again the optimum point will be identified by the lowest total cross-sectional area required of the spar caps. An example of this type of investigation has been provided in Appendix C.

B. INSTABILITY IMPLICATIONS

The shear flow in the skin, and thus minimum required skin thickness, will change similar to the change in spar cap size given a variation in material choices. However, the shear flow problem offers an additional consideration not associated with bending. The earlier analysis finished with solving for the skin thickness that sustained the ultimate expected load and complied with Navy design specifications. Now, the designer needs to consider the effects of increasing the skin thickness beyond the required minimum. As skin thickness rises, so does the load carried by the stiffeners. This increase tends to reduce the column length in response to increased buckling potential. However, as the

buckling column lengths are reduced (implying reduced rib-spacing, thus more ribs required along the span), the total number of stiffeners required is also reduced.

Aside from changing the skin thickness directly, rib spacing can also be affected by the value specified for the upper surface allowable stress design level. Additionally, for any given thickness chosen, if the stringer crushing strength proves to be unsatisfactory, the areas of the individual stringer elements can be varied. All of these changes impact the ratio of skin thickness to rib spacing. As both of these quantities change, so does the overall weight of the wing. For educational purposes it is recommended that at least one trade be conducted by the students and investigated over a reasonable range of parameters to introduce the concepts and gain an understanding of the extent of possibilities involved over the entire flight envelope of an aircraft.

C. ADVANCED MATERIAL CONSIDERATIONS

As a student's understanding and exposure to structural considerations grows, one more consideration that weighs heavily in all aviation designs remains for review. The design engineer must consider the effects of cyclic loading. This arena may force the complete exclusion of various materials for failing to meet minimum required life cycles. As a student completes his or her study in the area of fracture and fatigue, he or she can then analyze effectively the likelihood of a given design satisfying the Navy's expected life cycle requirements. This stage of the design could prove to be the most challenging in attempting to improve the strength to weight ratio of the structure while subjected to a

wide range of loads over a long lifetime. Structural fatigue has been a central issue in all Naval Aviation programs for the past 30 years.

VI. SUMMARY

A. FUTURE AREAS OF STUDY

1. Aerodynamic Investigations

During the validation and testing of PMARC, all of the work was completed without the use of the boundary layer routines that are built into the analysis portion. This was done to prevent overwhelming a student in his or her first exposure to such a complex code. The boundary layer routine may prove however to offer an interesting and effective means of determining the approximate c_{Lmax} based upon a reversal in the boundary layer shear stresses. A separate research project in itself would encompass a validation of the boundary layer routine and eventual incorporation into the user's guide that was developed as part of this thesis project.

Since most high lift devices are employed well below Mach 0.5, PMARC remains a good solution for those unusual design problems. However, the supersonic, transonic and high subsonic regimes cannot be addressed currently through the employment of PMARC. These regions comprise a major portion of the operational envelopes of today's tactical jet aircraft. To support the structures design of wing sections operating at high speeds, with all high lift devices stowed, a simplified CFD routine could be developed for student use. Such an undertaking would require earlier introduction of CFD methods into the current syllabus, a grid generation system that is readily adaptable to geometric iterations, and analysis routines that can respond to large variations in freestream

conditions. Having met all of those conditions, the output needs to be transformed into a usable format for structural analysis, in a fashion similar to that presented in this thesis, or like the pressure distribution analysis described in the next section. Given the magnitude of that challenge, the distinction between educational and industrial goals needs to be addressed at length prior to undertaking such a project.

2. Advanced Structural Analysis

Several areas of improvement were identified throughout this project and presented for consideration. The first point introduces the incorporation of Finite Element Analysis (FEA) into the advanced aircraft structures course. This is the first introduction to the subject for most students in the aerospace discipline at NPS. A logical building block on the original design project would be verification and comparison of results using the layout, sizing and material choices from the AA2021 class project.

If the initial class project were to be modified to include design and analysis of a swept wing, as depicted in Figure 27, the wing could be analyzed over the period of two quarters. The first quarter would be done using the methods presented here with an adjustment for loading based upon the leading edge sweep. The root section would require the use of FEA. The root section analysis would also necessitate the incorporation of the results of the straight wing approach applied at the boundary of the two regions. This project probably represents both the most extensive of follow-on suggestions, and the most beneficial to future design students.

If fewer fundamental concepts are presented in future instruction to accommodate increased FEA skills, there are two investigation areas to aid in expanded use of FEA. The first is oriented towards the reduction of time consumed to generate a finite element model. Since PMARC is already used to determine a wireframe model, incorporate the means to port that information into a FEA routine as a part of an input file. PMARC is written in FORTRAN 77; thus, only a minor modification should be required within the source code to generate an additional output data file. This project would only be available to students of U.S. citizenship however, due to restrictions on accessing the source code.

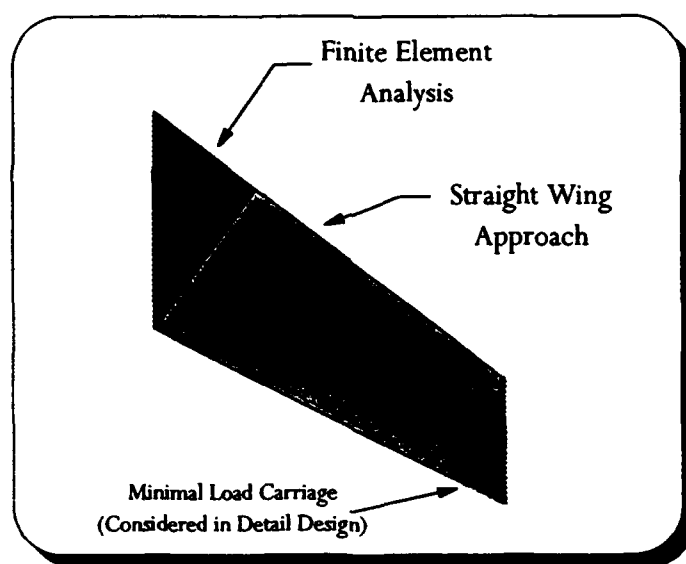


Figure 27

The second project entails the boundary conditions that are solved under FEA. As mentioned earlier, PMARC can generate output on the basis of pressure distribution (c_p) or force and moment coefficients. Since most FEA routines can solve an external

pressure problem, a modification to the source code to provide yet another output data file, could be used to input the boundary conditions to a particular FEA application. This project would parallel the previous one in development, with only slight differences resulting from the requirement of converting c_p to actual pressure.

B. CONCLUSION

The computer code developed to produce the outputs displayed in Appendix B represents a significant step forward for the aircraft design course offered to NPS students. It offers a means to reduce required computational time without sacrificing the importance of careful consideration of the impact of engineering decisions in establishing a baseline design. Hopefully the methods presented in the body of this thesis in conjunction with the sample calculations listed in Appendix C offer insight to the beginning design student that can build one's confidence level in that first design undertaking.

The intent for the software development on a spreadsheet format was to reinforce the student's understanding in a guided environment. As each portion of the series of spreadsheets becomes relevant in a student's classroom discussion, exact portions are worked out in the classroom. Ideally the project will support about four hours of in-class instruction (for all core structures courses), to allow the student the opportunity to derive the underlying equation used in every calculation found throughout the worksheets. Additionally, the classroom exercise should introduce the concept of working in engineering teams to achieve a final result in a reasonable amount of time. By constraining the project to an in-class basis, the instructor can ensure participation by all students and

provide valuable insight on stumbling blocks as they arise among individuals. This intermediate approach to design, should serve students extremely well as they prepare for eventual placement in the most demanding acquisition jobs the Navy can offer, both today and on the horizon ahead.

APPENDIX A

A. WAKE INITIALIZATION

The panel code used for this analysis, PMARC, allows for a wide range of computations. One of its most complex features includes the analysis of flow past an oscillating airfoil. To accomplish this task, the code requires the assembly and analysis of a wake. Unfortunately, that type of computation generally demands extensive CPU time on most computers. Recognizing that handicap, the creator of PMARC wanted to allow experienced users of the code several means by which they could reduce the overall run time during program execution, depending upon their individual requirements. As a result the user has the option to:

- Specify the number of timesteps over which the wake is calculated. This assumes analysis begins at time $t=0$, where the body under investigation is about to enter the freestream flow.
- Specify the length of the time increment used for completion of one time step.
- Allow PMARC to initialize the trailing wake and determine its development in direction and magnitude.
- Override the code and allow the user to specify the wake's initial size and direction upon startup. This option is designed to reduce overall run time if the user is simply trying to analyze a complex flow geometry at a steady-state condition.

Because of the availability of these two features, and the intent of developing several templates that would satisfy a wide range of student applications, a determination of the optimum settings for the student design requirement had to be accomplished. To review

the effects of varying the number of timesteps, a test matrix was conducted on a consistent wing geometry to observe when the outputs converged within a reasonable tolerance to a steady-state value. In reviewing Figure 28, the steady-state solution was found to occur to within four decimal place agreement following 10 timesteps. This test was performed using the geometry described as Planform 3 in Reference 5. The operating conditions for the test were the defaults listed for Planform 3 and AOA=0.00 degrees.

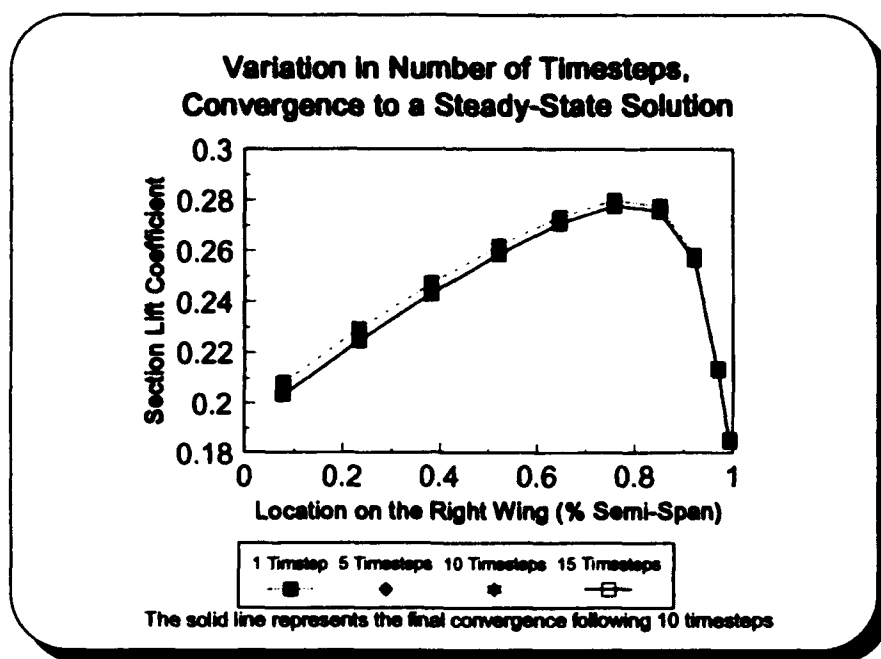


Figure 28

Turning to the question of which initialization method to employ, the user specification of wake attachment, or allowing PMARC to initialize the wake, prompted the development of a second test scenario. The first concern in this test questioned the existence of reasonable agreement between a user defined wake, and PMARC initiation of the wake. Since the wake's departing orientation is generally quite complex, it will not

immediately adopt the direction of the freestream, which can lead to errors in the analysis. Following that result came the question of the existence of any time savings afforded to the typical NPS student using the various initiation options. The final review would then focus on the accuracy of the results. Figure 29 is useful to demonstrate the first point. Using the same airfoil from the earlier test, the two methods of wake generation were compared at $AOA=0.00$ and $AOA=8.00$ degrees.

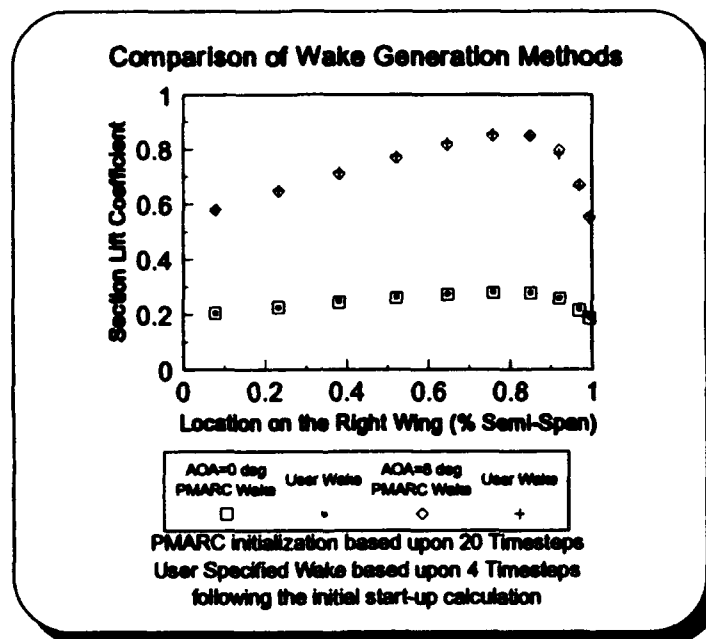


Figure 29

Reasonable agreement was obtained between the two methods, therefore a second test was conducted to determine the time savings involved by specifying the wake's initial direction and magnitude. Figure 30 is a summary of those results. At first inspection of Figures 29 and 30, one might assume a distinct advantage exists in user specification of the wake initial positioning. However, it should also be noted that the code rendered

good convergence for the problem after only 10 timesteps. At that iteration level, the time savings offered by the user specification mode is not considerable. An additional point involves how much time is required to actually develop the required information that is specified in the input data file to accomplish user initialization. From that aspect, coupled with the intent to develop templates to be available for general use, the determination was made to allow PMARC to specify the initial wake orientation and magnitude. The penalty of additional run time does not outweigh the advantage of significant potential errors that may be induced due to user specification of the wake.

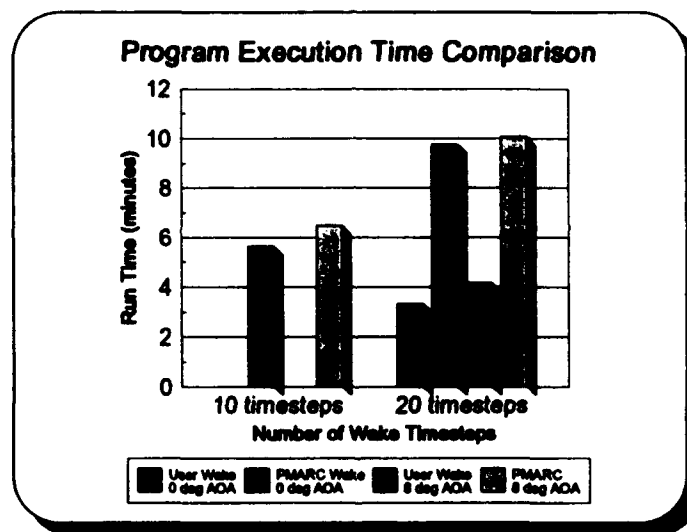


Figure 30

B. ANALYTICAL VALIDATION

Having established the desired input format, the next step in the process involved checking the output against other methods of calculation. The verification test first attempted to match the value of total lift for a wing against a prediction based upon a

conversion technique described in Nicholai. Knowing the characteristics of a two-dimensional airfoil (infinite span), Nicholai offers a means to convert those characteristics into a finite, three-dimensional wing. Equations (26) and (27) were employed to accomplish this conversion of data. In these equations the constant C1 was assumed to be 0.6, while the value for β was taken as 0.866. Note that β is a correction for compressibility which is not considered within PMARC. Equation (27) is actually the first to be solved since it determines the lift curve slope. [Ref. 3:pp. 2-8:2-9]

$$C_L = [C_{L_\alpha}]_{\alpha=0}(\alpha - \alpha_{0\ lift}) + C1(\alpha - \alpha_{0\ lift})^2 \quad (26)$$

$$C_{L_\alpha} = \frac{2\pi AR}{2 + \sqrt{4 + AR^2 \beta^2 \left(1 + \frac{\tan^2 \Lambda}{\beta^2}\right)}} \quad (27)$$

The results of this comparison are depicted in Figure 31. Since the approximation accounts for compressibility, it shows a slightly larger value of lift for any given AOA at the operating condition of 0.5 Mach.

Having attained a good correlation between total lift and AOA, the next task was to look at the lift distribution the code predicted along the span at a given AOA. Planform 3 was again chosen as the baseline configuration for the test. The analytic model chosen for the reference was based upon a modification of Schrenk's Lift Approximation as described by Raymer. The process begins by first solving for the average between a predicted chord

length determined via equation (28) and the actual (or trapezoidal) chord length at various stations along the span. The station points chosen were increments of 10% of the semi-span.

$$C(y) = \frac{4S}{\pi b} \sqrt{1 - \left(\frac{2y}{b}\right)^2} \quad (28)$$

The value of S is obtained from equation (29), note all other parameters are taken from the characteristics of Planform 3.

$$S = \frac{b}{2} C_r (1 + \lambda) \quad (29)$$

The trapezoidal chord length, $C(y)$, at a particular station location, y , can be found from equation (30).

$$C(y) = C_r \left[1 - \frac{2y}{b} (1 - \lambda) \right] \quad (30)$$

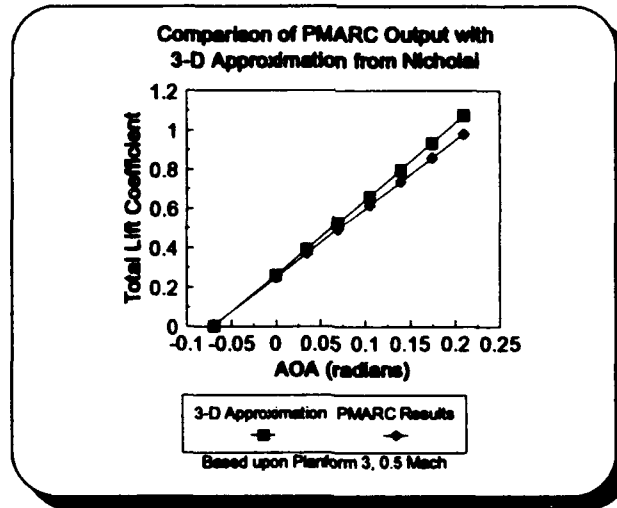


Figure 31

Once the elliptical chord length and trapezoidal chord length have been determined, Schrenk's Approximation states that the distribution of total lift along the span is proportional to the average of these two chord lengths. If this average chord length at a

given station is plotted against the station value, the total area under the resultant curve must sum to be equal to the total lift. [Ref. 4:pp. 342-343]

To accommodate a comparison between PMARC and Shrenk's Approximation, a somewhat different curve was developed using the same principles. Once the average chord values were determined for the approximation, they were normalized by dividing each individual value by the root chord length. Since this approximation was based upon lift, vice lift coefficient, the output of PMARC also required modification. Taking the local coefficient of lift for each spanwise station, that value would have to be multiplied by the dynamic pressure (q) and the area of that spanwise station. Having obtained the lift at each station, all values were then normalized by dividing the lift at the first output location (7.8% of the semi-span) of PMARC into all station lift values.

Since the lift distributions for both methods were based upon a location described by percentage of semi-span, it was then possible to overlay the two results for accurate comparison. These results are depicted in Figure 32. For reference, Table 6 provides a brief synopsis of the characteristics associated with Planform 3.

TABLE 6

Planform 3 Characteristics	
$-b$	36.7 ft
c_r	20.0 ft
λ	0.1445
S_{ref}	420 ft ²
Λ_{LE}	25 deg

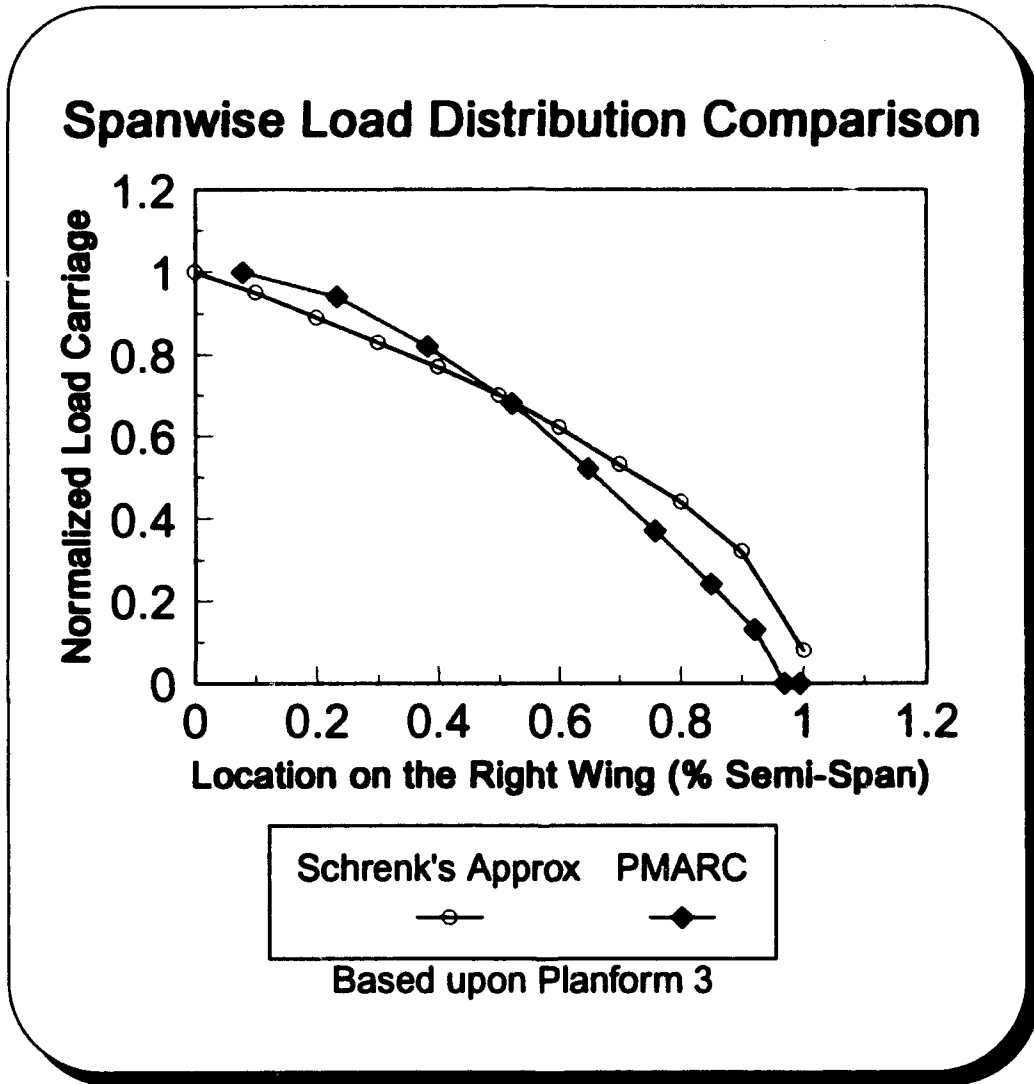


Figure 32

C. COMPUTER-BASED VERIFICATION

Having attained reasonable results from generalized approximations, the next step entailed comparing the output of PMARC with an independent panel code. The choice for this comparison was a panel code named SUB, which was developed by NASA Langley. The test involved nearly identical geometry and freestream conditions. However, two small differences did exist between the two codes. First, SUB did not permit easy identification of the wing's cross-section, as a result the airfoil considered in SUB was a flat plate. The cross-section used for PMARC was a NACA 0012 airfoil. The second difference was due to the selection of independent variable used by each code in their analysis routines. In SUB, the user specifies the desired total output c_l , whereas PMARC evaluates the input on the basis of operating angle of attack. Figure 33 depicts the actual wing chosen for this portion of validation testing.

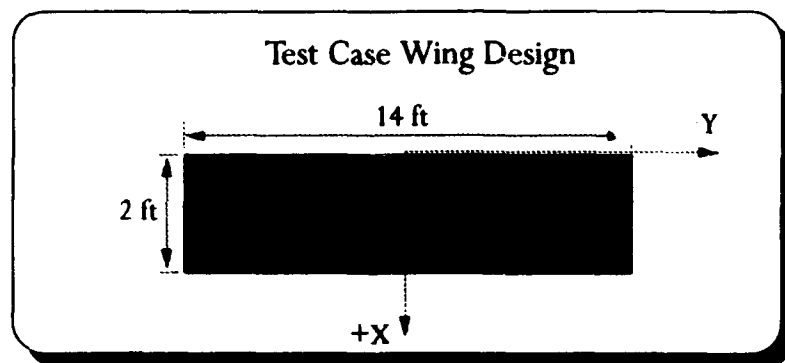


Figure 33

The results of those tests are illustrated in Figure 34. The runs were compared along the right wing for two different choices of AOA. Even with the subtle differences in the codes, the results demonstrated good correlation.

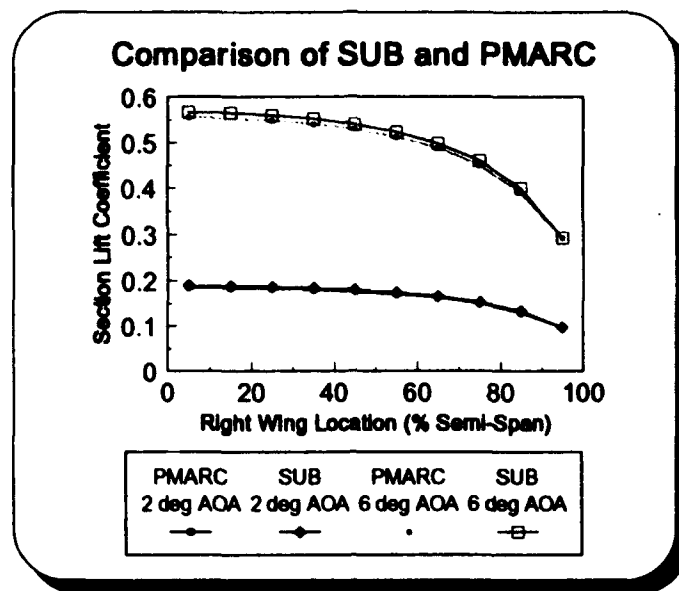


Figure 34

D. EXPERIMENTAL DATA COMPARISON

The last validation study included a check against actual wind tunnel results for a wing section that was built with a NACA 6 Digit airfoil cross-section. Data for the study were obtained from Bertin and Smith in their discussion of panel code methods [Ref. 6:pp. 253-256]. The test cross-section was a NACA 65-210 forming a 15 ft span wing similar in shape to Planform 1 used throughout the body of this thesis. Comparison of the wind tunnel results and PMARC output is displayed in Figure 35. The effects of non-linearity due to viscous effects can be observed at the higher values of AOA. With the conclusion of this test, PMARC was determined to be a good introductory tool for use by design students at NPS, that could also be readily validated by available references.

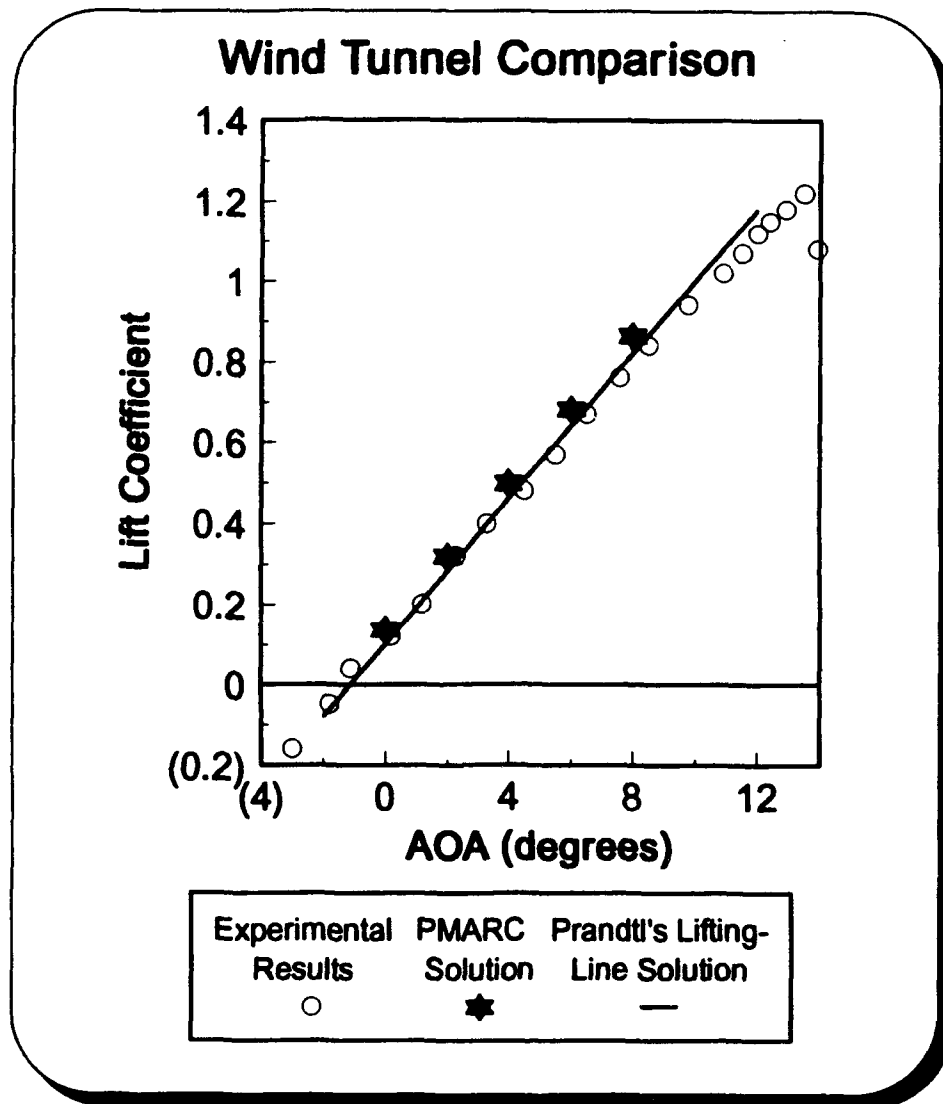


Figure 35

APPENDIX B

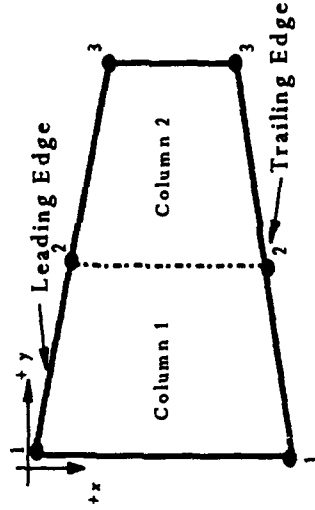
This appendix provides the output of the spreadsheet routines developed to support design students faced with the task of repetitive calculations based upon the principles presented in this thesis. The results provided are for flight conditions I, II, III and IV, which were previously described within chapter III of this thesis. These values are based upon the analysis of an aircraft wing geometry represented by Planform I throughout the thesis. The routines used to determine normal and axial loadings allow the inclusion of planform drag through the specification of c_{d0} . The values obtained at all four flight conditions used the airfoil section data at the appropriate velocity and Reynold's number from Abbot and von Doenhoff [Ref. 10:p. 493]. Anderson provides an example of using the section drag characteristics to solve for the expected lift and drag associated with a finite wing [Ref. 14:pp. 221-222].

Each page represents a complete output from individual worksheets that have been linked together in a 3-D spreadsheet format. The code was developed within LOTUS® 1-2-3 release 4.0 for Windows™. The code runs without delay on a 386-based machine or better that employs a math co-processor and at least 8 Mb of RAM. For those users with a color VGA or better monitor, the input cells have been shaded to further reduce the time required to conduct a preliminary design study. Those inputs dealing with a wing's physical geometry are indicated in light blue. Yellow cells pertain to material properties, while purple is used for those items that should always be updated with any

change to the operating conditions. Due to the reproduction limitations of this thesis, within Appendix B, all input cells are indicated by a grey background.

Panel Code Planform Area

Requires the spatial coordinates of the corner points for each column and column chord lengths.



Sample Layout:

Case: **Planform 1**

Location
Number

Leading Edge	X	Y
1	0.0000	0.0000
2	0.0000	7.8200
3	0.0000	15.4500
4	0.0000	22.7000
5	0.0000	29.3900
6	0.0000	35.3800
7	0.0000	40.4900
8	0.0000	44.5600
9	0.0000	47.5600
10	0.0000	49.3800
11	0.0000	50.0000
12		
13		
14		
15		
16		

Trailing Edge

X	Y
15.0000	0.0000
15.4400	7.8200
11.9100	15.4500
10.4600	22.7000
9.1200	29.3900
7.8300	35.3800
6.5100	40.4900
5.0900	44.5600
3.4900	47.5600
1.7200	49.3800
0.0000	50.0000

Column
Number

Area	Chord Length
111.20	14.249
96.71	12.700
81.09	11.203
65.50	9.812
50.89	8.544
37.77	7.435
26.65	6.514
17.37	5.802
9.71	5.318
3.14	5.072
0.00	
0.00	
0.00	
0.00	
0.00	
0.00	

Total Area: **500.02**

PMARC Output Summary

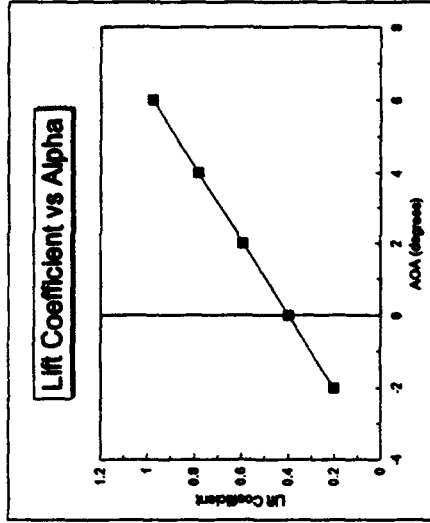
Condition: 1

Required Inputs: Cl, %SSPAN, Desired Cl, Corresponding AOA, Freestream Conditions, SSPAN

AOA (degree)	Cl
-2	0.3022
0	0.5972
2	0.8905
4	0.7541
6	0.5765
8	

Desired Cl: 1.200

Corresponding AOA: 0.028



Freestream Conditions:

C_{ns} = 0.110

Density = 0.0023760

Velocity = 500

SSPAN = 500

(slug/ft³)

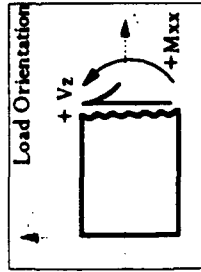
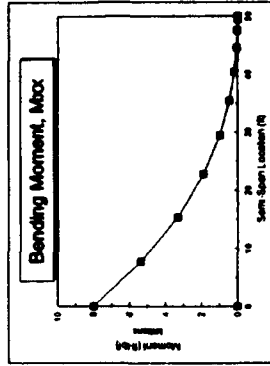
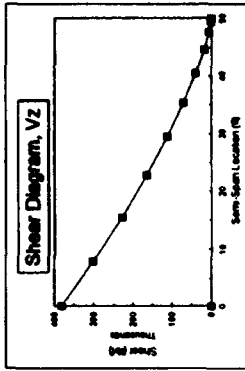
(ft/sec)

50,000

Spanwise Load and Moment Coefficients

Column	Column Center % of Semi-span	Column Center Location (ft)	Area (sqft)	C _L	Lift (lb)	C _D	Normal Force with C _{Do} (lb)	Induced Drag (lb)	C _{Ma}	Axial Force with C _{Do} (lb)	Axial Force with C _{Do} (lb)
1	7.8%	3.90	111.20	1.335	52,426	1.1535	52,639	2,328	0.0009	(5,925)	(928)
2	24.3%	11.65	96.71	1.2104	48,427	1.2033	48,833	2,012	0.0003	(5,606)	(1,263)
3	38.2%	19.10	81.09	1.2535	42,219	1.2803	42,523	1,577	0.0070	(5,066)	(1,421)
4	52.1%	26.05	65.50	1.2939	34,950	1.2905	35,171	1,187	0.0059	(4,311)	(1,367)
5	64.7%	32.35	50.89	1.3015	27,478	1.2955	27,640	889	0.0022	(3,432)	(1,145)
6	75.8%	37.90	37.77	1.2972	20,268	1.2860	20,394	683	0.0003	(2,505)	(907)
7	85.0%	42.50	26.85	1.2486	13,766	1.2409	13,871	547	0.0009	(1,618)	(421)
8	92.1%	46.05	17.37	1.1191	8,042	1.1142	8,131	407	0.0007	(659)	(79)
9	96.9%	48.45	9.71	0.7722	3,503	0.8711	3,588	248	0.0013	(304)	132
10	99.1%	49.70	3.14	0.5466	843	0.6076	866	216	0.0023	81	222
11		0.00	0.00		0		0	0		0	0
12		0.00	0.00		0		0	0		0	0
13		0.00	0.00		0		0	0		0	0
14		0.00	0.00		0		0	0		0	0
15		0.00	0.00		0		0	0		0	0
Totals:			500		251,923		250,389	10,093		(29,549)	

Condition: 1



Shear and Moment Diagram Construction (Normal Loading)

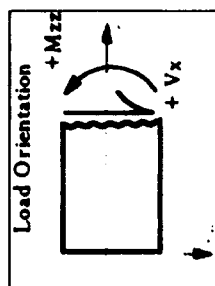
Span Point Location (ft)	Left Edge Location (ft)	Center Location (ft)	Limit Load (k)	Ultimate Load (k)	Shear (V _i) (k)	Bending Moment (M _i) (k-ft)
1	0.00	3.90	52.939	79.408	390.938	8,027.754
2	7.82	11.65	48.833	73.250	301.530	5,360.097
3	15.45	19.10	42.523	63.785	228.280	3,337.771
4	22.70	26.05	35.171	52.757	164.498	1,912.364
5	29.39	32.35	27.640	41.460	111.739	988.097
6	35.36	37.90	20.394	30.591	70.279	445.810
7	40.45	42.50	13.871	20.807	39.688	166.098
8	44.55	46.05	8.131	12.198	18.881	46.032
9	47.55	48.45	3.568	5.352	6.685	7.683
10	49.38	49.70	889	1,333	1,333	427
11	50.00	0.00	0	0	0	0
12	0.00	0.00	0	0	0	0
13	0.00	0.00	0	0	0	0
14	0.00	0.00	0	0	0	0
15	0.00	0.00	0	0	0	0

Moment Construction:

Column.1	Column.2	Column.3	Column.4	Column.5	Column.6	Column.7	Column.8	Column.9	Column.10	Column.11	Column.12	Column.13	Column.14	Column.15
500.642	290.547	232.614	178.735	122.721	77.701	42.864	18.294	4.617	0	0	0	0	0	0
853.390	716.462	569.222	464.963	370.329	290.361	228.280	180.374	130.374	88.297	42.814	20.872	9.696	2.897	0
1,210.298	981.758	790.873	626.177	492.827	392.164	304.774	237.800	187.800	142.333	108.008	82.008	62.008	46.032	7.683
1,574.314	1,017.012	806.787	626.177	492.827	392.164	304.774	237.800	187.800	142.333	108.008	82.008	62.008	46.032	7.683
1,941.228	1,250.177	981.758	790.873	626.177	492.827	392.164	304.774	237.800	187.800	142.333	108.008	82.008	62.008	46.032
2,310.396	1,481.758	1,166.462	931.758	740.873	581.758	451.758	351.758	271.758	201.758	151.758	101.758	71.758	41.758	21.758
2,681.521	1,712.821	1,392.821	1,092.821	842.821	642.821	492.821	392.821	302.821	232.821	182.821	132.821	82.821	32.821	12.821
3,052.646	1,943.946	1,623.946	1,273.946	973.946	723.946	523.946	373.946	273.946	203.946	153.946	103.946	73.946	43.946	23.946
3,423.771	2,175.071	1,855.071	1,485.071	1,135.071	835.071	635.071	485.071	385.071	315.071	245.071	195.071	145.071	95.071	45.071
3,794.896	2,406.196	2,086.196	1,686.196	1,286.196	986.196	786.196	636.196	536.196	466.196	396.196	346.196	296.196	246.196	196.196
4,166.021	2,637.321	2,317.321	1,887.321	1,487.321	1,087.321	887.321	737.321	637.321	567.321	497.321	447.321	397.321	347.321	297.321
4,537.146	2,868.446	2,548.446	2,118.446	1,718.446	1,318.446	1,118.446	968.446	818.446	748.446	678.446	628.446	578.446	528.446	478.446
4,908.271	3,099.571	2,779.571	2,349.571	1,949.571	1,549.571	1,349.571	1,199.571	1,049.571	979.571	929.571	879.571	829.571	779.571	729.571
5,279.396	3,330.696	3,010.696	2,580.696	2,180.696	1,780.696	1,580.696	1,430.696	1,280.696	1,210.696	1,160.696	1,110.696	1,060.696	1,010.696	960.696
5,650.521	3,561.821	3,241.821	2,811.821	2,411.821	2,011.821	1,811.821	1,661.821	1,511.821	1,441.821	1,391.821	1,341.821	1,291.821	1,241.821	1,191.821
6,021.646	3,792.946	3,472.946	3,042.946	2,642.946	2,242.946	2,042.946	1,892.946	1,742.946	1,672.946	1,622.946	1,572.946	1,522.946	1,472.946	1,422.946
6,392.771	4,024.071	3,704.071	3,274.071	2,874.071	2,474.071	2,274.071	2,124.071	1,974.071	1,904.071	1,854.071	1,804.071	1,754.071	1,704.071	1,654.071
6,763.896	4,255.196	3,935.196	3,505.196	3,105.196	2,705.196	2,505.196	2,355.196	2,205.196	2,135.196	2,085.196	2,035.196	1,985.196	1,935.196	1,885.196
7,135.021	4,486.321	4,166.321	3,736.321	3,336.321	2,936.321	2,736.321	2,586.321	2,436.321	2,366.321	2,316.321	2,266.321	2,216.321	2,166.321	2,116.321
7,506.146	4,717.446	4,397.446	3,967.446	3,567.446	3,167.446	2,967.446	2,817.446	2,667.446	2,597.446	2,547.446	2,497.446	2,447.446	2,397.446	2,347.446
7,877.271	4,948.571	4,628.571	4,198.571	3,798.571	3,398.571	3,198.571	3,048.571	2,898.571	2,828.571	2,778.571	2,728.571	2,678.571	2,628.571	2,578.571
8,248.396	5,179.696	4,859.696	4,429.696	4,029.696	3,629.696	3,429.696	3,279.696	3,129.696	3,059.696	3,009.696	2,959.696	2,909.696	2,859.696	2,809.696
8,619.521	5,410.821	5,090.821	4,660.821	4,260.821	3,860.821	3,660.821	3,510.821	3,360.821	3,290.821	3,240.821	3,190.821	3,140.821	3,090.821	3,040.821
8,990.646	5,641.946	5,321.946	4,891.946	4,491.946	4,091.946	3,891.946	3,741.946	3,591.946	3,521.946	3,471.946	3,421.946	3,371.946	3,321.946	3,271.946
9,361.771	5,873.071	5,553.071	5,123.071	4,723.071	4,323.071	4,123.071	3,973.071	3,823.071	3,753.071	3,703.071	3,653.071	3,603.071	3,553.071	3,503.071
9,732.896	6,104.196	5,784.196	5,354.196	4,954.196	4,554.196	4,354.196	4,204.196	4,054.196	3,984.196	3,934.196	3,884.196	3,834.196	3,784.196	3,734.196
10,104.021	6,335.321	6,015.321	5,585.321	5,185.321	4,785.321	4,585.321	4,435.321	4,285.321	4,215.321	4,165.321	4,115.321	4,065.321	4,015.321	3,965.321
10,475.146	6,566.446	6,246.446	5,816.446	5,416.446	5,016.446	4,816.446	4,666.446	4,516.446	4,446.446	4,396.446	4,346.446	4,296.446	4,246.446	4,196.446
10,846.271	6,797.571	6,477.571	6,047.571	5,647.571	5,247.571	5,047.571	4,897.571	4,747.571	4,677.571	4,627.571	4,577.571	4,527.571	4,477.571	4,427.571
11,217.396	7,028.696	6,708.696	6,278.696	5,878.696	5,478.696	5,278.696	5,128.696	4,978.696	4,908.696	4,858.696	4,808.696	4,758.696	4,708.696	4,658.696
11,588.521	7,259.821	6,939.821	6,509.821	6,109.821	5,709.821	5,509.821	5,359.821	5,209.821	5,139.821	5,089.821	5,039.821	4,989.821	4,939.821	4,889.821
11,959.646	7,490.946	7,170.946	6,740.946	6,340.946	5,940.946	5,740.946	5,590.946	5,440.946	5,370.946	5,320.946	5,270.946	5,220.946	5,170.946	5,120.946
12,330.771	7,722.071	7,402.071	6,972.071	6,572.071	6,172.071	5,972.071	5,822.071	5,672.071	5,602.071	5,552.071	5,502.071	5,452.071	5,402.071	5,352.071
12,701.896	7,953.196	7,633.196	7,203.196	6,803.196	6,403.196	6,203.196	6,053.196	5,903.196	5,833.196	5,783.196	5,733.196	5,683.196	5,633.196	5,583.196
13,073.021	8,184.321	7,864.321	7,434.321	7,034.321	6,634.321	6,434.321	6,284.321	6,134.321	6,064.321	6,014.321	5,964.321	5,914.321	5,864.321	5,814.321
13,444.146	8,415.446	8,095.446	7,665.446	7,265.446	6,865.446	6,665.446	6,515.446	6,365.446	6,295.446	6,245.446	6,195.446	6,145.446	6,095.446	6,045.446
13,815.271	8,646.571	8,326.571	7,896.571	7,496.571	7,096.571	6,896.571	6,746.571	6,596.571	6,526.571	6,476.571	6,426.571	6,376.571	6,326.571	6,276.571
14,186.396	8,877.696	8,557.696	8,127.696	7,727.696	7,327.696	7,127.696	6,977.696	6,827.696	6,757.696	6,707.696	6,657.696	6,607.696	6,557.696	6,507.696
14,557.521	9,108.821	8,788.821	8,358.821	7,958.821	7,558.821	7,358.821	7,208.821	7,058.821	6,988.821	6,938.821	6,888.821	6,838.821	6,788.821	6,738.821
14,928.646	9,339.946	9,019.946	8,589.946	8,189.946	7,789.946	7,589.946	7,439.946	7,289.946	7,219.946	7,169.946	7,119.946	7,069.946	7,019.946	6,969.946
15,300.771	9,571.071	9,251.071	8,821.071	8,421.071	8,021.071	7,821.071	7,671.071	7,521.071	7,451.071	7,401.071	7,351.071	7,301.071	7,251.071	7,201.071
15,671.896	9,802.196	9,482.196	9,052.196	8,652.196	8,252.196	8,052.196	7,902.196	7,752.196	7,682.196	7,632.196	7,582.196	7,532.196	7,482.196	7,432.196
16,043.021	10,033.321	9,713.321	9,283.321	8,883.321	8,483.321	8,283.321	8,133.321	7,983.321	7,913.321	7,863.321	7,813.321	7,763.321	7,713.321	7,663.321
16,414.146	10,264.446	9,944.446	9,514.446	9,114.446	8,714.446	8,514.446	8,364.446	8,214.446	8,144.446	8,094.446	8,044.446	7,994.446	7,944.446	7,894.446
16,785.271	10,495.571	10,175.571	9,745.571	9,345.571	8,945.571	8,745.571	8,595.571	8,445.571	8,375.571	8,325.571	8,275.571	8,225.571	8,175.571	8,125.571
17,156.396	10,726.696	10,406.696	9,976.696	9,576.696	9,176.696	8,976.696	8,826.696	8,676.696	8,606.696	8,556.696	8,506.696	8,456.696	8,406.696	8,356.696
17,527.521	10,957.821	10,637.821	10,207.821	9,807.821	9,407.821	9,207.821	9,057.821	8,907.821	8,837.821	8,787.821	8,737.821	8,687.821	8,637.821	8,587.821
17,898.646	11,188.946	10,868.946	10,438.946	10,038.946	9,638.946	9,438.946	9,288.946	9,138.946	9,068.946	9,018.946	8,968.946	8,918.946	8,868.946	8,818.946
18,269.771	11,420.071	11,100.071	10,670.071	10,270.071	9,870.071	9,670.071	9,520.071	9,370.071	9,300.071	9,250.071	9,200.071	9,150.071	9,100.071	9,050.071
18,640.896	11,651.196	11,331.196	10,901.196	10,501.196	10,101.196	9,901.196	9,751.196	9,601.196	9,531.196	9,481.196	9,431.196	9,381.196	9,331.196	9,281.196
19,012.021	11,882.321	11,562.321	11,132.321	10,732.321	10,332.321	10,132.321	9,982.321	9,832.321	9,762.321	9,712.321				

Span-Beam Location (ft)	Moment (ft-k)
0	0
10	96
20	192
25	240
30	240
35	240
40	240
45	240
50	240

Condition:



Plantom Column No.	Left Edge Location (in)	Center Location (in)	Limit Load (kips)	Ultimate Load (kips)	Shear (V ₂) (at Left Edge) (kips)	Bending Moment (M ₂) (at Left Edge) (ft-kips)
1	0.00	3.90	(928)	(1,391)	(10,614)	229,203
2	7.82	11.65	(1,263)	(1,894)	(9,223)	151,653
3	15.45	19.10	(1,421)	(2,132)	(7,329)	88,479
4	22.70	26.05	(1,367)	(2,051)	(5,197)	43,018
5	29.39	32.35	(1,145)	(1,717)	(3,146)	15,099
6	35.36	37.90	(907)	(1,211)	(1,429)	1,463
7	40.45	42.50	(421)	(631)	(219)	(2,705)
8	44.55	46.05	(79)	(118)	412	(2,308)
9	47.55	48.45	132	198	531	(694)
10	49.36	49.70	222	333	333	(106)
11	50.00	0.00	0	0	0	0
12	0.00	0.00	0	0	0	0
13	0.00	0.00	0	0	0	0
14	0.00	0.00	0	0	0	0
15	0.00	0.00	0	0	0	0

[illegible][illegible]

Area Distribution based upon Air Loads

Condition: I

Constants: $z1=$ 28.80 $z2=$ 25.65 $z4=$ 3.15 $x1=$ 27.00 $x2=$ 90.00

*All distances measured in inches

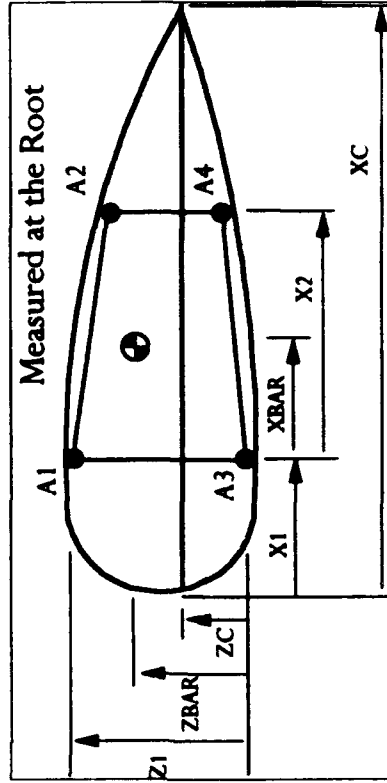
$zc=$ 9.90 $xc=$ 180.00

A1	A2	A3	A4	Area total	xbar	zbar	lx	lz	lzx
63	19	46	19	147	23.27	16.07	27,004	228,233	(5,695)

S1	S2	S3	S4
-43856	-39512	59373	41121

Allowable Stresses:

Upper: -44000
Lower: 60000



Torsion Across the Cross-Section

Condition: I

Required Inputs: Cm, XLE, CBAR and RMPX

Freestream Conditions:

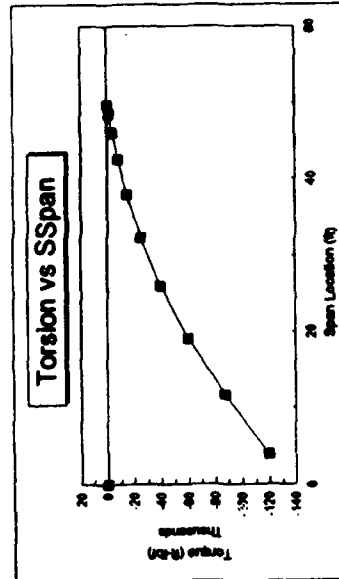
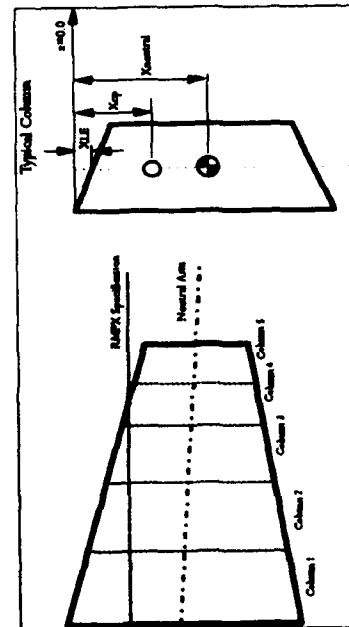
Density= 0.0023769 Velocity= 590

CBAR= 10.83

RMPX= 1.000

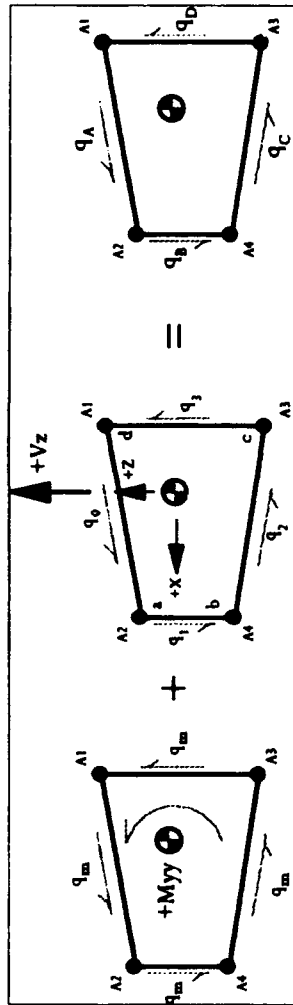
Note: zeros appear as blank cells

Column Number	Area (sq ft)	N (Column Normal Force)	Cm	M (Column Moment)	d (in)	XLE (in)	XCP (Column Center of Pressure)	Xneutral (in)	chord (in)	d' (in)	M2x (Column Moment Temporarily Transferred to a Station)	M2y (Column Moment Temporarily Transferred to a Station)	Max (Total Torque at a Station)
	CSAR=	Density=	0.0023769	Velocity=	RMPX=	1,000	Centroid=	27.93% (ftd Chord)		Centroid=	8.93% (ftd Chord)		
1	111.20	52.145	-0.3840	(191,316)	-3.67	-0.030	4.67	3.95	14.25	-0.72	(37,537)	5.180	(119,764)
2	96.71	48.143	-0.3522	(152,607)	-3.17	-0.026	4.17	3.52	12.70	-0.65	(31,264)	4.012	(87,407)
3	81.09	41.944	-0.3075	(111,720)	-2.66	-0.023	3.66	3.11	11.21	-0.56	(23,338)	2.814	(60,156)
4	65.50	34.704	-0.2569	(75,972)	-2.19	-0.020	3.19	2.72	9.81	-0.47	(16,281)	1.747	(39,631)
5	50.89	27.277	-0.2114	(48,204)	-1.77	-0.018	2.77	2.37	8.54	-0.40	(10,692)	921	(25,097)
6	37.77	20.124	-0.1676	(28,360)	-1.41	-0.016	2.41	2.06	7.44	-0.35	(7,024)	364	(15,125)
7	26.65	13.681	-0.1291	(15,415)	-1.13	-0.014	2.13	1.81	6.51	-0.32	(4,401)	49	(8,466)
8	17.37	8.007	-0.0929	(7,230)	-0.90	-0.012	1.90	1.61	5.80	-0.29	(2,360)	(82)	(4,114)
9	9.71	3.499	-0.0585	(2,545)	-0.73	-0.011	1.73	1.47	5.32	-0.25	(886)	(97)	(1,872)
10	3.14	868	-0.0689	(983)	-1.13	-0.011	2.13	1.41	5.07	-0.73	(631)	(56)	(669)



Shear Flow Calculation

Condition: I



*All shear flows expressed in lb/in

C1=	-14.17	$q_0 =$	-654	$q_m =$	-311
C2=	0.31	$q_1 =$	-3624		
$Q_{Ax} =$	182.11	$q_2 =$	-536	$q_A =$	-965
$Q_{Bx} =$	-245.39	$q_3 =$	10266	$q_B =$	-3935
$Q_{Cx} =$	-739.00			$q_C =$	-847
$Q_{Az} =$	1267.96			$q_D =$	9954
$Q_{Bz} =$	1267.96				
$Q_{Cz} =$	-1070.20				

Buckling Considerations Based Upon Material Properties

Condition: I

Shear Flow in the
Wing Upper Cover = 965

$\tau_{allow} = 32,000$
(lb/sq-in) $\sigma_{SE} = 44,000$

Minimum Thickness
Based upon $\tau_{allow} = 0.0302$
(in)

Minimum Gauge
Req'd Thickness = 0.0280
(in)

Desired Skin Thickness
in Buckling Analysis = 0.0400

Material Properties:

$K_s = 7.17$
(Shear Buckling Coefficient)

$E = 1.06E+07$
(lb-sq-in) $\nu = 0.330$

$K_C = 5.75$
(Compression Buckling Coefficient)

$K = 117.00$ $m = 5.00$

$\tau_{CR} = 24,127$
(lb/sq-in) $\sigma_{CR} = 19,348$
(lb/sq-in)

Distance Between Stringer Centerlines:

Number of Stringers:

Effective Width of Skin:

$b = 2.16$
(in)

$n = 41$

$W_e = 0.78$
(in)

Condition: I

Stringer Design and Rib Spacing

$$A_s = 0.1294 \quad t_b = 0.0420$$

Proposed Section Lengths:

L1 = 0.5049	L2 = 1.7825	L3 = 0.5348
L2 = 0.8750	A1 = 0.0242	zbar _{ST} = 0.2500
L3 = 0.3534	A2 = 0.0368	I _{xx} = 0.0132
t _w = 0.0480	A3 = 0.0119	r = 0.3198
	Ask _{in} = 0.0621	(Radius of Gyration)

$$L = 6.953$$

(Rib Spacing, inches)

$$C = 2.0000$$

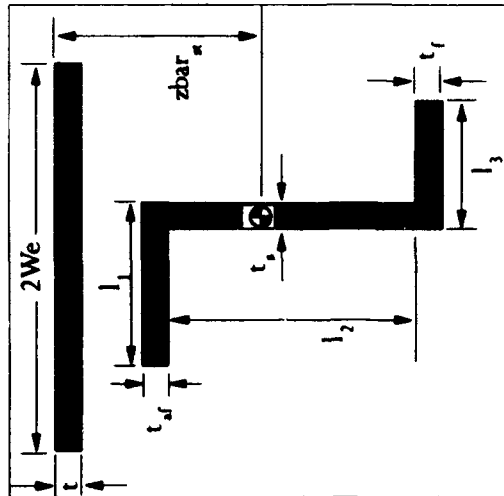
(Flexity Coefficient)

$$\sigma_{1\alpha} = 44,212$$

$$\sigma_{2\alpha} = 90,165$$

$$\sigma_{3\alpha} = 44,219$$

$$\sigma_{cc} = 44,000$$



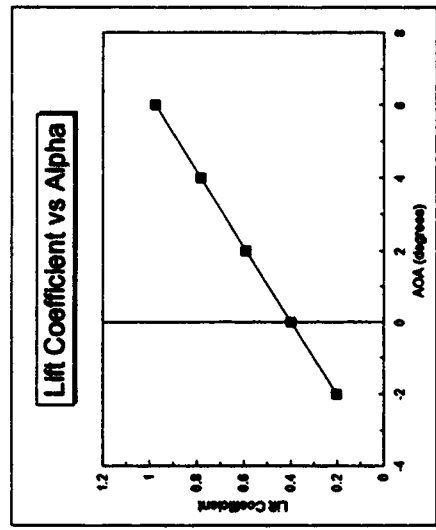
Condition: II

PMARC Output Summary

Required Inputs: Cl, %SSPAN, Desired Cl, Corresponding AOA, Freestream Conditions, SSPAN

AOA (degree)	Cl
-2	0.2022
0	0.3972
2	0.5905
4	0.7841
6	0.9755
8	

Desired Cl: -0.7155
Corresponding AOA: -11.5030

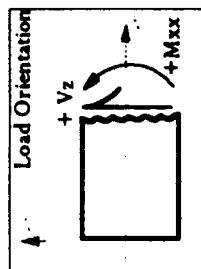
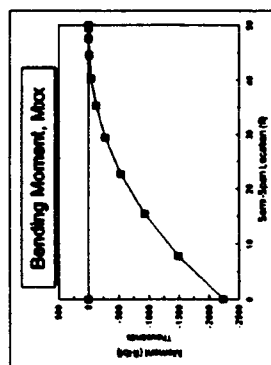
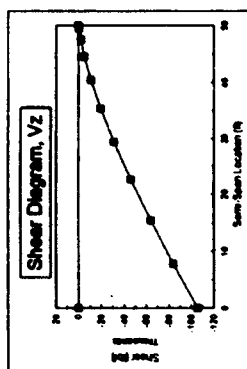


Freestream Conditions: Coo = 0.008

Density = 0.0023769 Velocity = 420 SSPAN = 50.00
(slugs/ft³) (ft/sec) (ft)

Spanwise Load and Moment Coefficients

Column	Column Center % of Semi-span	Column Center Location (ft)	Area (sqft)	C _L	Lift (lb)	C _D	Normal Force with C _D (lb)	Induced Drag (lb)	C _M	Axial Force (lb)	Axial Force with C _D (lb)
1	7.6%	3.90	111.20	-0.6270	(14,617)	-0.6188	(14,426)	511	0.0219	(2,415)	(2,210)
2	23.9%	11.65	96.71	-0.5719	(13,622)	-0.6627	(13,436)	440	0.0217	(2,287)	(2,108)
3	36.2%	19.10	81.09	-0.7035	(11,960)	-0.8935	(11,790)	352	0.0207	(2,040)	(1,890)
4	52.1%	26.05	65.50	-0.7246	(9,949)	-0.7139	(9,802)	269	0.0196	(1,720)	(1,599)
5	64.7%	32.35	50.89	-0.7346	(7,838)	-0.7237	(7,722)	204	0.0191	(1,364)	(1,269)
6	75.8%	37.90	37.77	-0.7290	(5,772)	-0.7182	(5,687)	151	0.0181	(1,002)	(933)
7	85.0%	42.50	26.65	-0.6979	(3,899)	-0.6379	(3,843)	114	0.0204	(666)	(617)
8	92.1%	46.05	17.37	-0.6237	(2,271)	-0.6157	(2,242)	83	0.0227	(372)	(340)
9	96.9%	48.45	9.71	-0.4906	(996)	-0.4863	(990)	57	0.0278	(143)	(126)
10	99.4%	49.70	3.14	-0.3746	(246)	-0.3802	(250)	43	0.0659	(7)	(1)
11		0.00	0.00		0		0	0		0	0
12		0.00	0.00		0		0	0		0	0
13		0.00	0.00		0		0	0		0	0
14		0.00	0.00		0		0	0		0	0
15		0.00	0.00		0		0	0		0	0
Totals:			500		(71,173)		(70,187)	2,223		(12,017)	

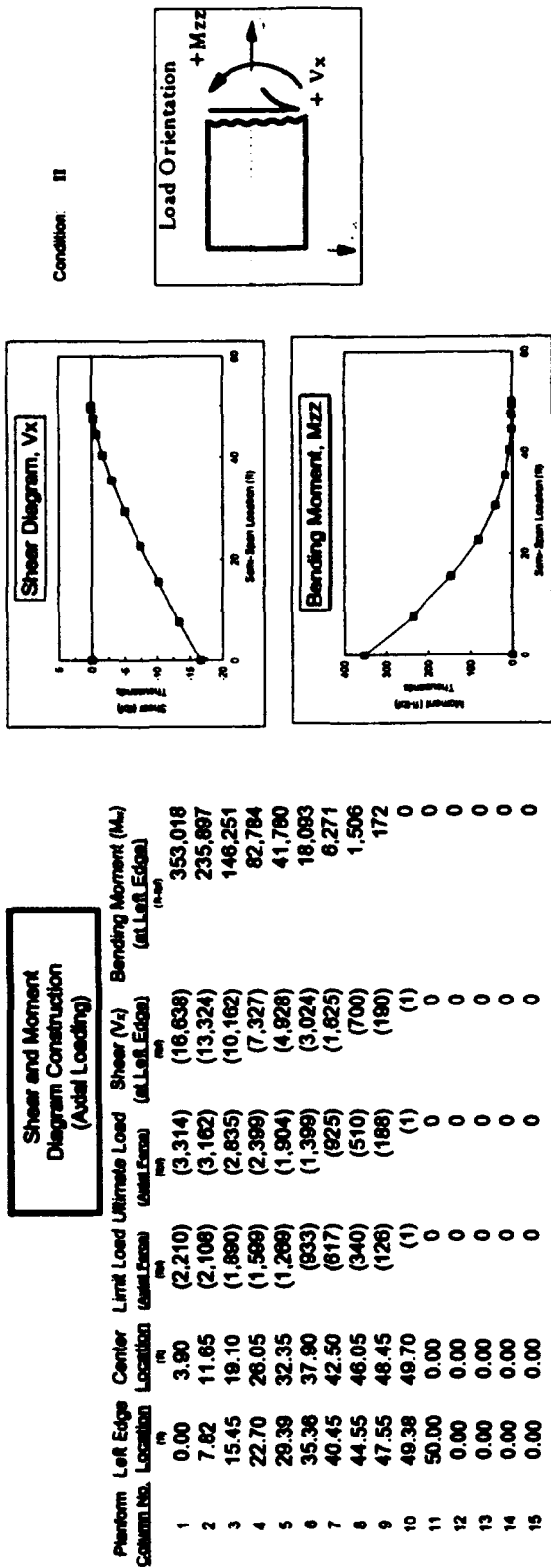


**Shear and Moment
Diagram Construction
(Normal Loading)**

[illegible]

Management Commentary:

[illegible]



Moment Construction:

Column 1	Column 2	Column 3	Column 4	Column 5	Column 6	Column 7	Column 8	Column 9	Column 10	Column 11	Column 12	Column 13	Column 14	Column 15
(12,826)	(12,111)	(26,640)	(8,037)	(5,636)	(3,553)	(1,898)	(786)	(169)	(0)	(0)	(0)	(0)	(0)	(0)
(84,181)	(31,980)	(10,346)	(18,376)	(11,904)	(6,068)	(2,866)	(734)	(3)	(0)	(0)	(0)	(0)	(0)	(0)
(62,494)	(43,734)	(25,430)	(21,262)	(12,127)	(5,453)	(2,506)	(734)	(7)	(0)	(0)	(0)	(0)	(0)	(0)
(61,601)	(46,710)	(32,181)	(18,316)	(8,498)	(2,485)	(1,506)	(734)	(12)	(0)	(0)	(0)	(0)	(0)	(0)
(53,016)	(42,077)	(31,404)	(11,910)	(3,569)	(18)	(0)	(0)	(0)	(0)	(0)	(0)	(0)	(0)	(0)
(36,314)	(25,022)	(15,008)	(4,849)	(26)	(0)	(0)	(0)	(0)	(0)	(0)	(0)	(0)	(0)	(0)
(23,486)	(19,500)	(8,214)	(34)	(0)	(0)	(0)	(0)	(0)	(0)	(0)	(0)	(0)	(0)	(0)
(8,123)	(7,651)	(43)	(0)	(0)	(0)	(0)	(0)	(0)	(0)	(0)	(0)	(0)	(0)	(0)
(63)	(53)	(0)	(0)	(0)	(0)	(0)	(0)	(0)	(0)	(0)	(0)	(0)	(0)	(0)
(0)	(0)	(0)	(0)	(0)	(0)	(0)	(0)	(0)	(0)	(0)	(0)	(0)	(0)	(0)
(0)	(0)	(0)	(0)	(0)	(0)	(0)	(0)	(0)	(0)	(0)	(0)	(0)	(0)	(0)
(0)	(0)	(0)	(0)	(0)	(0)	(0)	(0)	(0)	(0)	(0)	(0)	(0)	(0)	(0)
(0)	(0)	(0)	(0)	(0)	(0)	(0)	(0)	(0)	(0)	(0)	(0)	(0)	(0)	(0)
(383,018)	(234,697)	(146,251)	(82,784)	(41,780)	(18,093)	(6,271)	(1,506)	(172)	(0)	(0)	(0)	(0)	(0)	(0)

Area Distribution based upon Air Loads

Condition: II

Constants:

$z1 = 28.80$

$z2 = 25.65$

$z4 = 3.15$

$x1 = 27.00$

$x2 = 90.00$

*All distances measured in inches

$zc = 0.90$

$xc = 180.00$

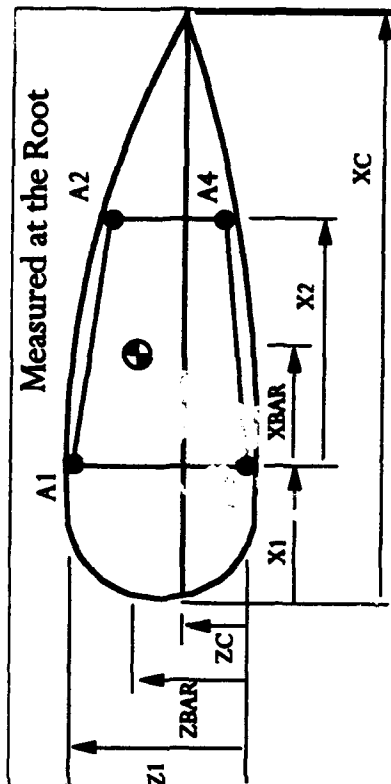
A1	A2	A3	A4	AreaTotal	xbar	zbar	ix	iz	izx
63	19	46	19	147	23.27	16.07	27,004	228,233	(5,695)

S1	S2	S3	S4
11758	12512	-17112	-10035

Allowable Stresses:

Upper: 80000

Lower: -44000



Torsion Across the Cross-Section

Condition: II

Required Inputs: Cm, XLE, CSAR and RMPX

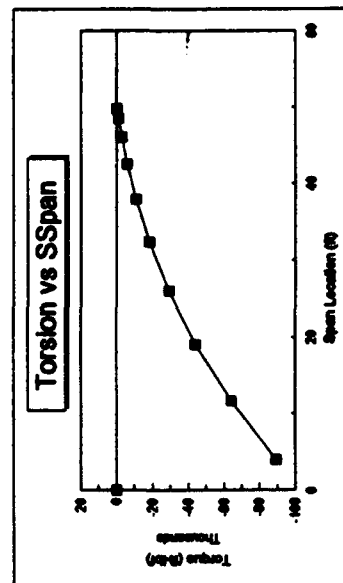
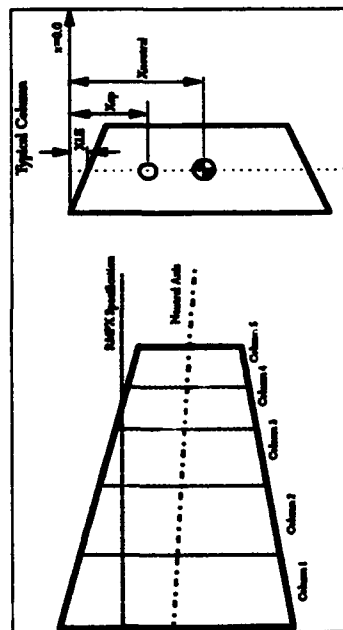
FreeStream Conditions:

Density= 0.0023769 Velocity= 420

CSAR= 10.83 RMPX= 1.000

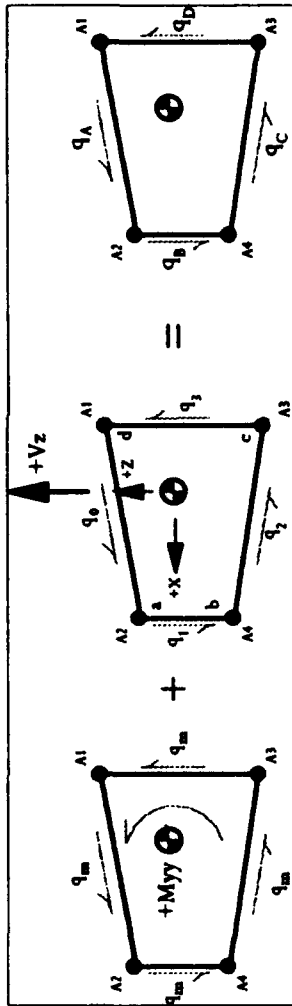
Note: zeros appear as blank cells

Column Number	area (sq ft)	N (Column Normal Force)	Cm	M (Column Moment)	d (ft)	XLE (ft)	XCP (Column Center of Pressure)	Xneutral (ft)	chord (ft)	d ² (ft ²)	Centroids=		I _{xx} (Column Moment of Inertia)	I _{yy} (Column Moment of Inertia)	I _{xy} (Column Product of Inertia)	Max (Field Torque at 0.5 Station)
											27.93% (Field Chord)	8.93% (Field Chord)				
1	111.20	(14,426)	0.1384	9,180		0.0530	1.64	3.95	14.25	2.31			(33,352)	8,120		(69,239)
2	96.71	(13,436)	0.1270	8,124		0.0228	1.60	3.52	12.70	1.92			(26,741)	6,798		(64,007)
3	81.09	(11,780)	0.1155	5,965		0.0223	1.51	3.11	11.21	1.60			(18,877)	3,901		(44,062)
4	65.50	(9,802)	0.1039	3,858		0.0200	1.37	2.72	9.81	1.35			(13,202)	2,462		(29,087)
5	50.89	(7,722)	0.1115	1,722		0.0118	1.22	2.37	8.54	1.14			(8,841)	1,442		(18,347)
6	37.77	(5,687)	0.1044	377		0.0116	1.07	2.08	7.44	0.99			(5,862)	770		(10,948)
7	26.65	(3,843)	0.1035	(381)		0.0114	0.90	1.81	6.51	0.90			(3,476)	362		(6,067)
8	17.37	(2,242)	0.1016	(651)		0.0112	0.71	1.61	5.80	0.90			(2,014)	139		(2,954)
9	9.71	(980)	0.1021	(509)		0.0111	0.49	1.47	5.32	0.99			(978)	35		(1,076)
10	3.14	(250)	0.1007	(33)		0.0111	0.87	1.41	5.07	0.54			(136)	0		(135)



Shear Flow Calculation

Condition: **II**



*All shear flows expressed in lb/in

C1=	3.95	q ₀ =	64	q _m =	-232		
C2=	-0.17	q ₁ =	999				
Q _{AX} =	182.11	q ₂ =	248	q _A =	-168		
Q _{BX} =	-245.39	q ₃ =	-2850	q _B =	767		
Q _{CX} =	-739.00			q _C =	17		
Q _{AZ} =	1267.96			q _D =	-3082		
Q _{BZ} =	1267.96						
Q _{CZ} =	-1070.20						

Buckling Considerations Based Upon Material Properties

Condition: **II**

Shear Flow in the Wing Upper Cover =	168	$\tau_{allow} = 32,000$ (lb/sq-in)	$\sigma_{se} = 44,000$
Minimum Thickness Based upon $\tau_{allow} =$	0.0053 (in)	Minimum Gauge Req'd Thickness =	0.0280 (in)
Desired Skin Thickness in Buckling Analysis =	0.0400	<u>Material Properties:</u>	
$K_s = 7.17$ (Shear Buckling Coefficient)	$K_c = 5.75$ (Compression Buckling Coefficient)	$E = 1.06E+07$ (lb-sq-in)	$\nu = 0.330$
$\tau_{cr} = 4,208$ (lb/sq-in)	$\sigma_{cr} = 3,374$ (lb/sq-in)	$K = 117.00$	$m = 5.00$
Distance Between Stringer Centerlines:	Number of Stringers:	Effective Width of Skin:	
$b = 5.16$ (in)	$n = 16$	$W_e = 1.39$ (in)	

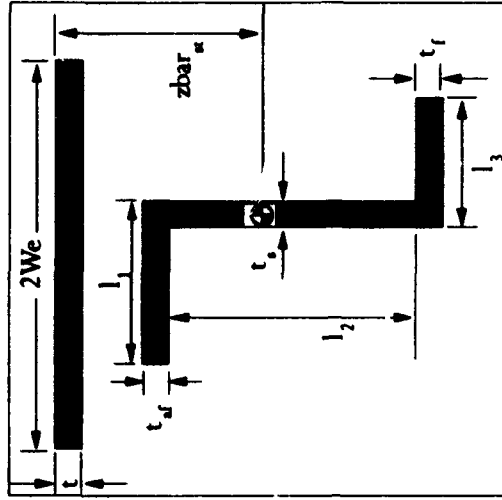
Condition: II

Stringer Design and Rib Spacing

$$A_s = 0.3099 \quad t_s = 0.0420$$

Proposed Section Lengths:

$L_1 = 0.5049$	$L_2 = 1.8293$	$L_3 = 1.2805$	
$L_2 = 0.8750$	$A_1 = 0.0242$	$z_{bar_{ST}} = 0.1886$	
$L_3 = 0.3534$	$A_2 = 0.0368$	$I_{xx} = 0.0151$	
$W_y = 0.0480$	$A_3 = 0.0119$	$r = 0.2211$	
$b = 0.0336$	$A_{skin} = 0.1112$	(Radius of Gyration)	
$C = 2.0000$	$\sigma_{1\alpha} = 44,212$	$L = 4.806$	
(Flexity Coefficient)	$\sigma_{2\alpha} = 90,165$	(Rib Spacing, inches)	
	$\sigma_{3\alpha} = 44,219$	$\sigma_{cc} = 44,000$	



PMARC Output Summary

Condition:

Required Inputs: Cl, %SSPAN, Desired Cl, Corresponding AOA, Freestream Conditions, SSPAN

AOA (degrees)	Cl
-2	0.2022
0	0.3972
2	0.5905
4	0.7841
6	0.9765
8	

Desired Cl: 0.2455

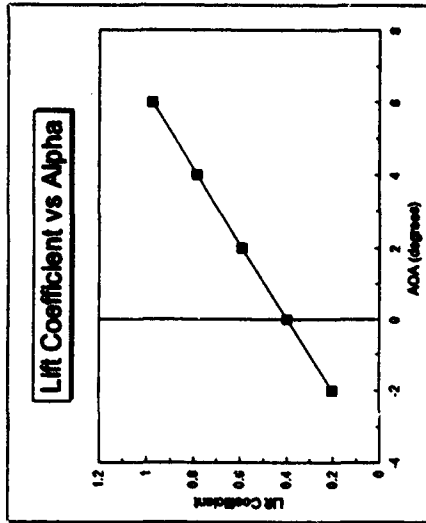
Corresponding AOA: 0.6414

Freestream Conditions:

Cos = 0.007

Density= 0.0023769 Velocity= 717 ft/sec

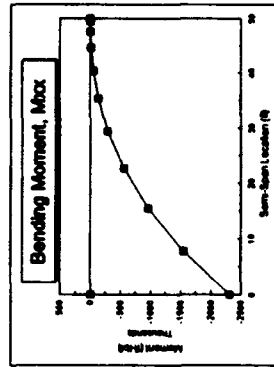
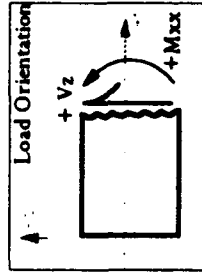
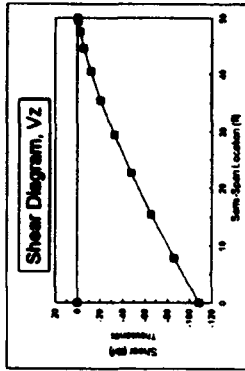
SSPAN= 50.00 ft



Spanwise Load and Moment Coefficients

Column	Column Center % of Semi-span	Column Center Location (ft)	Area (sq ft)	C _L	Lift (lb)	C _D	Normal Force with C _{do} (lb)	Induced Drag (lb)	C _{Ma}	Axial Force with C _{do} (lb)	Axial Force with C _{do} (lb)
1	0.00	3.90	111.20	-0.2146	(14,580)	-0.2141	(14,801)	516	0.0173	(1,175)	(703)
2	2.31	11.85	96.71	-0.2341	(13,832)	-0.2335	(13,845)	502	0.0187	(1,105)	(684)
3	4.62	19.10	81.09	-0.2448	(12,128)	-0.2441	(12,134)	421	0.0189	(988)	(641)
4	6.93	26.05	65.50	-0.2506	(10,026)	-0.2499	(10,032)	332	0.0207	(828)	(550)
5	9.24	32.35	50.89	-0.2533	(7,882)	-0.2530	(7,882)	258	0.0212	(659)	(443)
6	11.55	37.90	37.77	-0.2540	(5,861)	-0.2532	(5,861)	192	0.0212	(489)	(329)
7	13.86	42.50	26.65	-0.2499	(4,053)	-0.2482	(4,054)	140	0.0202	(329)	(216)
8	16.17	46.05	17.37	-0.2113	(2,455)	-0.2308	(2,450)	100	0.0176	(186)	(112)
9	18.48	48.45	9.71	-0.1692	(1,122)	-0.1883	(1,123)	69	0.0104	(62)	(20)
10	20.79	49.70	3.14	-0.1422	(273)	-0.1436	(275)	38	0.0050	6	19
11	23.10	0.00	0.00	0.00	0	0	0	0	0	0	0
12	25.41	0.00	0.00	0.00	0	0	0	0	0	0	0
13	27.72	0.00	0.00	0.00	0	0	0	0	0	0	0
14	30.03	0.00	0.00	0.00	0	0	0	0	0	0	0
15	32.34	0.00	0.00	0.00	0	0	0	0	0	0	0
Totals:			500		(72,224)		(72,036)	2,598		(5,813)	

Condition: III



**Shear and Moment
Diagram Construction
(Normal Loading)**

Platform Column No.	Left Edge Location ft	Center Location ft	Limit Load Normal Force lb	Ultimate Load Normal Force lb	Shear (V ₁) (at Left Edge) lb	Bending Moment (M ₁) (at Left Edge) ft-lb
1	0.00	3.90	(14,601)	(21,901)	(108,424)	(2,314,075)
2	7.82	11.65	(13,845)	(20,767)	(86,523)	(1,552,051)
3	15.45	19.10	(12,134)	(18,201)	(65,756)	(970,798)
4	22.70	26.05	(10,032)	(15,048)	(47,555)	(559,589)
5	29.39	32.35	(7,892)	(11,838)	(32,507)	(291,707)
6	35.36	37.90	(5,861)	(8,792)	(20,868)	(133,275)
7	40.45	42.50	(4,054)	(6,082)	(11,877)	(50,492)
8	44.55	46.05	(2,459)	(3,889)	(5,795)	(14,286)
9	47.55	48.45	(1,126)	(1,691)	(2,108)	(2,414)
10	49.38	49.70	(277)	(415)	(415)	(133)
11	50.00	0.00	0	0	0	0
12	0.00	0.00	0	0	0	0
13	0.00	0.00	0	0	0	0
14	0.00	0.00	0	0	0	0
15	0.00	0.00	0	0	0	0

Moment Construction

Column 1	Column 2	Column 3	Column 4	Column 5	Column 6	Column 7	Column 8	Column 9	Column 10	Column 11	Column 12	Column 13	Column 14	Column 15
(85,418) (241,335) (347,635) (362,011) (362,947) (333,215) (256,472) (146,857) (61,949) (20,821)	(79,537) (206,366) (274,352) (290,362) (294,466) (210,913) (141,913) (86,722) (17,378)	(66,433) (159,513) (260,046) (197,378) (164,519) (112,898) (55,917) (14,216)	(60,412) (114,239) (132,637) (120,417) (85,127) (43,864) (11,262)	(58,941) (74,819) (79,731) (81,491) (52,289) (8,427)	(22,331) (43,429) (39,439) (22,141) (5,869)	(12,467) (20,869) (13,531) (3,839)	(5,533) (8,597) (2,157)	(1,522) (662)	(133)	0	0	0	0	0
(2,314,075)	(1,552,051)	(970,798)	(559,589)	(291,707)	(133,275)	(50,492)	(14,286)	(2,414)	(133)	0	0	0	0	0

The graph shows the bending moment distribution along the span of the bridge. The x-axis represents the transverse distance in meters, ranging from -10 to 10, and the span-end location in meters, ranging from 0 to 10. The y-axis represents the bending moment M_{zz} in kNm, ranging from 0 to 140. The curve is parabolic, with the maximum bending moment occurring at the center of the span (0m).

Transverse Distance (m)	Span-End Location (m)	Bending Moment M_{zz} (kNm)
-10	0	0
-8	2	10
-6	4	35
-4	6	70
-2	8	110
0	10	120
2	8	110
4	6	70
6	4	35
8	2	10
10	0	0

	Column 1	Column 2	Column 3	Column 4	Column 5	Column 6	Column 7	Column 8	Column 9	Column 10	Column 11	Column 12	Column 13	Column 14	Column 15
--	----------	----------	----------	----------	----------	----------	----------	----------	----------	-----------	-----------	-----------	-----------	-----------	-----------

	Column 1	Column 2	Column 3
1	(4,112)	(3,988)	(3,512)
2	(12,129)	(10,863)	(8,748)
3	(18,377)	(15,042)	(11,230)
4	(21,496)	(16,300)	(11,071)
5	(21,487)	(14,833)	(8,762)
6	(18,689)	(11,220)	(6,119)
7	(13,750)	(6,419)	(5,138)
8	(7,732)	(2,146)	(1,012)
9	(1,480)	1,198	990
10	1,422	0	0
11	0	0	0
12	0	0	0
13	0	0	0
14	0	0	0
15	0	0	0
16	0	0	0
17	0	0	0
18	0	0	0
19	0	0	0
20	0	0	0
21	0	0	0
22	0	0	0
23	0	0	0
24	0	0	0
25	0	0	0
26	0	0	0
27	0	0	0
28	0	0	0
29	0	0	0
30	0	0	0
31	0	0	0
32	0	0	0
33	0	0	0
34	0	0	0
35	0	0	0
36	0	0	0
37	0	0	0
38	0	0	0
39	0	0	0
40	0	0	0
41	0	0	0
42	0	0	0
43	0	0	0
44	0	0	0
45	0	0	0
46	0	0	0
47	0	0	0
48	0	0	0
49	0	0	0
50	0	0	0
51	0	0	0
52	0	0	0
53	0	0	0
54	0	0	0
55	0	0	0
56	0	0	0
57	0	0	0
58	0	0	0
59	0	0	0
60	0	0	0
61	0	0	0
62	0	0	0
63	0	0	0
64	0	0	0
65	0	0	0
66	0	0	0
67	0	0	0
68	0	0	0
69	0	0	0
70	0	0	0
71	0	0	0
72	0	0	0
73	0	0	0
74	0	0	0
75	0	0	0
76	0	0	0
77	0	0	0
78	0	0	0
79	0	0	0
80	0	0	0
81	0	0	0
82	0	0	0
83	0	0	0
84	0	0	0
85	0	0	0
86	0	0	0
87	0	0	0
88	0	0	0
89	0	0	0
90	0	0	0
91	0	0	0
92	0	0	0
93	0	0	0
94	0	0	0
95	0	0	0
96	0	0	0
97	0	0	0
98	0	0	0
99	0	0	0
100	0	0	0
101	0	0	0
102	0	0	0
103	0	0	0
104	0	0	0
105	0	0	0
106	0	0	0
107	0	0	0
108	0	0	0
109	0	0	0</

[illegible][illegible][illegible]

Area Distribution based upon Air Loads

Condition: III

Constants: $z1=$ 28.80 $z2=$ 25.85 $z4=$ 3.15 $x1=$ 27.00 $x2=$ 90.00

*All distances measured in inches

$z_c=$ 9.90 $x_c=$ 180.00

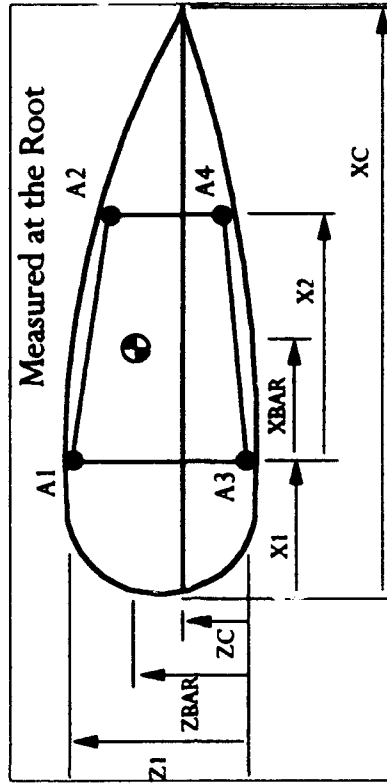
A1	A2	A3	A4	Area total	xbar	zbar	I	Iz	Izx
83	19	46	19	147	23.27	16.07	27.004	228,233	(5,695)

S1	S2	S3	S4
12444	12058	-17374	-11231

Allowable Stresses:

Upper: 60000

Lower: -44000



Torsion Across the Cross-Section

Condition: III

Required Inputs: Cm, XLE, CBAR and RMPX

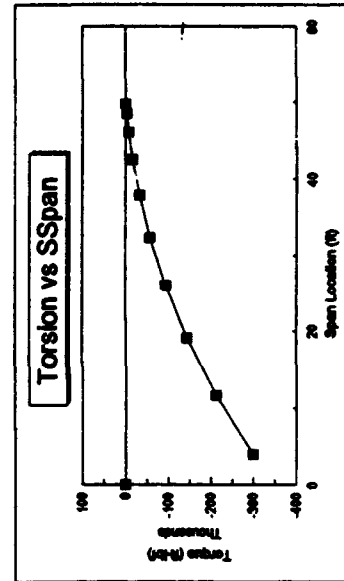
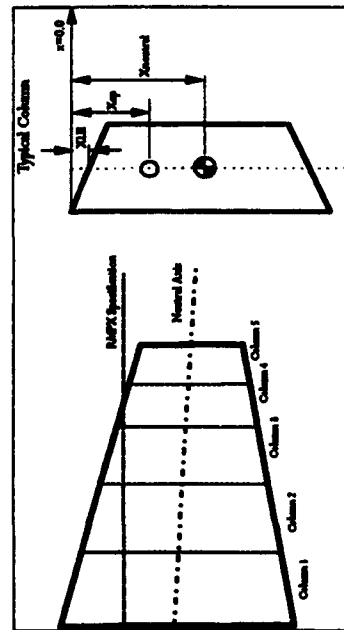
FreeStream Conditions:

Density= 0.0023789 Velocity= 717

CBAR= 10.83 RMPX= 1.000

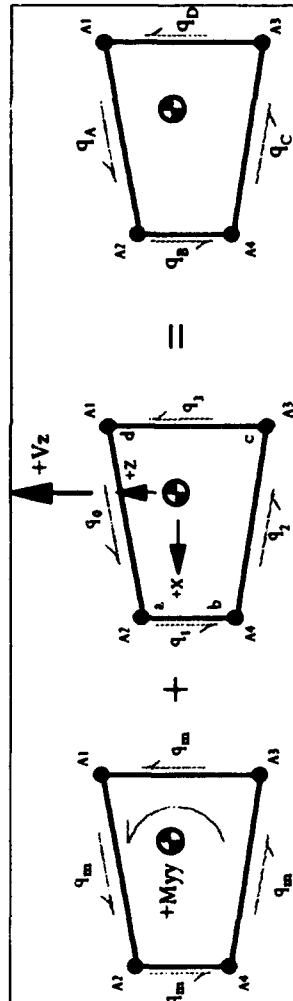
Note: zeros appear as blank cells

Column Number	area (sq.in.)	N (Column Normal Force) (lb)	Cm	M (Column Moment) (lb-in)	d (in.)	XLE (in.)	XCP (Column Center of Pressure) (in.)	Xneutral (in.)	chord (in.)	d _c (Moment Arm from Column Centerline) (in.)	Centroid=		I _{yy} (Column Moment of Inertia) (in ⁴)	I _{zz} (Column Moment of Inertia) (in ⁴)	M _{zz} (Total Torque at a Station) (lb-in)
											27.93% (Half Chord)	8.93% (Half Chord)			
1	111.20	(14,546)		(46,281)			-2.18	3.95	14.25	6.13			(89,178)	2,701	(298,979)
2	96.71	(13,797)		(34,491)			-1.50	3.52	12.70	5.02			(89,268)	1,949	(212,502)
3	81.08	(12,084)		(26,345)			-1.18	3.11	11.21	4.28			(51,828)	1,320	(145,184)
4	65.50	(10,000)		(19,948)			-0.98	2.72	9.81	3.70			(37,048)	832	(94,678)
5	50.89	(7,867)		(14,413)			-0.83	2.37	8.54	3.20			(25,176)	483	(58,460)
6	37.77	(5,843)		(9,971)			-0.71	2.08	7.44	2.77			(18,168)	251	(33,769)
7	26.65	(4,041)		(6,489)			-0.61	1.81	6.51	2.41			(9,743)	110	(17,854)
8	17.37	(2,450)		(3,950)			-0.57	1.61	5.80	2.18			(5,341)	34	(8,222)
9	9.71	(1,123)		(1,895)			-0.89	1.47	5.32	2.18			(2,427)	0	(2,915)
10	3.14	(275)		(372)			-0.35	1.41	5.07	1.76			(483)	(5)	(488)



Shear Flow Calculation

Condition: III



*All shear flows expressed in lb/in

C1=	4.04	$q_0 =$	135	$q_m =$	-777
C2=	-0.13	$q_1 =$	1029		
$Q_{Ax} =$	182.11	$q_2 =$	196	$q_A =$	-642
$Q_{Bx} =$	-245.39	$q_3 =$	-2924	$q_B =$	252
$Q_{Cx} =$	-739.00			$q_C =$	-581
$Q_{Az} =$	1267.96			$q_D =$	-3701
$Q_{Bz} =$	1267.96				
$Q_{Cz} =$	-1070.20				

Buckling Considerations Based Upon Material Properties

Condition: III

Shear Flow in the
Wing Upper Cover = 642 $\tau_{allow} = 32,000$ $\sigma_{SE} = 44,000$
(lb/sq-in)

Minimum Thickness
Based upon $\tau_{allow} = 0.0201$ Minimum Gauge
(in) Req'd Thickness = 0.0280
(in)

Desired Skin Thickness
in Buckling Analysis = 0.0400

Material Properties:

$K_S = 7.17$ $E = 1.06E+07$ $\nu = 0.330$
(Shear Buckling Coefficient) (lb-sq-in)

$K_C = 5.75$ $K = 117.00$ $m = 5.00$
(Compression Buckling Coefficient)

$\tau_{CR} = 16,059$ $\sigma_{CR} = 12,878$
(lb/sq-in) (lb/sq-in)

Distance Between Stringer Centerlines:

Number of Stringers:

Effective Width of Skin:

$b = 2.64$
(in)

$n = 33$

$W_e = 0.85$
(in)

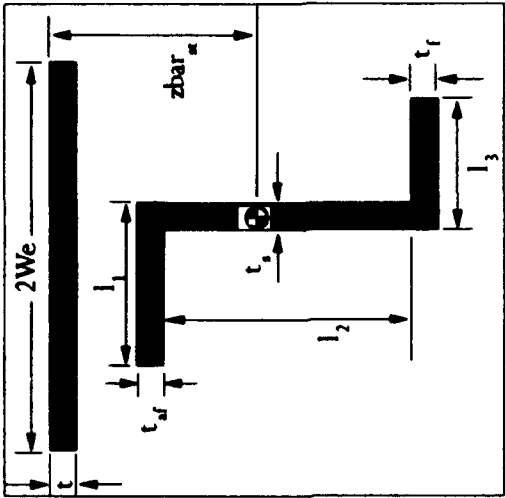
Stringer Design
and
Rib Spacing

Condition: III

$$A_s = 0.1586 \qquad t_s = 0.0420$$

Proposed Section Lengths:

L1 = 0.5049	L2 = 2.1849	L3 = 0.6555	
L2 = 0.8750	A1 = 0.0242	zbar _{st} = 0.2398	
L3 = 0.3534	A2 = 0.0368	I _{xx} = 0.0136	
t _w = 0.0480	A3 = 0.0119	r = 0.2923	
t _b = 0.0336	Ask _{in} = 0.0683	(Radius of Gyration)	
C = 2.0000	σ1 _α = 44,212	L = 6.355	
(Flexity Coefficient)	σ2 _α = 90,165	(Rib Spacing, inches)	
	σ3 _α = 44,219	σ _{cc} = 44,000	



PMARC Output Summary

Condition: IV

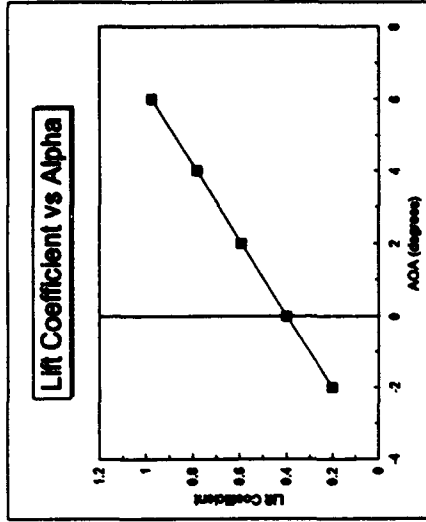
Required Inputs: Cl, %SSPAN, Desired Cl, Corresponding AOA, Freestream Conditions, SSPAN

AOA (degrees)	Cl
-2	0.2022
0	0.5072
2	0.8005
4	0.7841
6	0.9765
8	

Desired Cl: 0.8503
Corresponding AOA: 4.7806

Freestream Conditions: $C_{\infty} = 0.007$
Density: 0.0023769 Velocity: 717
(slugs/ft³) (ft/sec)

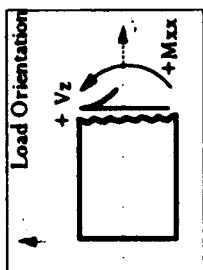
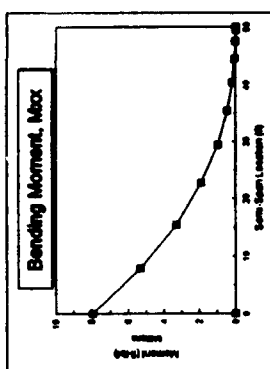
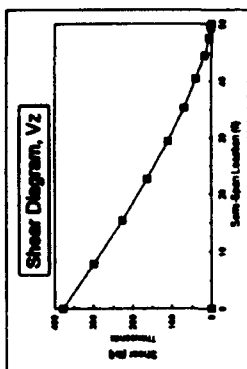
SSPAN= 50.00



Spanwise Load and Moment Coefficients

Column	Column Center % of Semi-span	Column Center Location (ft)	Area (sqft)	C_L	Lift (lb)	C_D	Normal Force with Cdo (lb)	Induced Drag (lb)	C_{Di}	Axial Force (lb)	Axial Force with Cdo (lb)
1	7.8%	3.90	111.20	0.7746	52,840	0.1741	52,832	1,892	0.0249	(2,704)	(2,230)
2	23.3%	11.85	96.71	0.5070	48,504	0.2502	48,483	1,507	0.0165	(2,547)	(2,134)
3	38.2%	19.10	81.09	0.3002	42,222	0.3512	42,201	1,194	0.0071	(2,334)	(1,988)
4	52.1%	26.05	65.50	0.1739	34,930	0.4718	34,909	908	0.0027	(2,009)	(1,730)
5	64.7%	32.35	50.89	0.1024	27,438	0.5811	27,398	684	0.0017	(1,608)	(1,391)
6	76.8%	37.90	37.77	0.0734	20,200	0.6742	20,186	521	0.0008	(1,168)	(1,007)
7	88.0%	42.50	26.85	0.0403	13,885	0.7597	13,882	407	0.0003	(738)	(624)
8	92.1%	46.05	17.37	0.0209	8,031	0.7867	8,037	306	0.0001	(306)	(282)
9	95.8%	48.45	9.71	0.0100	3,588	0.8030	3,582	205	0.0001	(85)	(54)
10	98.5%	49.70	3.14	0.0048	847	0.8171	858	156	0.0001	85	98
11		0.00	0.00		0		0	0		0	0
12		0.00	0.00		0		0	0		0	0
13		0.00	0.00		0		0	0		0	0
14		0.00	0.00		0		0	0		0	0
15		0.00	0.00		0		0	0		0	0
Totals:			500		252,086		251,835	7,580		(13,482)	

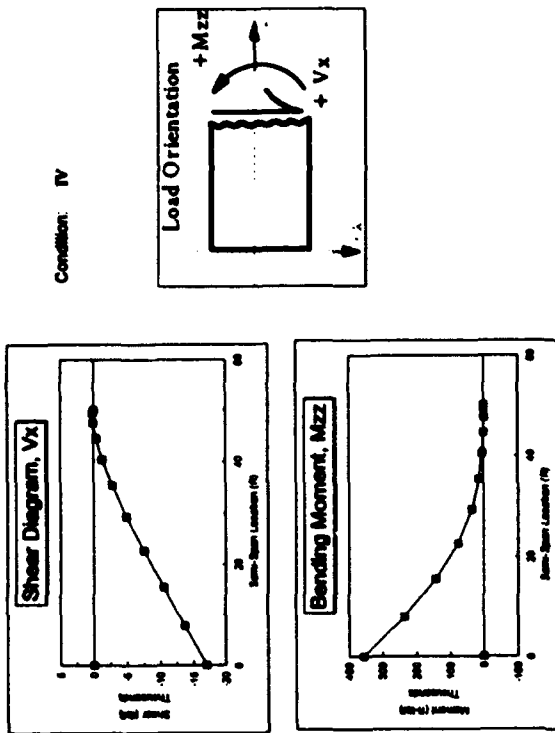
Condition: IV



Shear and Moment Diagram Construction (Normal Loading)			
Pier/Column No.	Left Edge Location (ft)	Center Location (ft)	Limit Load Ultimate Load (kips)
1	0.00	3.90	52.632
2	7.82	11.65	48.468
3	15.45	19.10	42.201
4	22.70	26.05	34.909
5	29.39	32.35	27.416
6	35.36	37.90	20.186
7	40.45	42.50	13.682
8	44.55	46.05	8.037
9	47.55	48.45	3.596
10	49.38	49.70	856
11	50.00	0.00	0
12	0.00	0.00	0
13	0.00	0.00	0
14	0.00	0.00	0
15	0.00	0.00	0

Moment Contributions

Column No.	Column 1	Column 2	Column 3	Column 4	Column 5	Column 6	Column 7	Column 8	Column 9	Column 10	Column 11	Column 12	Column 13	Column 14	Column 15
1	397.837	278.919	221.680	175.417	121.726	78.907	42.071	19.093	10.000	0	0	0	0	0	0
2	947.468	714.041	565.081	396.644	287.689	146.532	87.508	21.034	6.529	2.787	0	0	0	0	0
3	1,350.382	1,084.263	864.391	684.232	509.682	328.889	198.089	43.146	0	0	0	0	0	0	0
4	1,147.882	916.778	678.750	496.349	359.837	250.899	158.678	70.586	0	0	0	0	0	0	0
5	872.213	711.728	565.136	391.468	282.837	182.796	112.808	41.142	0	0	0	0	0	0	0
6	558.135	460.695	368.095	251.678	182.796	112.808	70.586	41.142	0	0	0	0	0	0	0
7	281.204	219.128	177.979	138.678	102.796	70.586	43.146	21.034	6.529	2.787	0	0	0	0	0
8	63.971	53.066	44.064	34.753	26.142	16.456	11.808	6.529	2.787	0	0	0	0	0	0
9	0	0	0	0	0	0	0	0	0	0	0	0	0	0	0
10	0	0	0	0	0	0	0	0	0	0	0	0	0	0	0
11	0	0	0	0	0	0	0	0	0	0	0	0	0	0	0
12	0	0	0	0	0	0	0	0	0	0	0	0	0	0	0
13	0	0	0	0	0	0	0	0	0	0	0	0	0	0	0
14	0	0	0	0	0	0	0	0	0	0	0	0	0	0	0
15	0	0	0	0	0	0	0	0	0	0	0	0	0	0	0
16	7,689.843	6,312.466	3,308.927	1,883.656	979.222	441.363	184.632	46.745	7.821	412	0	0	0	0	0



Shear and Moment Diagram Construction (Axial Loading)				
Platform Column No.	Left Edge Location (ft)	Center Location (ft)	Limit Load (ft-lb)	Ultimate Load (ft-lb)
1	0.00	3.90	(2,230)	(3,345)
2	7.82	11.65	(2,134)	(3,202)
3	15.45	19.10	(1,988)	(2,982)
4	22.70	26.05	(1,730)	(2,594)
5	29.39	32.35	(1,391)	(2,086)
6	35.36	37.90	(1,007)	(1,510)
7	40.45	42.50	(624)	(936)
8	44.55	46.05	(292)	(438)
9	47.55	48.45	(54)	(81)
10	49.38	49.70	98	147
11	50.00	0.00	0	0
12	0.00	0.00	0	0
13	0.00	0.00	0	0
14	0.00	0.00	0	0
15	0.00	0.00	0	0

Moment Construction				
Column 1	Column 2	Column 3	Column 4	Column 5
(13,046)	(12,263)	(10,864)	(8,981)	(6,175)
(37,309)	(33,836)	(27,501)	(22,130)	(12,860)
(66,964)	(47,287)	(35,254)	(18,533)	(12,271)
(87,988)	(51,171)	(33,869)	(10,231)	(7,300)
(87,227)	(46,419)	(25,319)	(2,080)	(1,547)
(20,791)	(22,461)	(13,408)	3,980	2,984
(20,177)	(18,791)	(2,878)	0	0
(3,533)	(3,288)	0	0	0
7,327	6,174	5,049	0	0
0	0	0	0	0
0	0	0	0	0
0	0	0	0	0
0	0	0	0	0
(368,161)	(238,122)	(143,884)	(78,847)	(37,148)

Column 6	Column 7	Column 8	Column 9	Column 10	Column 11	Column 12	Column 13	Column 14	Column 15
(3,835)	(1,919)	(657)	(73)	47	0	0	0	0	0
(6,883)	(2,454)	(317)	(317)	317	0	0	0	0	0
(4,884)	(849)	756	0	0	0	0	0	0	0
(1,053)	2,114	1,364	0	0	0	0	0	0	0
(14,151)	(3,886)	(215)	244	47	0	0	0	0	0

Area Distribution based upon Air Loads

Condition: IV

Constants: $z1=$ 28.80 $z2=$ 25.65 $z4=$ 3.15 $x1=$ 27.00 $x2=$ 90.00

*All distances measured in inches

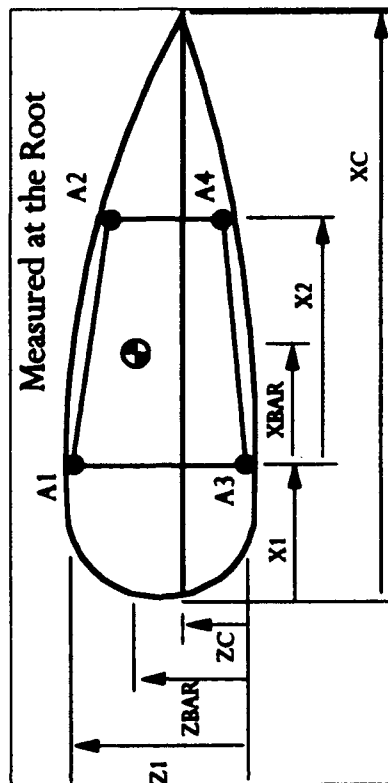
$z_c=$ 9.90 $x_c=$ 180.00

A1	A2	A3	A4	Area total	xbar	zbar	ix	iz	izx
63	19	46	19	147	23.27	16.07	27.004	228.233	(5.695)

s1	s2	s3	s4
-43619	-38706	58683	41205

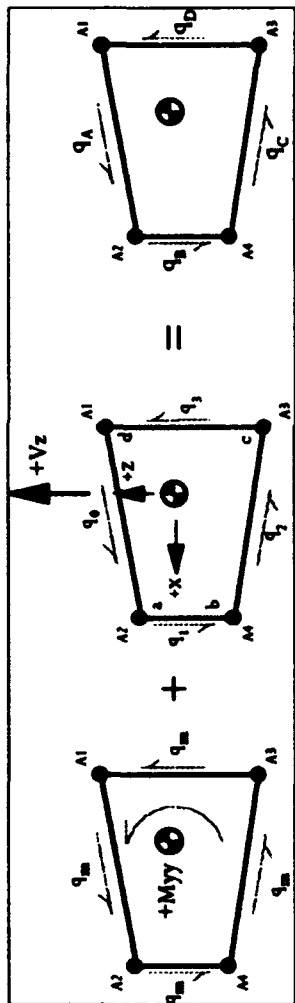
Allowable Stresses:

Upper: -44000
Lower: 60000



Shear Flow Calculation

Condition: IV



*All shear flows expressed in lb/in

C1=	-14.06	$q_0 =$	-688	$q_m =$	-550
C2=	0.28	$q_1 =$	-3598		
$Q_{Ax} =$	182.11	$q_2 =$	-499	$q_A =$	-1238
$Q_{Bx} =$	-245.39	$q_3 =$	10185	$q_B =$	-4148
$Q_{Cx} =$	-739.00			$q_C =$	-1049
$Q_{Ax} =$	1267.96			$q_D =$	9635
$Q_{Bx} =$	1267.96				
$Q_{Cx} =$	-1070.20				

Condition:

Shear Flow in the Wing Upper Cover =	1238	$\tau_{allow} = 32,000$ (lb/in ²)	$\sigma_{sg} = 44,000$
--------------------------------------	------	--	------------------------

Minimum Thickness Based upon Tau_{allow}	Minimum Gauge Req'd Thickness =
0.0387 (in)	0.0280 (in)

**Desired Skin Thickness
in Buckling Analysis = 0.0400**

Material Properties:

$K_S = 7.17$ (Shear Buckling Coefficient)	$K_C = 5.75$ (Compression Buckling Coefficient)	$E = 1.06E+07$ (lb-sq-in)	$\nu = 0.330$
		$K = 117.00$	$m = 5.00$

$$\tau_{cr} = 30,948 \text{ (lb/sq-in)} \quad \sigma_{cr} = 24,818 \text{ (lb/sq-in)}$$

Distance Between Stringer Centerlines:

Number of Stringers:

Effective Width of Skin:

$$b = 1.90 \text{ (in)}$$
$$n = 46$$
$$We = 0.74 \quad (m)$$

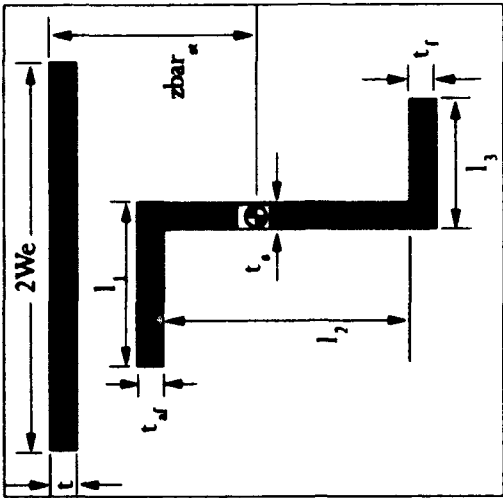
Stringer Design
and
Rib Spacing

Condition: IV

$$A_s = 0.1143 \qquad t_s = 0.0420$$

Proposed Section Lengths:

	L1 =	0.6745	L2 =	1.5739	L3 =	0.4722	
L1 =	0.5049		A1 =	0.0242		zbar _{str} =	0.2544
L2 =	0.8750		A2 =	0.0368		l _{xx} =	0.0131
L3 =	0.3534		A3 =	0.0119		r =	0.3386
l _w =	0.0480		A _{sk_{in}} =	0.0596		(Radius of Gyration)	
b =	0.0336					L =	7.362
C =	2.0000		σ _{1α} =	44,212		(Rib Spacing, inches)	
(Fltly Coefficient)			σ _{2α} =	90,165			
			σ _{3α} =	44,219		σ _{cc} =	44,000



APPENDIX C

This appendix was developed to demonstrate the process of design variation for optimization, more commonly known as a trade-study. This appendix will consider two specific cases that support study within the current core structures curriculum at NPS. The first study is intended for use within the introductory structures course, while the second study is aimed at the advanced structures student.

A. LOCATING THE FORWARD SPAR

Earlier in Chapter III, it was presented that the forward spar location will generally fall between the 12% and 17% chord position, assuming a conventional two spar configuration. Since this range of decisions is available to the designer, he or she must determine the final location. Since the average introductory level engineer lacks considerable design experience, a reasonable and quantitative process must be devised to lead one to that final decision.

One recommendation is to begin first by reviewing what parameters have been used as inputs in determining the strength of the wing box. Considering the spar cap area sizing spreadsheet, one observes that several inputs are affected by changing the location of the forward spar. These inputs include X_1 , X_2 , Z_1 and Z_c . Through the use of a scale drawing of the wing's cross-section, it is possible to locate the inputs required for a wide range of spar locations.

However, before entering a long trial and error process of arbitrarily entering a series of spar locations into the spreadsheet, a short review of anticipated outputs can prove very beneficial in reducing computation time and increasing one's understanding of the principles at work. One or more specific outputs should be identified as being uniquely related to specific inputs. For this problem, the first obvious output to consider is total area of the spar caps. Since maximum strength in comparison to structural weight is sought, the smaller the total area at a fixed allowable stress, the greater the overall strength-to-weight ratio. However, moving the structure's centroid may also affect the shear flow due to torsion around the body. As shear flow increases, so does skin thickness, which serves to increase total weight. Table 7 is a summary of data for moving the forward spar within the range of 12%-17% of chord.

TABLE 7

Spar Location	Total Area (in ²)	Shear Flow, q_A (lb/in)
12%	152	998
13%	150	1,007
14%	148	1,015
15%	147	965
16%	142	1,018
17%	142	960

As observed in Table 7, moving the spar aft to 17% reduces the total area without a major fluctuation in shear flow in the upper wing cover. Returning to the discussion on anticipation of results. Consider the NACA 4418 airfoil used in the wing cross section. For the 12%-17% chord range, as one moves aft a sizeable increase in the wingbox height

occurs. This implies that \bar{z} is also increasing in the calculation of the bending stresses. Yet, \bar{x} is decreasing at the same time, so why the inconsistency in results? The answer lies in the sensitivity to change of the two parameters. The chord change from 12% to 13% produces a relative increase in \bar{z} compared to the height of the forward spar that is much greater than the reduction in \bar{x} compared to the overall length of the wingbox.

This revelation should lead the designer to two additional considerations. The first issue that should come to mind is the question of consistency. Does this trend in improved structural performance hold for moving the forward spar aft for all airfoils? Hopefully, the beginning student would respond no, since the rate of vertical change to horizontal change is a function unique to every airfoil design. Second, what other assumptions were made in the development of Table 7? Recall, the rear spar was fixed at 65% chord. That fact should warrant at least an investigation of the points in Table 7 at a different rear spar location. A good place to start might be the forward limit of travel for the rear spar, which is generally taken to be 50 % of the chord.

B. RIB SPACING CONSIDERATIONS

In Chapter IV of this thesis, a method was developed based upon previous design experience to optimize a stringer size and location for material strength. When the issue of total weight enters that process, often very different design decisions will result that will change one's recommendations rather drastically. Recall that as the rib spacing is increased, the stringer cross-sectional area must also increase to preclude column buckling of the stiffener. Also an increase in the wing skin thickness reduces the effective working

shear flow carried in the skin. As the shear flow drops, the distance between stringers increases. This distance increase will imply a reduction in the total number of stringers, and hence lower total stringer weight.

These points should lead the designer to consider the effect of increasing skin thickness on total weight of the wing. Does an optimum condition exist that will carry the applied loads for lowest total wing weight? Additionally, what input parameters must be considered in such a study? These types of questions are fundamental for efficient and effective work in the field of engineering design.

To determine the input parameters, consider those variables in the current structure that add weight to the wing. The components considered thus far include the spar caps, the wing skin and the ribs. Knowing the density of the material and the dimensions of each structure, it is possible to estimate the weight of each of these components. In the case of the spar caps, the cross-section area times the length of the semi-span yields the volume. Yet this volume does not change when the skin thickness is varied, therefore it does not enter into this particular trade study.

For a quick example of trade study calculations that are relevant, the following assumptions are made for analysis:

- Only the wing skin on the top of the wing between the forward and rear spar will be considered for total wing weight estimation.
- The initial study will consider a wing of constant chord, equal to the root chord dimension (a rectangular wing).
- The only wing skin associated variable affecting total weight will be skin thickness.

Note that to properly determine the location of the rib spacing, the actual wing chord at various spanwise stations must be accounted for. Turning to the only remaining variable, some estimation process must be derived for the weight of the ribs. For the results depicted in Figure 36, the following steps were used to calculate individual rib weight:

- Determine the cross-sectional area bounded by the four spar caps to use as the external boundary of the rib.
- Assume only 70% of that area contains sheet metal, that allows for cutouts and weight reduction.
- The rib weight is the product of the reduced cross-sectional area, material density and specified rib skin thickness. For illustration purposes, three different skin thickness were used, beginning with the minimum gauge value. Actual determination of the required rib skin thickness is generally a detail design procedure.

Figure 36 is the result of the spreadsheet that follows at the end of this appendix. The calculations are based upon the same equations developed in chapter IV of this thesis. However, one distinction is made for this method that differs from the previous development. Recall earlier, the rib spacing (L), was determined by first specifying the stringer cross-section geometry, and then solving for I_{xx} and the radius of gyration. When L is specified first, the designer must then solve for the radius of gyration and required moment of inertia. The geometry must then be developed to satisfy the resultant moment of inertia and radius of gyration. This method appears to require a bit more iteration on the part of the designer, but does lead to an overall reduced weight. Hopefully, these

studies offer some insight into the nature of optimization that serves to build a skill that can be applied to a wide range of engineering decisions.

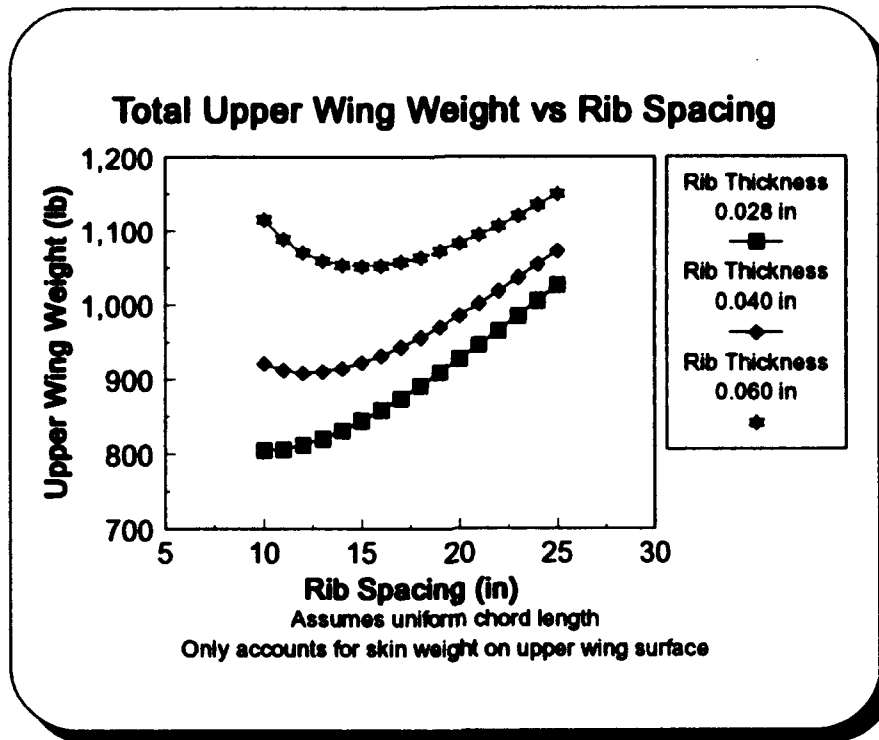


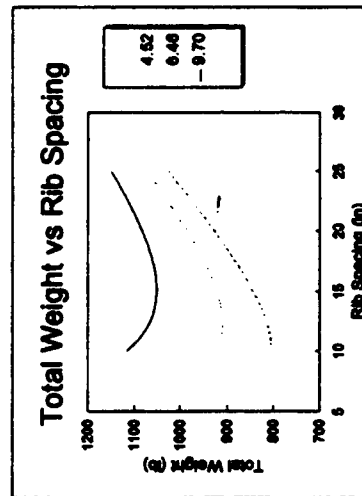
Figure 36

Rib Spacing Trade Study

Skin		Effective Shear Stress		Stiffener Spacing		Normal Buckling Stress		Effective Skin Width		Total Stiffeners (Wing Root)		Stringer Area		Total Stringer Weight		Upper Skin Weight	
Thickness	t	Effective Shear Stress	τ	Stiffener Spacing	Min. Lb	Buckling Stress	σ_{cr}	Effective Skin Width	W _{eff}	Total Stiffeners (Wing Root)	A _{st}	Stringer Area	W _{st}	Total Stringer Weight	W _{st}	Upper Skin Weight	W _{us}
(in)	(in)	(ksi)	(ksi)	(in)	(in)	(ksi)	(ksi)	(in)	(in)	(in)	(in)	(in)	(in)	(lb)	(lb)	(lb)	(lb)
0.040	0.040	30,950	1,904	1,904	24,820	23,639	23,639	0.745	46	46	0.114	0.114	317.144	218.00	218.00	218.00	218.00
0.042	0.042	29,476	2,049	2,049	22,694	21,583	21,583	0.787	43	43	0.129	0.129	332.455	228.80	228.80	228.80	228.80
0.044	0.044	28,136	2,197	2,197	20,664	19,558	19,558	0.831	40	40	0.145	0.145	347.700	237.80	237.80	237.80	237.80
0.046	0.046	26,913	2,348	2,348	19,093	18,396	18,396	0.875	37	37	0.162	0.162	362.877	248.40	248.40	248.40	248.40
0.048	0.048	25,792	2,503	2,503	17,729	17,118	17,118	0.920	35	35	0.180	0.180	377.966	259.20	259.20	259.20	259.20
0.050	0.050	24,760	2,661	2,661	16,547	16,013	16,013	0.966	33	33	0.200	0.200	393.024	270.00	270.00	270.00	270.00
0.052	0.052	23,808	2,823	2,823	15,513	15,043	15,043	1.012	31	31	0.220	0.220	407.990	280.80	280.80	280.80	280.80
0.054	0.054	22,928	2,987	2,987	14,600	14,183	14,183	1.059	29	29	0.242	0.242	422.893	291.60	291.60	291.60	291.60
0.056	0.056	22,107	3,154	3,154	13,758	13,364	13,364	1.106	28	28	0.265	0.265	437.701	302.40	302.40	302.40	302.40
0.058	0.058	21,345	3,325	3,325	12,988	12,613	12,613	1.155	26	26	0.289	0.289	452.444	313.20	313.20	313.20	313.20
0.060	0.060	20,633	3,498	3,498	12,275	11,913	11,913	1.204	25	25	0.315	0.315	467.108	324.00	324.00	324.00	324.00
0.062	0.062	19,968	3,675	3,675	11,600	11,218	11,218	1.253	23	23	0.342	0.342	481.695	334.80	334.80	334.80	334.80
0.064	0.064	19,344	3,854	3,854	11,000	10,643	10,643	1.303	22	22	0.370	0.370	496.201	345.60	345.60	345.60	345.60
0.066	0.066	18,758	4,036	4,036	10,480	10,158	10,158	1.354	21	21	0.400	0.400	510.625	356.40	356.40	356.40	356.40
0.068	0.068	18,208	4,221	4,221	9,999	9,709	9,709	1.405	20	20	0.431	0.431	524.966	367.20	367.20	367.20	367.20
0.070	0.070	17,688	4,409	4,409	9,549	9,243	9,243	1.457	19	19	0.463	0.463	539.226	378.00	378.00	378.00	378.00

Total Rib Cross-Sectional Area, without cutouts: 23,953 (sq-in)

Rib		Rib Thickness		Rib Weight		Upper Wing Wt	
Spacing	L	(in)	(in)	(lb)	(lb)	(lb)	(lb)
10	10	0.040	0.040	4.52	4.52	1115	1115
11	11	0.042	0.042	4.52	4.52	1088	1088
12	12	0.044	0.044	4.52	4.52	1070	1070
13	13	0.046	0.046	4.52	4.52	1059	1059
14	14	0.048	0.048	4.52	4.52	1053	1053
15	15	0.050	0.050	4.52	4.52	1051	1051
16	16	0.052	0.052	4.52	4.52	1052	1052
17	17	0.054	0.054	4.52	4.52	1057	1057
18	18	0.056	0.056	4.52	4.52	1063	1063
19	19	0.058	0.058	4.52	4.52	1072	1072
20	20	0.060	0.060	4.52	4.52	1082	1082
21	21	0.062	0.062	4.52	4.52	1094	1094
22	22	0.064	0.064	4.52	4.52	1108	1108
23	23	0.066	0.066	4.52	4.52	1120	1120
24	24	0.068	0.068	4.52	4.52	1135	1135
25	25	0.070	0.070	4.52	4.52	1150	1150



APPENDIX D

Common Sheet Metal Gauges

	<i>gauge</i>	<i>American Standard</i>	<i>Webb & Moen</i>	<i>Birmingham Std</i>	<i>U.S. Standard</i>	<i>gauge</i>	<i>American Standard</i>	<i>Webb & Moen</i>	<i>Birmingham Std</i>	<i>U.S. Standard</i>
7-0		.490		.500		18	.040	.047	.049	.050
6-0	.580	.461		.468		19	.035	.041	.042	.043
5-0	.516	.430	.500	.437		20	.032	.034	.035	.037
4-0	.460	.393	.454	.406		21	.028	.031	.032	.034
3-0	.409	.362	.425	.375		22	.025	.028	.028	.031
2-0	.364	.331	.380	.343		23	.022	.025	.025	.028
0	.324	.306	.340	.312		24	.020	.023	.022	.025
1	.289	.283	.300	.281		25	.017	.020	.020	.021
2	.257	.262	.284	.265		26	.015	.018	.018	.018
3	.229	.243	.259	.250		27	.014	.017	.016	.017
4	.204	.225	.238	.234		28	.012	.016	.014	.015
5	.181	.207	.220	.218		29	.011	.015	.013	.014
6	.162	.192	.203	.203		30	.010	.014	.012	.012
7	.144	.177	.180	.187		31	.008	.013	.010	.010
8	.128	.162	.165	.171		32	.008	.012	.009	.010
9	.114	.148	.148	.156		33	.007	.011	.008	.009
10	.101	.135	.134	.140		34	.006	.010	.007	.008
11	.090	.120	.120	.125		35	.005	.009	.005	.007
12	.080	.105	.109	.109		36	.005	.009	.004	.007
13	.072	.091	.095	.093		37	.004	.008		.006
14	.064	.080	.083	.078		38	.004	.008		.006
15	.057	.072	.072	.070		39	.003	.007		
16	.050	.062	.065	.062		40	.003	.007		
17	.045	.054	.058	.056						

REFERENCES

1. Allen, D. H., and Haisler, W.E., *Introduction to Aerospace Structural Analysis*, John Wiley & Sons, Inc., 1985.
2. Sechler, E. E., and Dunn, L.G., *Airplane Structural Analysis and Design*, John Wily & Sons, Inc., 1942.
3. Nicholai, L. M., *Fundamentals of Aircraft Design*, Domicone Printing Services, 1975.
4. Raymer, D. P., *Aircraft Design: A Conceptual Approach*, 2d ed., American Institute of Aeronautics and Astronautics, Inc., 1992.
5. Burris, S. A., *Subsonic Load Analysis Manual*, Technical Manual prepared for the Naval Postgraduate School, Department of Aeronautics and Astronautics, 1994.
6. Bertin, J. J., and Smith, M. L., *Aerodynamics for Engineers*, 2d ed., Prentice Hall, 1989.
7. Anderson, J. D. Jr., *Fundamentals of Aerodynamics*, 2d ed., McGraw-Hill, Inc., 1991.
8. Interview between Mr. Dave McNally, and others, Northrop Aircraft Corporation, and the author, 30 July 1993.
9. Niu, M. C., *Airframe Structural Design*, CONMILIT PRESS LTD., 1988.
10. Abbott, I. H., and von Doenhoff, A. E., *Theory of Wing Sections*, Dover Publications, Inc., 1959.
11. McDonnell Douglas Corporation, *DATCOM, USAF Stability and Control Data Compendium*, by Fink, R. D., and Hoak, D. E., April 1978.
12. Popov, E. P., *Introduction to Mechanics of Solids*, Prentice-Hall, Inc., 1968.
13. Naval Air Systems Command, General Specification for Design and Construction of Aircraft Weapon Systems, v. 1, Fixed Wing Aircraft, 2 June 1982.

14. Anderson, J. D. Jr., *Introduction to Flight*, 3d ed., McGraw-Hill, Inc., 1989.

INITIAL DISTRIBUTION LIST

	No. of Copies
1. Defense Technical Information Center Cameron Station Alexandria VA 22304-6145	2
2. Library, Code 052 Naval Postgraduate School Monterey CA 93943-5002	2
3. Department Chairman, AA Department of Aeronautics and Astronautics Naval Postgraduate School Monterey CA 93943	1
4. Prof. Gerald H. Lindsey Code AA/Li Department of Aeronautics and Astronautics Naval Postgraduate School Monterey CA 93943	3
5. Prof. Edward M. Wu Code AA/Wu Department of Aeronautics and Astronautics Naval Postgraduate School Monterey CA 93943	2
6. Prof. M. Platzer Code AA/Pl Department of Aeronautics and Astronautics Naval Postgraduate School Monterey CA 93943	2
7. Stephen A. Burris c/o George R. Burris, Jr. 2223 Viburnum Lane Worthington OH 43235	2

- | | | |
|-----|--|---|
| 8. | Prof. R. Ball | 2 |
| | Code AA/Ba | |
| | Department of Aeronautics and Astronautics | |
| | Naval Postgraduate School | |
| | Monterey CA 93943 | |
| 9. | Prof. C. Newberry | 4 |
| | Code AA/Ne | |
| | Department of Aeronautics and Astronautics | |
| | Naval Postgraduate School | |
| | Monterey CA 93943 | |
| 10. | Dr. O. Lynn Webb, Ph.D. | 1 |
| | 30 NW Quail Creek Drive | |
| | Lawton OK 73501 | |